TOSHIBA
Leading Innovation >>>

TOSHIBA CORPORATION

1-1,SHIBAURA 1-CHOME, MINATO-KU TOKYO 105-8001,JAPAN

TOS-CR-4S-2011-0001
Project Number 0760

September 26, 2011

U.S. Nuclear Regulatory Commission
Document Control Desk
Washington, DC 20555-0001

Subject: Submittal of Technical Report "4S Core Nuclear Design Codes and Methods Validation"

Enclosed is a copy of the non-proprietary "4S Core Nuclear Design Codes and Methods Validation" for the 4S (Super-Safe, Small and Simple) reactor plant that is currently the subject of a pre-application review among NRC, Toshiba, and its 4S affiliates including Japan's Central Research Institute for Electric Power Industry (CRIEPI).

The pre-application review for the 4S reactor commenced in the fourth quarter of 2007. Pre-application review meetings were held among NRC, Toshiba and the 4S affiliates in October 2007, and February, May and August 2008.

Additional technical reports pertaining to the 4S design will be submitted as the pre-application review progresses. If you have any questions regarding this document, please contact Mr. Tony Grenci of Westinghouse at (623) 271-9992, or grencit@westinghouse.com.

Very truly yours,

Tetsuya Noda

Tetsuya Noda
Senior Manager, Plant Project Engineering Department
Nuclear Energy Systems & Services Division, Power Systems Company
Toshiba Corporation

Enclosures: Technical Report "4S Core Nuclear Design Codes and Methods'Validation"

cc: Michael Mayfield (NRO/DNRL)
Tom Kevern (NRO/DNRL)
Bill Reckley (NRO/DNRL)
Don Carlson (NRO/DNRL)
Nobuyuki Ueda (CRIEPI)
Tony Grenci (Westinghouse)
Sam Binger (Westinghouse)
Abdellatif M. Yacout (Argonne National Laboratory)

D104
NRO

Document Number: AFT-2011-000082rev004(0)
PSN Control Number: PSN-2011-1034

4S Core Nuclear Design Codes and Methods Validation

September 2011

TOSHIBA CORPORATION

Summary

The purpose of this report is to inform the United States Nuclear Regulatory Commission of the core nuclear design codes and methods for the reflector-controlled fast reactor 4S, its validation by the comparison between the measured and calculated results, and the derived analysis uncertainties.

The 4S core is small and is reflector-controlled for operation through core lifetime. The design methods which are a combination of analysis methods and nuclear data sets have been selected to treat neutron leakage with high accuracy in small fast reactors. The selected design methods are as follows:

a) The continuous-energy Monte Carlo code, MVP, which can rigorously treat detail geometries of the core and reflectors in analytical modeling.

b) The discrete ordinate transport codes, THREEDANT and TWODANT for deterministic calculations.

c) The evaluated cross-section file JENDL_3.3 based library MVPlib_J33 for the MVP code and the 70 energy group constant set JFS-3-J3.3 generated by the cell homogenization code SLAROM from the evaluated cross section file JENDL-3.3 for the discrete ordinate transport codes.

These two types of transport methods a) and b) are used for the design in a complementary fashion.

The nuclear design methods have been validated by analysis of benchmark critical experiments and the experimental reactor data. Three kinds of physical benchmark data were used for the validation.

1) Critical experimental data of various core characteristics of the FCA XXIII core which was constructed as a physics mockup assembly of the 4S core to demonstrate reflector-controlled core characteristics in the leakage-dominant situation. The measured data used in this validation were criticality, reflector worth, power distributions, spectrum indexes, absorber reactivity worth, and sodium void worth distributions.

2) Critical experimental data which were obtained from the critical experiments in fast spectra tests other than from FCA XXIII. The measured data used in this validation were criticality, spectrum indexes, sample Doppler reactivity and effective delayed neutron fractions.

3) Data from the experimental reactor JOYO MK-1 tests.

Validated characteristics are criticality, reflector reactivity worth, power distribution, absorber reactivity worth, sodium void worth, Doppler reactivity, effective delayed neutron fraction and burnup reactivity worth. A multi-component bias method was applied, especially to improve the

accuracy of sodium void reactivity worth. The bias factors and uncertainties for each component derived by perturbation calculations are determined by utilizing approximately one hundred sets of measured data from the FCA XXIII experiments of sodium void reactivity worth.

Through these validation results, it has been confirmed that the 4S core nuclear design code and method provides good accuracy for neutronic characteristics. The analysis uncertainty of each characteristic is less than 10% for the nominal value, and the uncertainty of criticality is less than 0.3% in C/E.

TABLE OF CONTENTS

Section	Title	Page No.
LIST OF TABLES		IV
LIST OF FIGURES		VI
LIST OF ACRONYMS AND ABBREVIATIONS		VII
1	INTRODUCTION	1-1
2	4S CORE DESIGN AND ITS METHODS	2-1
2.1	Outline of Core Design and Characteristics	2-1
2.2	Core Design Methods	2-3
3	VALIDATION OF NUCLEAR DESIGN METHODS	3-1
	(1) Criticality	3-2
	(2) Reflector reactivity worth	3-3
	(3) Power distribution	3-4
	(4) Absorber reactivity worth	3-4
	(5) Sodium void reactivity worth	3-5
	(6) Doppler reactivity	3-5
	(7) Effective Delayed Neutron Fraction	3-6
	(8) Burnup reactivity losses	3-6
4	APPLICABILITY OF THE CRITICAL ANALYSIS RESULTS TO THE 4S CORE NUCLEAR DESIGN	4-1
4.1	Sensitivity and Uncertainty (S&U) Analysis Using Critical Analysis Results	4-1
4.2	Prediction Accuracies of the Selected Characteristics of the Target Cores	4-3
	4.2.1 Cross-Section Sensitivity Coefficients	4-3
	4.2.2 Prediction Accuracies by Application of the Bias Factors	4-3
4.3	Direct Application of the Measured Sodium Void Worth Results to the Target Cores	4-5
	4.3.1 Multi-Component Approach for Predicting Core Sodium Void Worth	4-5
	4.3.2 Estimated Uncertainty of Core Sodium Void Worth	4-7
5	CONCLUSIONS	5-1
APPENDIX. EXPERIMENTAL ANALYSES BY THE 4S NUCLEAR DESIGN METHODS		1

LIST OF TABLES

Table No. **Title** **Page No.**

Table 2.1-1. Reference Values of Doppler, Density, and Geometry Reactivity Coefficients..... 2-8

Table 2.1-2. Isotope Content at BOL and EOL..... 2-8

Table 3-1. Outline of the Selected Fast-Spectrum Cores..... 3-8

Table 3-2. C/E Values for Effective Multiplication Factors..... 3-8

Table 3-3. Examples of Sn-order Effects on the Effective Multiplication Factor..... 3-9

Table 3-4. C/E Values for Criticality of JOYO MK-1 Core 3-9

Table 3-5. Criticality C/E Values for the Enriched Uranium Cores from JENDL-3.3 Library ... 3-10

Table 3-6. C/E Values with 900 Energy Group S8 Calculations for ZPPR-21 Benchmark Cores..... 3-10

Table 3-7. C/E-values for Reactivity Changes for Drawer Replacements from Reflector Cell to Cavity Cell in the Reflector Worth Measurements in the FCA XXIII Cores 3-11

Table 3-8. C/E-Values for Reactivity Changes for Drawer Replacements from Reflector Cell to Cavity Cell in the Reflector Worth Measurements in the FCA XXIII Cores 3-12

Table 3-9. C/E-Values for Reactivity Changes for Drawer Replacements from Sodium Cell to Cavity Cell in the Reflector Worth Measurements in the FCA XXIII Cores 3-13

Table 3-10. C/E Values for Relative Reaction Rate Distributions for U-235(n,f) Reaction Rate..... 3-13

Table 3-11. C/E Values of Hf Worth at Central 3x3 Zone in FCA XXIII-1DU Core 3-14

Table 3-12. C/E Values of B_4C Worth at Central 3x3 Zone in FCA XXIII-1DU Core 3-14

Table 3-13. C/E-Values for Axially Integrated Sodium Void Reactivity Worth in the Core Variants of FCA XXIII 3-15

Table 3-14. Examples of C/E Values for Doppler Reactivity by the Simplified Homogeneous Models..... 3-16

Table 3-15. Outline of the Cores and Measured Characteristics..... 3-17

Table 3-16. C/E Values for the Benchmark Data..... 3-17

Table 3-17. C/E Values for Spectral Indices (70 energy group, P0-S8) 3-18

Table 3-18. Burnup Reactivity Loss and Component-Wise Fractions in 4S 3-19

Table 3-19. C/E Values for Spectral Indices (70 Energy Group, P0-S8) 3-20

Table 3-20. C/E Values for the Benchmark Data 3-20

Table 4.1-1. Measured Integral Parameters and their Identification Numbers 4-9

Table 4.1-2 Measured Integral Parameters and their Errors 4-10

Table 4.1-3 Analysis Results (C/E Values) and the Examples of Method Uncertainties 4-10

Table 4.1-4. Nuclides and Reactions for Cross-Section Sensitivity Analysis 4-11

Table 4.2-1 Examples of Evaluated Uncertainties for Core Characteristics of FCA XXIII Core 4-12

Table 4.2-2 Examples of Evaluated Uncertainties for Core Characteristics of the Target Core 4-12

Table 4.3-1. Fitted Bias Factors by One Energy Group from the FCA XXIII Results 4-13

Table 4.3-2. Predicted Average Bias for the FCA XXIII Results 4-13

Table 4.3-3. Fitted Bias Factors by Two-Energy Group from the FCA XXIII Results 4-13

Table 4.3-4. Core-Wide Sodium Void Worth at the EOL Core in the Target Core 4-14

Table 4.3-5. Predicted Sodium Void Worth Using Fitted Bias Factors 4-14

Table 5-1. Summary Analysis Accuracies Obtained from the FCA XXIII Experiments and Analyses 5-2

LIST OF FIGURES

Figure No.	Title	Page No.
Fig. 2.1-1	Reactor Structure	2-9
Fig. 2.1-2	Fuel Assembly	2-9
Fig. 2.1-3	Reflector and Cross-Section of Core	2-10
Fig. 2.1-4	Orifice Zones	2-10
Fig. 2.2-1	Effective Multiplication Factor Analysis Flow	2-11
Fig. 2.2-2	Reflector Reactivity Worth Analysis Flow	2-12
Fig. 2.2-3	Flooded Coolant Worth at Cavity Region Analysis Flow	2-13
Fig. 2.2-4	Power Distribution Analysis Flow	2-14
Fig. 2.2-5	Absorber Reactivity Worth Analysis Flow	2-15
Fig. 2.2-6	Sodium Void Reactivity Worth Analysis Flow	2-16
Fig. 2.2-7	Reactivity Coefficient Analysis Flow	2-17
Fig. 2.2-8	Effective Delayed Neutron Fraction Analysis Flow	2-18
Fig. 2.2-9	Burnup Reactivity Loss Analysis Flow	2-19
Fig. 3-1	Geometry and Models for FCA XXIII-1 Core	3-21
Fig. 3-2	Core Geometries and Models for the Reflector Worth and Sodium Void Measurement and Analyses	3-22
Fig.3-3	Effect due to Variation of Reflector Position to Axial Distribution of U235 fission of FCAXXIII Test	3-23
Fig.3-4	Comparison of Radial Relative Profiles for Measured and Caluclated U235 (n,f) Reaction Rate ar Core Midplane of JOYO Experiment	3-23
Fig.4.3-1	Energy Dependence of Calculated Components of Sodium Void Worth for the FCA XXIII	4-15

LIST OF ACRONYMS AND ABBREVIATIONS

4S	Super-Safe, Small and Simple
C/E	Calculation/Experimental Ratio
FCA	Fast Critical Assembly (JAEA)
GPT	Generalized Perturbation Theory
HEU	High Enrichment Uranium
JENDL-3.3	Japanese Evaluated Nuclear Data Library Version 3 Revision 3
LANL	Los Alamos National Laboratory
LEU	Low Enrichment Uranium
MEU	Medium Enrichment Uranium
MSM	Modified Source Multiplication
OECD/NEA	Nuclear Energy Agency (NEA) within the Organization for Economic Co-operation and Development (OECD)
ZPPR	Zero Power Physics Reactor (ANL)
ZPR	Zero Power Reactor (ANL)

1 INTRODUCTION

The 4S core nuclear characteristics are predominantly determined by the balance between lateral neutron leakage and reflected neutrons by means of reflector movement to maintain criticality. The six annular reflector segments move in unison very slowly in overlapping the active fuel portion of the core, from the lower toward the upper core. Although the 4S core is small, somewhat higher prediction accuracies are required to achieve long life, enhanced safety goals, and near-zero sodium void reactivity, to provide a viable design.

A specific design method (combination of prediction methods and data sets) has been selected for the nuclear design of the 4S. It includes application of:

a) The continuous-energy Monte Carlo code, MVP [1-1]

b) Discrete-ordinate transport codes, THREEDANT and TWODANT [1-2], for deterministic calculations

c) The evaluated cross-section file JENDL-3.3[1-4] based library for MVP code and 70 energy group constant set for fast reactor JFS-3-J3.3 with cell homogenization code SLAROM [1-3]

These two types of transport methods a) and b) are used for the design in a complementary fashion. The basic codes and libraries have been developed by JAEA (Japan) and LANL (USA) and are widely used by various organizations. Bias factors and uncertainties for the major characteristics were determined by application of the C/E values obtained from the physics benchmark experiments FCA XXIII series, which was structured to mock up the reflector-controlled geometry.

References

[1-1] Mori T., Nakagawa M., Sasaki M.: "Vectorization of Continuous Energy Monte Carlo Method for Neutron Transport Calculation", J. Nuclear. Sci. Technol., Vol. 29, [4], 325 (1992).

[1-2] R. E. Alcouffe, et al., "DANTSYS: A Diffusion Accelerated Neutral Particle Transport Code System," LA-12969-M (1995).

[1-3] M. Nakagawa, et al., "A Code for Cell Homogenization of Fast Reactor," JAERI 1294 (1984)

[1-4] K. Shibata, et al. "Japanese Evaluated Nuclear Data library Version 3 Revision-3: JENDL-3.3' J. Nucl. Sci. Technol. Vol.39. [11], 1125 (2002).

2 4S CORE DESIGN AND ITS METHODS

2.1 Outline of Core Design and Characteristics

4S uses a pool-type, sodium-cooled reactor. The reactor structure is shown in Figure 2.1-1 [2-1]. The reactor structure includes the fuel assemblies, primary electromagnetic (EM) pumps, an intermediate heat exchanger (IHX), reactor core support structure, vertical shroud, radial shield, reflector, fixed absorber, and reactor instrumentation, which are all installed inside the reactor vessel. The reactor vessel is fabricated of Type 304 stainless steel and has a 3.5 m inner diameter. The primary heat transport system is completely enclosed within the reactor vessel. The two sequential main circulating EM pumps are installed suspended from the bottom of the IHX, which is itself supported from the top of the reactor vessel. These pumps are immersed in sodium, and circulate the sodium coolant. The pumps are annular in configuration, and are located in the perimeter of the core shroud near the reactor vertical center. The rated flow is 10.6 m^3/min, and the total rated pump head is 0.1 MPa for the two pumps in series. A motor-generator set for the EM pumps supplies residual power to provide flow coast down when the normal power supply is lost.

Figure 2.1-2 [2-1] shows the fuel assembly configuration. There are 169 pins in each assembly. The pins contain fuel columns made of U-10%Zr alloy, for which substantial previous operating experience in sodium fast reactors exists. The cladding and duct material is HT-9, which was chosen for its excellent properties for this application, including its resistance to void swelling. The fuel slug portion of each pin is 2500 mm high, and the fission gas plenum just above the fuel is 2700 mm high. The large fission gas plenum is necessary to accommodate the long fuel life. The pins incorporate a sodium bond between the fuel slug and cladding. The fuel smear density inside the cladding is 78 percent of the theoretical maximum density, which compensates for any fuel swelling saturation associated with interconnection of porosity and fission gas release over core life. The low smear density is made possible by incorporating a sodium thermal bond between the fuel pin and the clad to promote thermal conductivity.

Based on the past experience with metal fuel design and consistency to the plant design conditions, the core design conditions were determined as follows:

(1) Reactor thermal power: 30 MW

(2) Reactor inlet/outlet temperature: 355/510°C

(3) Core pressure drop: 0.1 MPa or less

(4) Main reactivity control system: reflector of modified 9Cr-1Mo with a thickness of about 38cm

(5) Backup shutdown system: the shutdown rod located at the core center

(6) Fuel composition: U-Zr binary alloy (enrichment of less than 20%HM)

(7) Fuel pin: a diameter of 15 mm or less with HT-9 cladding

(8) Core height: 2.5 m or less

(9) Maximum cladding temperature: 650°C or less

(10) Cladding thickness: sufficient to maintain integrity for 30 years

(11) Fuel smear density ratio: 78%

(12) Coolant void condition: voiding of the sodium over intra-assembly for the height of active core and fission gas plenum

The distinctive characteristic of the 4S core design is the reflector-controlled core. Figure 2.1-3 shows the core cross-section and the reflector configuration [2-1]. The core consists of 18 hexagonal fuel assemblies and one central assembly containing a shutdown rod and fixed absorber. The 4S core is narrow relative to its height, with an equivalent core diameter of 0.95 m. The core average burnup is 34,000 MWd/t. Core reactivity and power are controlled by the six-segment cylindrical reflector surrounding the core. The reflecting region of the reflector assembly is positioned to cover the core partially to reach criticality, by reflecting fast neutrons back into the fuel. Reflector is designed to covers entire active core height at the end of life. As the metallic fuels elongate to axial direction by 8.5% due to swelling, the core height increase to 2.7m from 2.5m of the height at beginning of life. So the reflector length is set 2.7m for covering the end of life core height. Lowering of the reflector assembly to below the core region by gravity provides for scram shutdown. The reflector has sufficient worth to enable shutdown without using any additional means, even assuming one stuck segment.

Reactivity balance for the 4S reactor is achieved by gas-filled cavity cans above the reflecting region, along with a Hf fixed absorber, located in the center assembly. The cavity cans constitute the portion of the reflector assembly installed above the reflecting region, and enhance the increase in neutron leakage from the core relative to the surrounding sodium coolant. Each of the six segments of the reflector assembly contains six cavity cans, for a total of 36 cavity cans, thus restricting the insertion of positive reactivity by sodium intrusion as a result of the failure of a single can. The reactivity coefficients are shown in Table 2.1-1.

The fixed absorber is fan-shaped and includes a Hf-sheeted element or stainless steel pins filled with B_4C pellets. It is positioned surrounding the shutdown rod and allows a large excess reactivity at the beginning of life, which is necessary to maintain criticality for 30 years [2-1]. At approximately the middle of core life, the fixed absorber is retracted from the core, adding positive reactivity, and allowing repositioning of the reflector lower on the core, so that sufficient reflector movement is available to maintain criticality until end of life (EOL).

There are two distinct flow zones across the reactor. The flow distribution is set using an orifice to adjust the individual assembly flow to accommodate the power distribution across the core. Figure 2.1-4 shows the orifice zone map [2-1].

During normal operating conditions, reactor core power is controlled by the movable reflector. The reflector drive consists of a combination of fine and fast adjustment mechanisms. The fast adjustment mechanisms are used to position the reflector for startup and shutdown, and the fine adjustment is used incrementally and automatically to compensate for core burnup.

To scram the reactor, the clutch of the fast adjustment mechanism is released and the reflector falls by gravity, causing the reactor to shut down. The shutdown rod at the core center position is also inserted upon a scram to provide an independent and redundant means of shutting down the reactor. Either the reflector or the shutdown rod is capable of inserting enough negative reactivity by itself to shut down the reactor.

Burnup reactivity compensation and margins for uncertainties in temperature effects, criticality, and fissile enrichment are considered in the reflector and fixed neutron absorber design.

The radial reflector segments are adjustable, and they are incrementally raised very slowly during the service life of the core using the fine adjustment mechanism to maintain neutron flux and power levels as burnup progresses.

Table 2.1-2 shows the change of U and Pu isotope contents over core life. The Pu contents accumulate to around 1% at EOL.

2.2 Core Design Methods

The 4S core consists of 18 fuel subassemblies and a central subassembly which includes the shutdown rod and a fixed absorber as shown in figure 2.1-3 and figure 2.1-4. The reflectors surround the core. Metallic fuel expands axially due to swelling over the core life time, and the core geometry change due to swelling at various stages of burnup is considered in the analysis of core characteristics.

4S core power and criticality are controlled by adjusting neutron leakage with the positioning of the reflectors. Neutron leakage behavior must be predicted accurately for evaluating core characteristics over the 30 year core lifetime. In order to evaluate these core characteristics, it is considered that statistical and deterministic transport calculation methodologies are an adequate design method. The continuous-energy Monte Carlo code is adopted for neutron balance of the small size core, because it can treat the exact geometry of the core and reflector in modeling. On the other hand, statistical error is taken into account for the calculated results by Monte Carlo methods. A deterministic discrete ordinate transport method is used for evaluation of local integral characteristics.

A particular design methodology which is a combination of prediction methods and data sets has been selected for the nuclear design of the 4S. It includes application of:

a) The continuous-energy Monte Carlo code, MVP

b) Discrete ordinate transport codes, THREEDANT and TWODANT, for deterministic

calculations.

JFS3-3-J3.3, the group constant set with 70 energy group structure generated from JENDL3.3 is used for the deterministic transport calculations. The fast reactor cell homogenization code SLAROM is used to calculate the 70 energy group effective cross section for use with the deterministic discrete-ordinate transport code.

The evaluated number data file JENDL3.3 was selected, because it was the latest cross-section library available at the time of the 4S design.

As for the applicability of these codes, evaluation by MVP with the continuous-energy JENDL 3.3 based library is used for reference, because it can calculate with the exact geometries and detail cross section by using the continuous-energy JENDL 3.3 based library. For calculation of small difference values such as evaluating reactivity coefficients, deterministic discrete-ordinary transport methods were adopted.

Uncertainty evaluation in the 4S design is performed by considering design method uncertainty, nuclide density uncertainty due to tolerance, and uncertainty of temperature, etc. This report focuses on evaluation of the uncertainty of the design method. The design method uncertainty is deduced by evaluation of critical experiments at room temperature.. The uncertainty of analysis method combined with the nuclear cross section set are confirmed to be determined adequately by application of C/E values and the sensitivity analysis of validation by estimating the critical experiments. The validation results are described in chapter 3 and chapter 4.

The design methods for evaluating each nuclear characteristic are as follows:

(1) Criticality

Evaluation of the effective multiplication factor (k_{eff} Value) is necessary to determine uranium enrichment and reflector geometry which will maintain the reactivity for 30 years. The continuous-energy Monte Carlo calculations are selected for evaluation of effective multiplication because it can simulate the geometry such as reflector position and hexagonal subassembly

Cross section file; MVPlib_J33
Analysis method; Continuous-energy Monte Carlo Code, MVP

Fig. 2.2-1 shows the flow of the analysis.

(2) Reflector reactivity worth

As for evaluation of reflector reactivity worth, the three items evaluated are 1) reactivity worth for full stroke movement, 2) the stroke curve of worth, and 3) the flooded coolant worth at the cavity region. The reactivity worth for full stroke is defined as the difference between the effective multiplication factor of the core covered by reflector and that of the core uncovered by the

reflector. The continuous-energy Monte Carlo method is selected as the reference design method for evaluation of the multiplication factor. Deterministic calculations are adopted for evaluating the stroke- worth curve of the reflector using a two-dimensional RZ model. In this case, the homogenized model is used for the core, reflector and cavity regions. The total worth from the deterministic calculation is normalized to full stroke worth using a Monte Carlo calculation for stroke curve characteristics. The Monte Carlo method is adopted to evaluate the reactivity of flooded sodium at the cavity region, because it treats the geometry at the cavity region exactly, taking into account statistical errors associated with the calculation method. For additional estimations of the uncertainty of coolant intrusion into the cavity, a multi component bias factor is applied. The cavity worth components which compose the reactivity change, 'neutron leakage term' and 'neutron nonleakage term' are evaluated by a deterministic perturbation code with a homogeneous model. This approach with multi component bias factors is described in chapter 4.

1) Reflector reactivity
Cross section file: MVPlib_J33
Analysis method: Continuous-energy Monte Carlo Code, MVP

2) Reflector stroke-worth curve
Cross section file: JFS-3-J3.3 Group constant set with a 70 energy group structure generated from JENDL-3.3
Effective cross section preparation: Cell homogenized code SLAROM
Analysis method: Discrete-ordinate transport code: TWODANT

3) Flooded coolant worth at cavity region
Cross section file: JENDL3.3 based library
Analysis method: Continuous-energy Monte Carlo Code, MVP
Analysis method: Discrete-ordinate transport code: TWODANT, SNPERT
Cross section file: JFS-3-J3.3 Group constant set with a 70 energy group structure
Effective cross section preparation: cell homogenized code SLAROM

Fig. 2.2-2 and Fig. 2.2-3 show the flow of the analysis.

(3) Power distribution

Fuel power distribution is estimated for the neutron fission reaction. Integral subassembly power is evaluated by continuous-energy Monte Carlo calculations. Detailed power distributions such as the axial and radial distributions in a subassembly are calculated by deterministic transport calculations.

1) Subassembly power
Cross section file: MVPlib_J33
Analysis method: Continuous-energy Monte Carlo Code, MVP

2) Power peaking factor

Analysis method: Discrete-ordinate transport code: TWODANT
Cross section file: JFS-3-J3.3 Group constant set with a 70 energy group structure

Fig 2.2-4 shows the flow of the analysis.

(4) Absorber reactivity worth

The shutdown rod and fixed absorber in the central subassembly contain neutron absorbers such as B_4C or Hf. Because the shutdown rod has self-shielding and heterogeneous effects caused by geometry and material, the continuous-energy Monte Carlo calculations are adopted with detailed geometry models.

Deterministic calculations are also adopted for evaluating stroke-curves of absorbers which require evaluating small reactivity changes due to reflector movement.

1) Absorber reactivity worth
Cross section file: MVPlib_J33
Analysis method: Continuous-energy Monte Carlo Code, MVP

2) Absorber stroke-worth curve
Cross section file: JFS-3-J3.3 Group constant set with a 70 energy group structure
Effective cross section preparation: cell homogenized code SLAROM
Analysis method: Discrete-ordinate transport code TWODANT

Fig. 2.2-5 shows the flow of the analysis.

(5) Sodium void reactivity worth

Void reactivity is the reactivity from replacement of sodium with voids in the coolant flow area of a fuel subassembly. Evaluation of void reactivity requires the analysis of small reactivity changes from a non-void condition to the void condition. For estimation of the uncertainty of void reactivity, multi-component bias factors are applied, the same as for flooded coolant worth in a cavity,. The sodium void worth components which comprise reactivity change, "neutron leakage term" and "neutron nonleakage term", are calculated using a deterministic perturbation code with a homogeneous model. This approach of multi-component bias factors is described in chapter 4. The same approach is also adopted for estimation of coolant density coefficients for the coolant temperature coefficient.

Cross section file: JFS-3-J3.3 Group constant set with a 70 energy group structure
Effective cross section preparation: cell homogenized code SLAROM
Analysis method: Discrete-ordinate transport codes TWODANT, SNPERT

Fig. 2.2-6 shows the flow of the analysis.

(6) Doppler reactivity

The deterministic discrete transport calculation which can use perturbation methods is adopted for evaluating this reactivity coefficient .

Cross section file: JFS-3-J3.3 Group constant set with a 70 energy group structure
Effective cross section preparation: cell homogenized code SLAROM
Analysis method: Discrete-ordinate transport codes TWODANT, SNPERT

Fig 2.2-7 shows the flow of the analysis. We describe the validation of Doppler reactivity in chapter 3.

(7) Effective Delayed Neutron Fraction

The deterministic discrete transport calculation is adopted for evaluating effective delayed neutron fraction.

Cross section file: JFS-3-J3.3 Group constant set with a 70 energy group structure
Analysis method: Discrete-ordinate transport code: TWODANT
Delayed neutron fraction and yield data: data stored in JENDL-3.3 were processed for the 70-group energy structure by NJOY code

Fig 2.2-8 shows the flow of the analysis.

(8) Burnup reactivity loss

The same method as for criticality is adopted for reactivity burnup loss. Burnup reactivity loss is estimated by considering power distribution changes due to the gradual shift of reflector position from BOL to EOL. Burnt fuel composition are provided for models of MOL and EOL in order to calculate various characteristics.

Cross section file; MVPlib_J33
Analysis method; Continuous-energy Monte Carlo Code, MVPBURN

Fig. 2.2-9 shows the flow of the analysis.

References

[2-1] Y. Tsuboi et al., "Development of the 4S and Related Technology (1) Plant System Overview and Current Status", Proceedings of ICAPP '09, Tokyo, Japan, May 10-14, 2009.

Table 2.1-1. Reference Values of Doppler, Density, and Geometry Reactivity Coefficients

		Region			
Attribute	**Definition**	**Core**	**Shutdown Rod**	**Inside Core Barrel**	**Reflector**
Doppler Reactivity Coefficient	Tdk/dT	-3.8×10^{-3}	-	-	-
Fuel Density Coefficient	dk/kk'/ dρ/ρ	3.6×10^{-1}	-	-	-
Coolant Density Coefficient	dk/kk'/ dρ/ρ	2.8×10^{-4}	-1.2×10^{-3}	1.5×10^{-2}	3.3×10^{-3}
Structure Density Coefficient	dk/kk'/ dρ/ρ	-1.5×10^{-2}	-4.9×10^{-4}	-	-
Core Support Structure Expansion	dk/kk'/°C	-5.9×10^{-6}			

Table 2.1-2. Isotope Content at BOL and EOL

(WT%)

	BOL	EOL
U-234	0.54	0.51
U-235	18.33	15.30
U-236	0.00	0.73
U-238	81.13	81.83
Pu-238	0.00	1.37E-03
Pu-239	0.00	1.59
Pu-240	0.00	0.03
Pu-241	0.00	4.32E-04
Pu-242	0.00	6.75E-06
	100.00	100.00

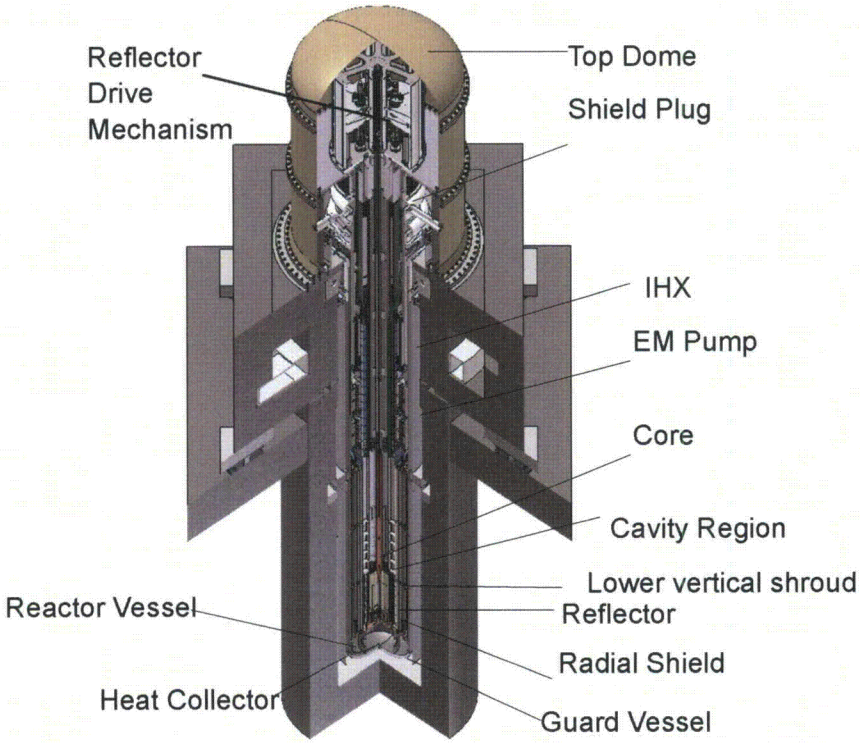

Fig. 2.1-1. Reactor Structure [2-1]

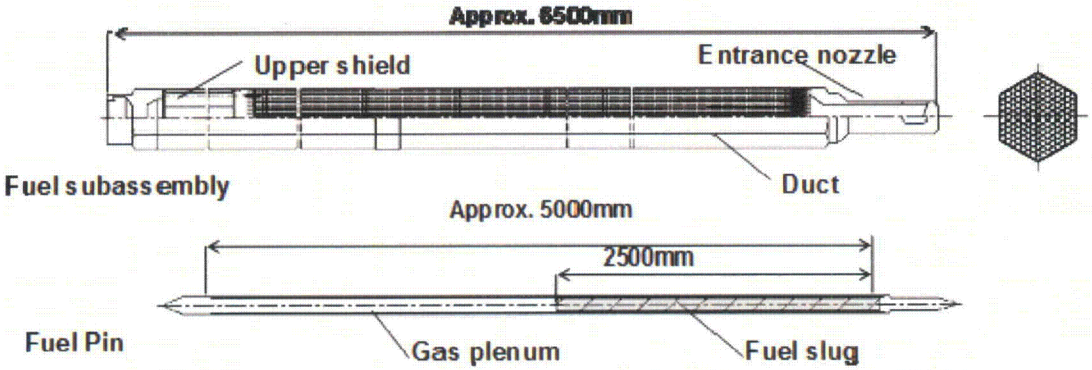

Fig. 2.1-2. Fuel Assembly [2-1]

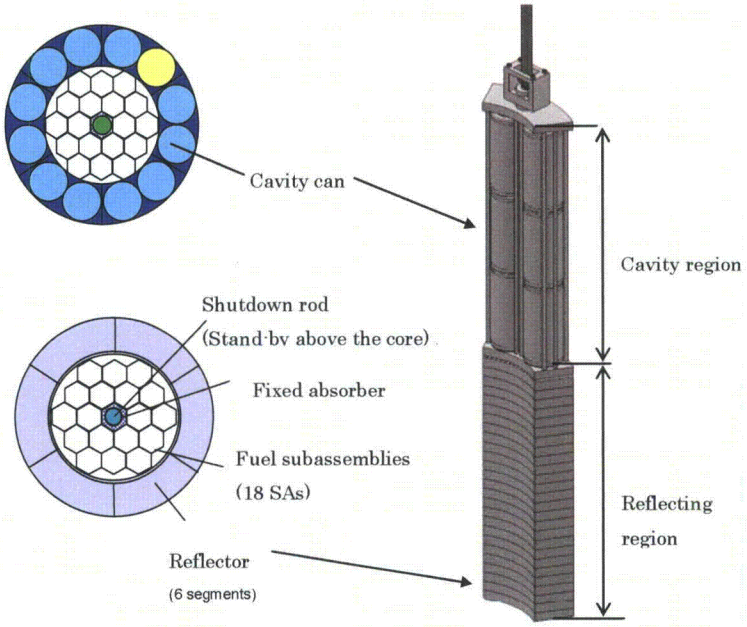

Fig. 2.1-3. Reflector and Cross-Section of Core [2-1]

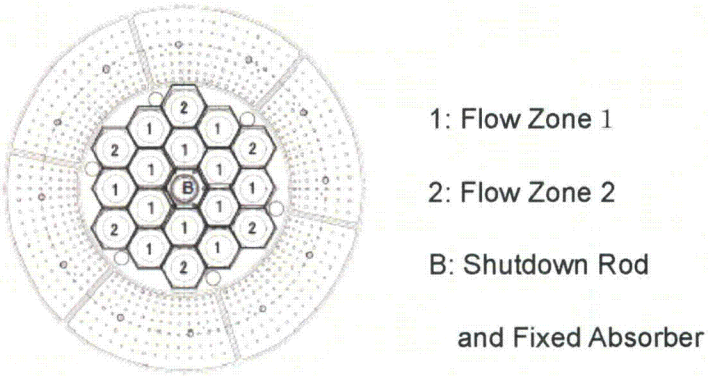

Fig. 2.1-4. Orifice Zones [2-1]

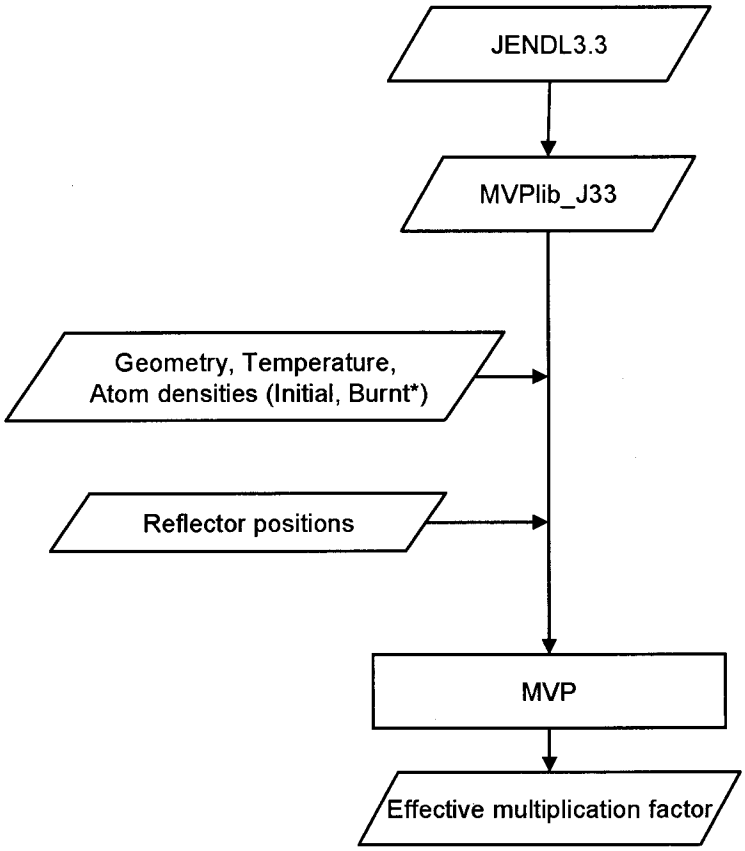

(*) Burnt atomic densities are calculated by MVPBURN (See figure 2.2-9)

Fig. 2.2-1. Effective Multiplication Factor Analysis Flow

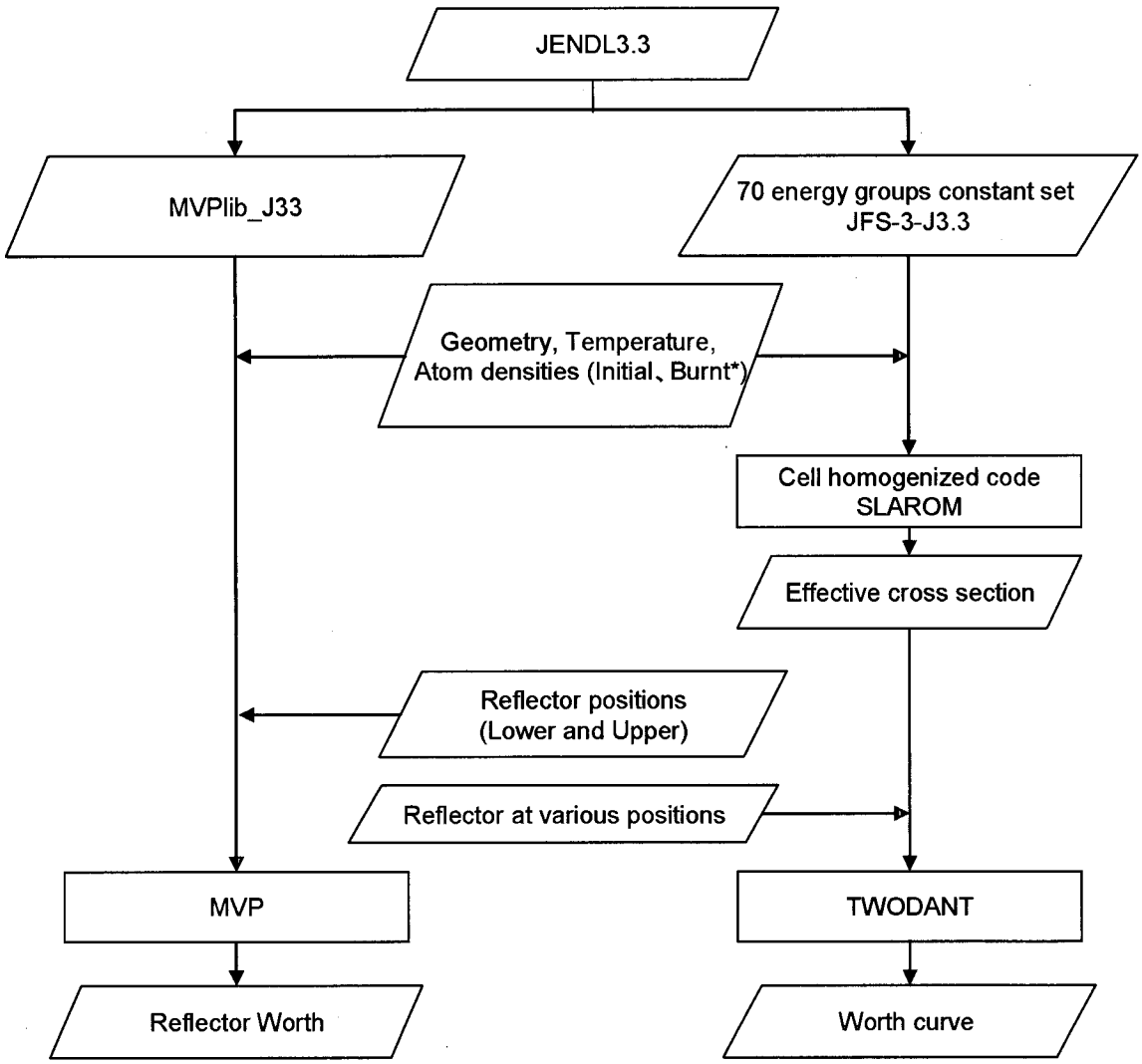

(*) Burnt atomic density is calculated by MVPBURN (See figure 2.2-9.)

Fig. 2.2-2. Reflector Reactivity Worth Analysis Flow

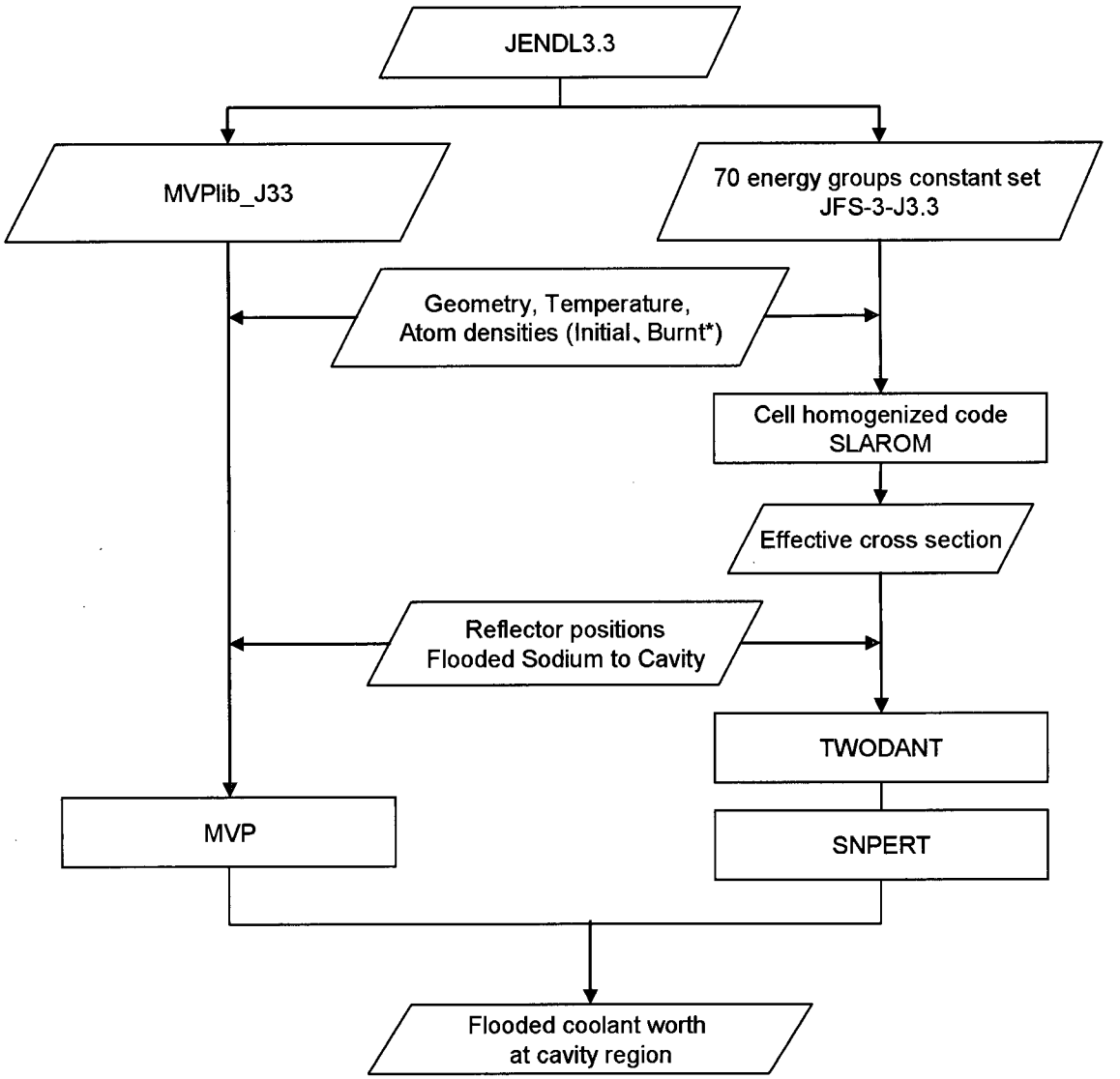

(*) Burnt atomic densities are calculated by MVPBURN (See figure 2.2-9.)

Fig. 2.2-3. Flooded Coolant Worth at Cavity Region Analysis Flow

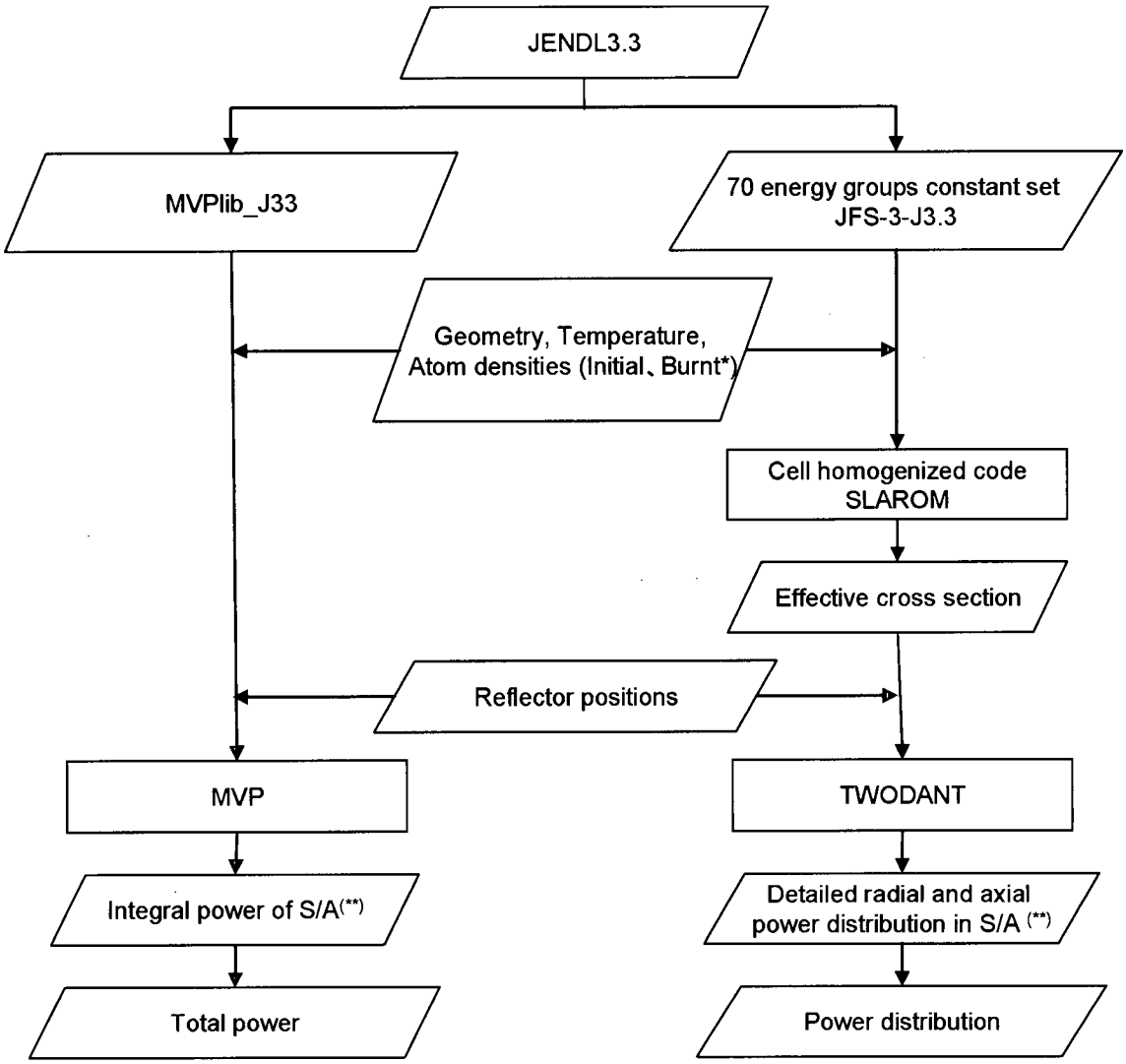

(*) Burnt atomic densities are calculated by MVPBURN (See figure 2.2-9.)

(**)S/A: subassembly

Fig. 2.2-4. Power Distribution Analysis Flow

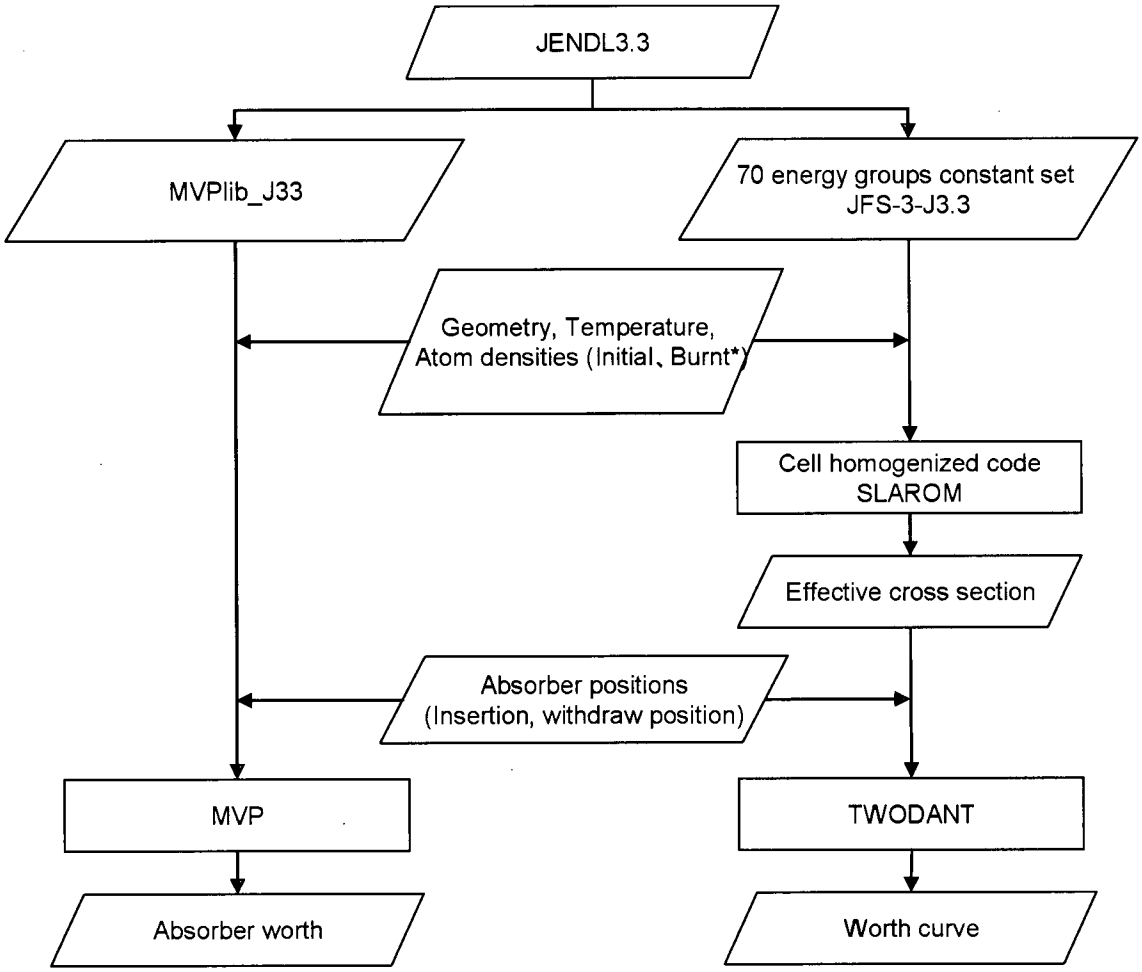

(*) Burnt atomic densities are calculated by MVPBURN (See figure 2.2-9.)

Fig. 2.2-5. Absorber Reactivity Worth Analysis Flow

(Absorber means shutdown rod and fixed absorber)

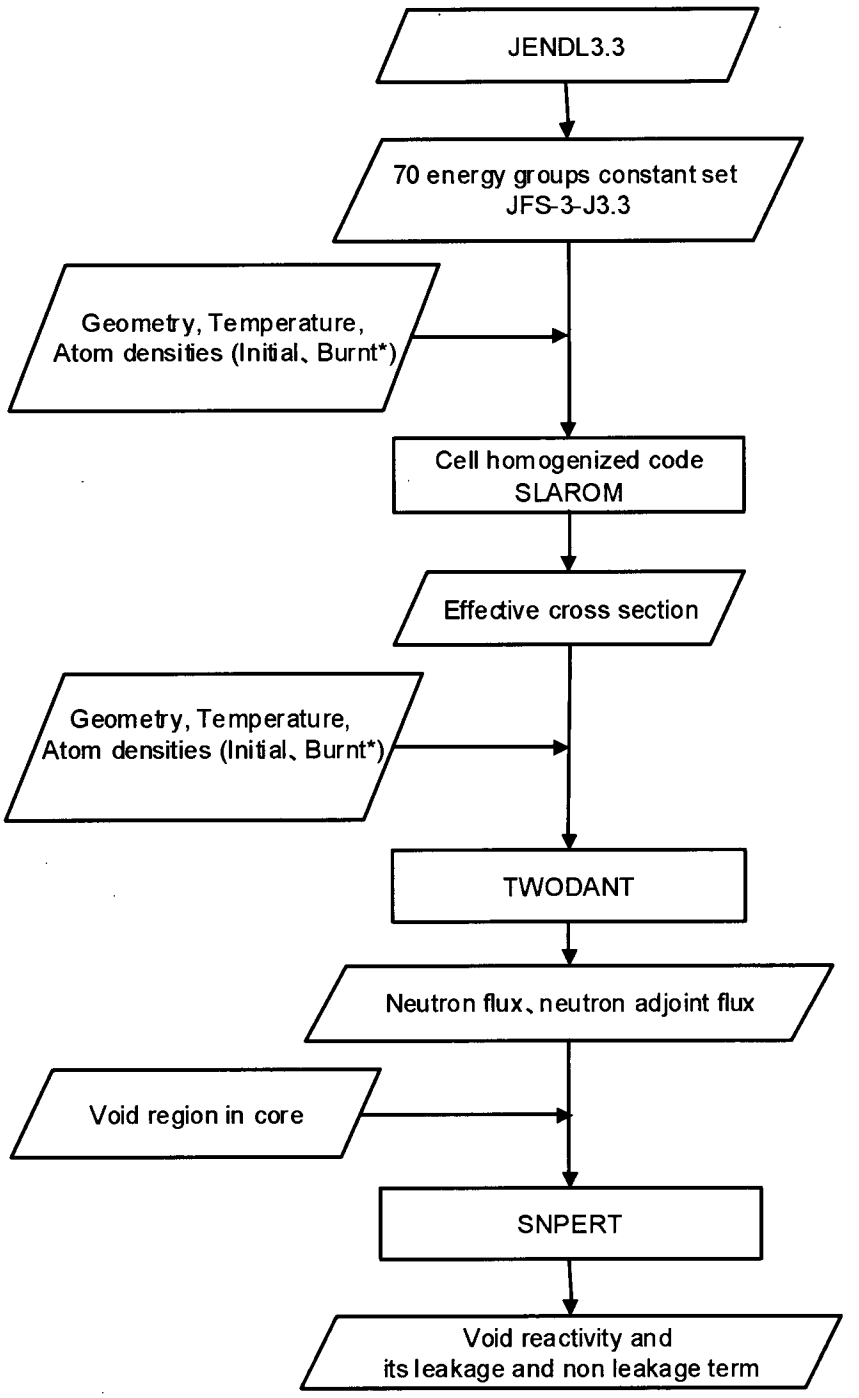

(*) Burnt atomic densities are calculated by MVPBURN (See figure 2.2-9.)

Fig. 2.2-6. Sodium Void Reactivity Worth Analysis Flow

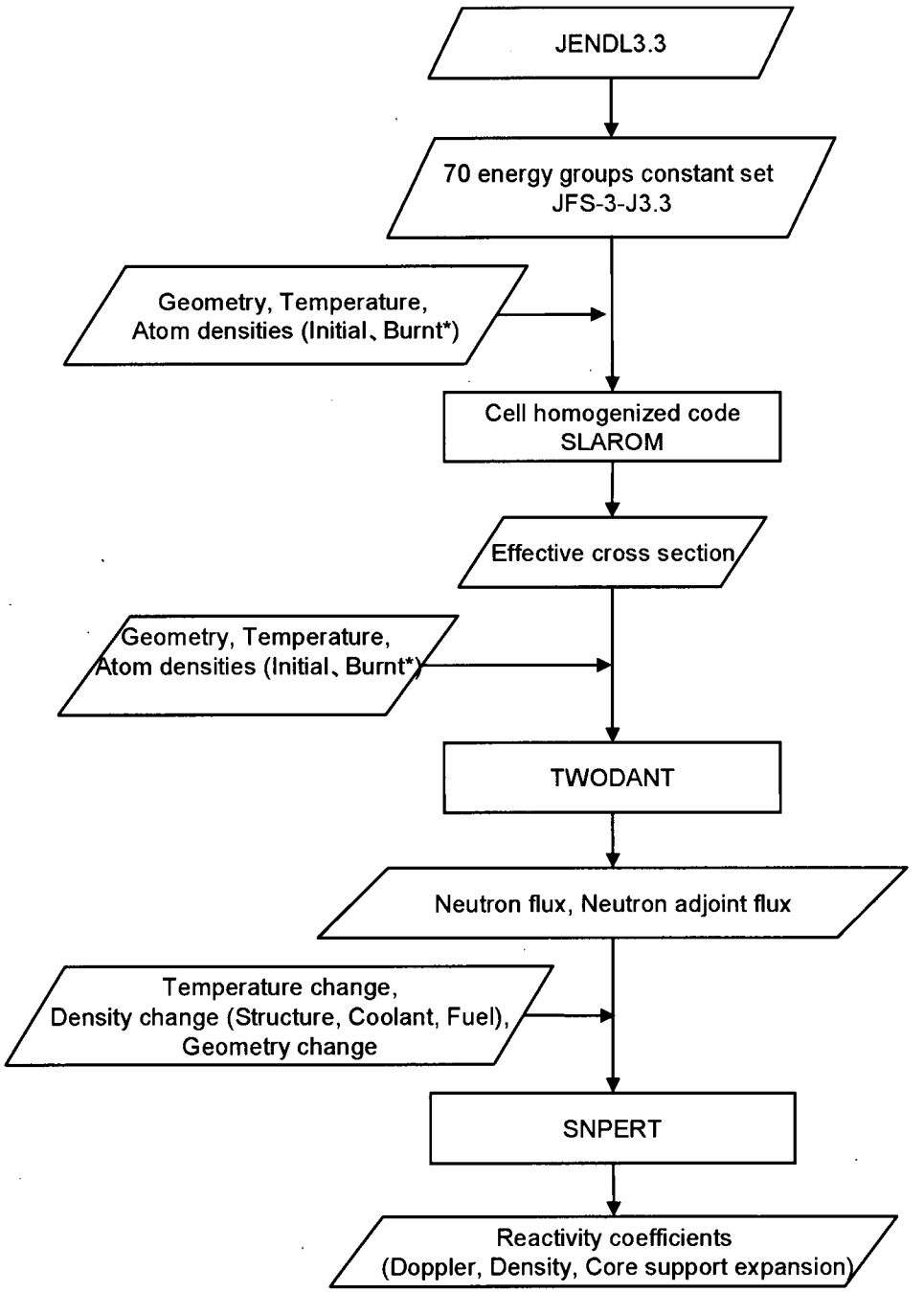

(*) Burnt atomic densities are calculated by MVPBURN (See figure 2.2-9.)

Fig.2.2-7. Reactivity Coefficient Analysis Flow

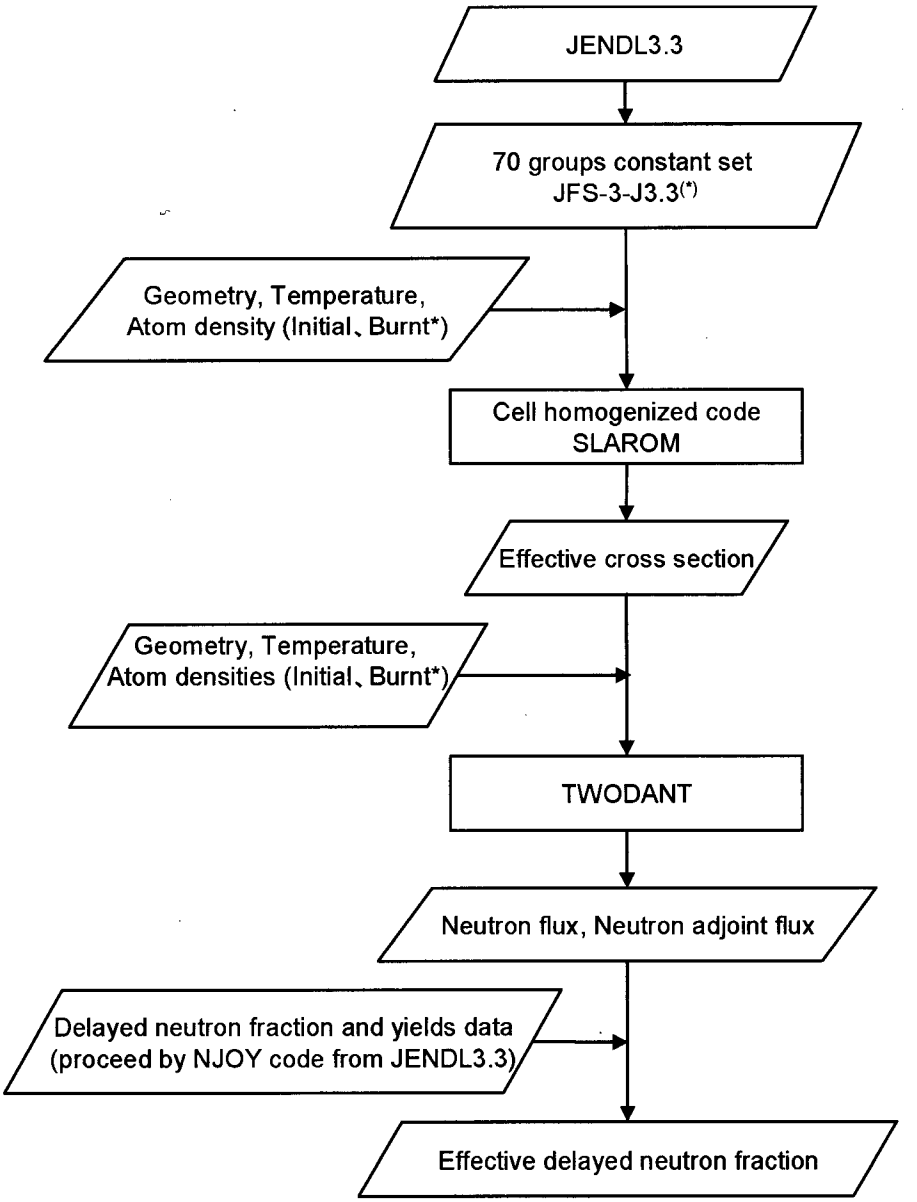

(*) Burnt atomic densities are calculated by MVPBURN (See figure 2.2-9.)

Fig. 2.2-8. Effective Delayed Neutron Fraction Analysis Flow

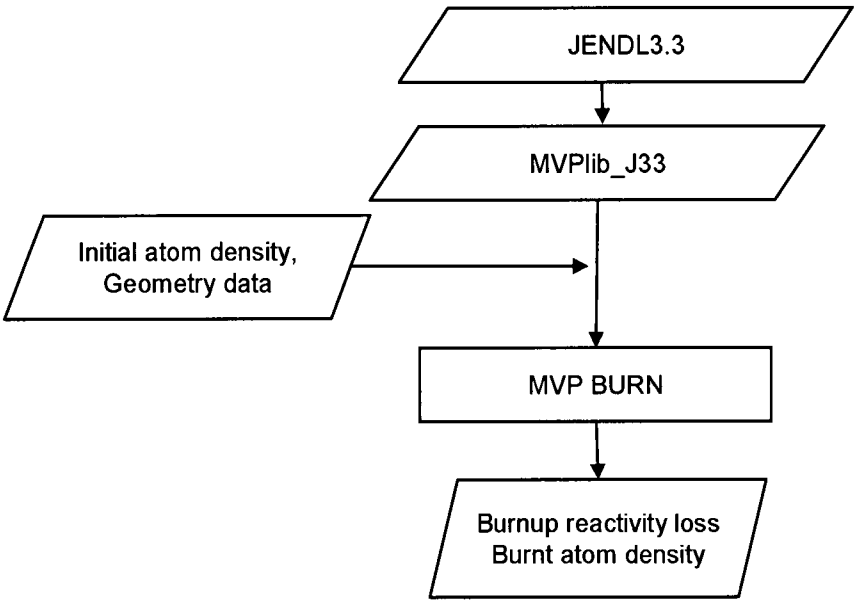

Fig. 2.2-9. Burnup Reactivity Loss Analysis Flow

3 VALIDATION OF NUCLEAR DESIGN METHODS

In this chapter, validation of the design method is described.

Three kinds of physical benchmark database sets are used for validation of the nuclear design methods (combination of analysis method and nuclear cross section library):

1) Critical experimental data of various core characteristics of the FCA XXIII core, which was constructed as a physics mockup assembly of the 4S core to demonstrate major core characteristics in the simulated layouts for reflector-controlled core.

2) Critical experimental data which were obtained from critical experiments in fast neutron spectra apart from the FCA XXIII core, and

3) Data from the experimental reactor JOYO MK-1 tests

Table 3.1 includes a comparison between the 4S core system and FCA XXIII core system. Core equivalent diameter of FCA XXIII is approximately 60% of 4S and the height is half of 4S. The neutron leakage of FCA XXIII is relatively larger than that of 4S. The composition of the 4S initial core is approximately 18% enriched U and composition at EOL is 15% U and 2-3 % Pu. The fraction of U-235 was approximately two third of that for the 4S. The sum of the U-235 and Pu fractions is approximately 26% for FCA XXIII.

In the FCA XXIII cores, important nuclear characteristics were measured for sodium void reactivity, reflector worth, fission rate distributions, absorber reactivity worth of B_4C and Hf-plates, and reaction rate ratios. Through the experiment and the analysis, the focus was on understanding the relationships between reflector positions controlling core-wide neutron leakage and the major characteristics, such as criticality, reflector worth, power distribution and sodium void reactivity worth. Fig. 3-1 shows the geometry and models for FCA XXIII cores and Fig. 3-2 shows core geometries and models for the reflector worth and sodium void measurements.

Therefore, in order to confirm the applicability of the nuclear design methods for the 4S core design, data from the FCA XXIII measurements are given primary priority as the main part of the benchmark data for validation of the reflector-controlled core.

Criticality is sensitive to the core composition. Prediction accuracy of criticality can also be dependent on the fractions of the U-235 and Pu isotopes. In order to evaluate applicability of the cross section library used in the 4S design methodology, analyses were done for benchmark data originating from criticality experiments performed in the ZPR and ZPPR cores with low enrichment (less than 20% of U-235).

The selected enriched U fast-spectrum cores are outlined in Table 3-1. Criticality benchmark from the ZPPR-21 series, which parametrically covered a wide range of combinations of the Pu

and enriched U fractions, were analyzed for assessment of the applicability of the cross section library.

The metallic fuel core of 4S has a relatively higher energy neutron spectrum than that of an oxide fuel core fast reactor. In order to evaluate accuracy of the Doppler coefficient, Doppler reactivity measured by sample-sized DU in the FCA XVI core was analyzed using the 4S design methods.

As for the validation of effective delayed neutron fraction, which is also sensitive to core composition, the benchmark data of FCA XIX was analyzed to evaluate applicability of the delayed neutron data used in the 4S design calculation. Through analyses, additional C/E values were obtained for criticality and fission rate ratios.

As for precedent fast reactors, the criticality and power distributions measured in the experimental fast reactor JOYO were analyzed by the 4S design methods to confirm the applicability of the design method in "pin" fuel geometry.

A summary of validation results is as follows.

(1) Criticality

The multiplication factors were analyzed by a continuous-energy Monte Carlo method using the MVP code with MVPlib_J33. The FCA XXIII core which simulates a reflector-controlled core is used for validation. The FCA XXIII core is composed of Pu and enriched U due to the lack of enriched U. As for the analysis of FCA XXIII criticality, the plate type fuel is modeled exactly at 20°C so temperature corrections are not necessary. The FCA XXIII data set is considered the main benchmark data for validation of the reflector-controlled core. The calculated multiplication factor (k_{eff} value) was compared with the measured one in the form of calculation-to-experiment ratio (C/E value) in table 3-2. The reference model provided C/E values of 0.9965 for the FCA XXIII-1 core and of 0.9976 for the FCA XXIII-1DU core. Biases are consistent between the two. Calculated values using MVP resulted in underestimating the experimental values by 0.2 to 0.3%.

For the deterministic calculation method, the effects of discrete–ordinate number (Sn-order) on criticality were surveyed in the course of the FCA XXIII analysis. Table 3-3 shows criticality values from the discrete-ordinate calculation results. A survey of Sn-order number from 2 to 16 with mesh size of 2.5cm shows that S8 is accurate enough in comparison to 16 of Sn. The combination of S8 and mesh size 2.5cm are selected as the reference for the design method of the discrete-ordinate transport calculation.

Criticality of the JOYO MK-1 initial core is also analyzed. This core was a small core composed of mixed uranium and Pu. The pin type fuel is modeled as the exact geometry at 200°C. Table 3-4 shows that the criticality calculated by MVP is in good agreement. This analysis supports the conclusion that the 4S design method is adequate for past actual fast cores.

In order to identify the effect of fuel composition on accuracy, low enrichment U benchmark cores and mixed Pu composition cores were analyzed. The criticality of ZPR-U9, ZPPR-3/41 and ZPR6-6A are evaluated in Table 3-1. In this evaluation, comparisons of the C/E values are made in terms of understanding the relationships between the 70 energy group cross section set and continuous-energy cross section library. As an advanced cross section set, 900 group cross section set was used with the deterministic transport code for criticality calculations.

Table 3-5 shows the results of this analysis. Though the C/E of MVP is 1.005 for high enrichment fuel, the C/E is 0.9936 for low enrichment fuel. The tendency of C/E is therefore different when uranium enrichment changes. For 4S cores, which use low enrichment (less than 20%), the results of the low enrichment cases in table 3-5 are used for the uncertainty evaluation. The C/E is 0.9936 and uncertainty is 0.3%. This is consistent with the result of MVP, S8 900 energy groups. Table 3-6 shows the result of estimating ZPPR-21 experience. C/E value of S8 900 energy groups is consistent with MVP. The plutonium content of 4S is approx. 2% and the results with low Pu content in table 3-6 shows the Pu contents effect on C/E values for the criticality estimation is small. This result shows the 4S design method is adequate for evaluating from BOL to EOL.

The validation result is C/E=0.997 and uncertainty = ±0.003 in C/E (Estimated with 2 sigma - level)

(2) Reflector reactivity worth

The continuous-energy Monte Carlo code MVP is selected as the design method for reflector reactivity worth for full stroke movement. The deterministic discrete ordinate code TWODANT is adopted for evaluating the stroke-worth curve of the reflector. Reflector worth measurements of FCA XXIII are used for validation.

Table 3-7 and Table 3-8 summarize the validation results for the reactivity changes due to replacing reflector drawers with cavity (void) drawers in the FCA XXIII experiments performed in the small and larger test regions for the reflector reactivity worth measurements. The measurements covered various patterns for neutron leakage situations with changing sizes and shapes of the substitution of reflector drawers and void drawers in the test regions.

Table 3-7 shows the C/E values and estimated errors associated with measurements and MVP Monte Carlo calculations. Detailed geometry models were used in the MVP calculations. Through the comparisons for various patterns for the measurements, it is revealed that the combination of MVP and detailed models provides good accuracy with stable results.

S8-transport calculations employing simple homogeneous cell models are used for the reflector drawers and void drawers. Table 3-8 compares C/E-values obtained by the S8 XYZ 70 group calculations. The Average C/E value of 1.06 ±0.045 is generally good. More precisely, the analysis indicates that C/E values show dependence on the number of drawer replacements of reflector drawers and void drawers with a magnitude of up to about 8%.

Table 3-9 summarizes the reactivity changes due to replacement of sodium drawers with cavity (void) drawers and C/E values obtain by MVP calculations with the detailed geometry model. It is confirmed that a combination of MVP and detailed models provides good accuracy with stable results, as well.

From this data, it is confirmed that selection of the design method is adequate with the combination of using MVP for absolute reactivity changes and S8 calculations for the relative stroke curve. It is judged that the MVP calculation with a detailed geometry model predicts within 5% for reflector worth and sodium flood worth in the cavity region for the selected design configurations.

(3) Power distribution

Fuel power distribution is estimated by analyzing the neutron fission reaction. Integral subassembly power is evaluated by continuous-energy Monte Carlo calculations. Detailed power distribution such as the axial and radial distribution in a subassembly is evaluated by deterministic transport calculations to avoid requirements for large calculation resources.

Comparisons of the measured and calculated (by S8 transport calculation) U-235 fission reaction rate distributions for the A1 core and A6 core of FCA XXIII are shown in Fig 3-3. The A1 core was fully covered by reflector drawers, whereas the A6 core was only covered by cavity for half the height of the core region. The U235 fission rate difference between A1 and A6 is shown in Figure 3-3 (marked with a red triangle). Both C/E values of A1 and A6 are approximately 1.00 in the core region. Comparisons shows that power distribution and power distortion by different reflector positions are well predicted by the S8 transport code. The C/E value is 1.01 and uncertainty is ±0.01.

The U-234 fission rate of the JOYO experiment is estimated using the Monte Carlo code MVP which is used for fuel subassembly power. In this comparison, statistical accuracy of the foil detector is confirmed to have enough reliability in the core region. Table 3-17 and Fig. 3-4 show the comparison of calculations and measured values for U-235 (n, f) as an example. From this result, the C/E value of MVP is 1.007 and uncertainty is ±0.03 and the C/E value of S8 transport is 1.01 and uncertainty is ±0.01. Therefore, it is adequate that the fuel subassembly integral power is estimated by MVP and the power distribution in the subassembly is estimated by the S8 transport code..

(4) Absorber reactivity worth

Absorber reactivity worth is measured by using absorber tests arranged in the center region of the FCAXXIII core. The test results of FCA XXIII are estimated using continuous-energy Monte Carlo code MVP for total absorber reactivity and S8 discrete-ordinate transport code TWODANT for stroke worth curve. Table 3-11 shows the results for Hf and Table 3-12 shows the results for B_4C. From these results, the S8 transport calculation is confirmed to show good agreement with the measured values for small reactivity changes. It is shown to be adequate that total reactivity worth is estimated by MVP and small reactivity changes such as the stroke-worth curve are

estimated by the S8 discrete ordinate code TWODANT. As for MVP, the C/E value for B_4C is 0.94 and uncertainty is ±0.03, the C/E value for Hf is 0.88 and uncertainty is ±0.03. For TWODANT, the C/E value for B_4C is1.02 and uncertainty is ±0.03, the C/E value for Hf is 0.94 and uncertainty is ±0.03.

(5) Sodium void reactivity worth

The sodium void worth measured by the FCA XXIII core is estimated by the S8 discrete ordinate transport code TWODANT with JEF-3-J3.3. Table 3-13 shows the comparison between the measured and calculation results.

As for the general trends, the best agreement is found with slight biases between measured and values by the P0-S8 transport calculations with the 70 energy group JFS-3-J3.3 library in absolute value near zero sodium reactivity changes

The results confirmed that P0-S8 transport calculations provided stable agreement in the upper and lower halves of the core, where asymmetric replacement of reflector and void regions in the 1/6-sector portion were used for reflector reactivity worth measurements. As anticipated, diffusion calculations provided more negative-worth distribution due to overestimation of the leakage effects.

The P0-S8 transport calculations provide good agreement with unity for wide ranges of the near-zero sodium reactivity changes. C/E is1.01 and uncertainty is ±0.01. For the estimation of uncertainty of void reactivity a multi component bias factor is applied. The sodium void worth components which compose reactivity change, "neutron leakage term" and "neutron nonleakage term"' are evaluated using a deterministic perturbation code with a homogeneous model. This approach of a multi component bias factor is described in chapter 4.

(6) Doppler reactivity

The Doppler reactivity measurements in metallic fuelled FCA XVI cores are analyzed by the S8 discrete ordinate transport code TWODANT with 70-group library JEF-3-J3.3 and compared between measured and calculation results. Table 3-14 shows these results. For metallic fuel, the averaged C/E value is 0.85±0.03 for application of the 70 energy group library. Base on the homogeneous composition models for the benchmarked FCA XVI cores, the calculated Doppler reactivity changes of the FCA samples of NU-metal and NUO2 were corrected by the heterogeneous plate cell" effects around 1.05 and "XYZ/RZ" effects about 1.001. Cause of the large deviation of the averaged C/E value from unity for the metal fueled mockup cores is inferred as some insufficiency in the preparation of the self-shielding factors provided in the standard 70 groups library JFS-3-J3.3. To take account of the resonance shielding effect in the Doppler region, additional calculations using 900 groups library were done as shown in the Appendix. The new results showed that the averaged C/E value was improved as 0.95±0.03. From those data, it is judged that the C/E value is 0.85 with uncertainty ±0.10 for the 4S design method.

(7) Effective Delayed Neutron Fraction

Delayed neutron fraction analyses were made to estimate the uncertainty of the delayed neutron fractions (beta-effective) in the 4S core, applying the 4S nuclear design methods using the JENDL-3.3 file. The analyses selected the international benchmark experiments for effective delayed neutron fraction from the FCA XIX core series. Three cores, FCA XIX-1, -2 and -3, cover a wide variety of contributions from U-235, U-238 and Pu-239 fission within the fast spectrum ranges. The outline of the core is provided is table 3-15. Delayed neutron fraction analyses were made to estimate the uncertainty of the delayed neutron fractions (beta-effective) in the 4S core, applying the 4S nuclear design methods using the JENDL-3.3 file. Table 3-16 show these results. The C/E value by TWODANT with JFS-3.J3.3 is 0.994-0.975. Table 3-17shows the reaction rate ration of FCA XXIII. The C/E value is from 0.96 to 1.04. So for a uranium core, the C/E value is 0.994 and uncertainty is ±0.02.

Considering above FCA XXIII results, the C/E value for effective delayed neutron fraction is 1.00 and uncertainty is ±0.03.

(8) Burnup reactivity losses

Burnup reactivity losses of the 4S core are calculated by continuous-energy Monte Carlo code MVPBURN2 using the detailed geometry models, taking into account the slow movement of the reflector along the core. Table 3-18 shows the calculated value of the burnup reactivity loss for 30 years. Reactivity changes due to number density variations from the initial fuel compositions to the burnt compositions were analyzed by the two-dimensional RZ model using 70 energy group S8-transport calculations. Three major contributors, decreases of U-235, yield of Pu-239 and accumulation of fission products, are confirmed by the normalized fractions of the burnup reactivity loss shown in Table 3-18.

The prediction accuracies for the burnup reactivity loss are significantly governed by the accuracies of absorption rates of U-235 and capture rates of U-238 for generation of Pu-239 and absorption rates of FPs.

C/E-values for reaction rate ratios are tabulated in Tables 3-19 and 3-20. Although accuracies of absorption rates of U-235 are not definitely defined from the analysis results of the related critical experiments, prediction accuracies for criticality are well achieved by using recent evaluated cross section data. Fission reaction rate ratios for Pu-239 fission-to- U-235 fission are also well predicted within a few percent deviations of unity of C/E-values. More importantly, the facts of good prediction accuracies for ratios capture rates of U-238 between fission rates of U-235 support that prediction accuracies of Pu-239 generation are well anticipated within a magnitude of a few percent in the 4S design methods.

Limited information on accuracies of absorption rates for FP elements through integral experiments is available for fast reactor cores. However, when we assume large uncertainties around 20% for FP contribution in addition to uncertainties of several percent in decrease of U-235 and yield of Pu-239, estimated total uncertainties are of a magnitude of 5 to 10 percent.

As a result current prediction accuracies for burnup reactivity loss are judged to be within 10 percent with the 4S design method.

The prediction accuracy of burnup reactivity losses will be validated through analyses of measured burnup loss for JOYO and other cases.

Table 3-1. Outline of the Selected Fast-Spectrum Cores

Assembly	Pu(1)	U5(2)	R(cm)(3)	H(cm)	Core
4S(BOL)	-	17.6	47	250	Zr 29a%
FCA XXIII	15	11	32	112	Zr 23a%
ZPR-9/34	-	93	62.2	183.2	EU/Fe
ZPR-3/23	-	93	30.8	50.9	HEU
ZPR-6/6A	-	16.5	91.2	91.2	EU/oxide
ZPR-3/41	-	17.0	41.6	81.5	EU/Al
ZPR-U9	-	9.0	41.0	76.4	EU
ZPPR-21F	-	62	19.0	41.4	EU
ZPRR-21E	7.8	51.3	19.0	41.4	Pu/EU
ZPPR-21D	18.1	37.7	19.0	41.4	Pu/EU
ZPPR-21C	27.8	28.5	19.0	41.4	Pu/EU
ZPPR-21B	41.6	10.7	19.0	41.4	Pu/EU
ZPPR-21A	52.3	0.1	19.0	41.4	Pu
JOYO	17.7	23	36	60	Pu/EU

Notes:
(1) Pu=Pu fraction in total heavy metal (Pu+U)
(2) U5=U-235 fraction in total heavy metal
(3) Equivalent radius of core

Table 3-2. C/E Values for Effective Multiplication Factors

FCA Cores	Measured Values		C/E Values	
	Value	Uncertainty	MVP (Continuous-Energy Monte Carlo)*	P0-S8 Transport (70g)*
XXIII-1	1.00209	±0.00023	0.9965±0.0002	0.9926

Note:
(*) Calculated by using the JENDL-3.3-based-libraly

Table 3-3. Examples of Sn-order Effects on the Effective Multiplication Factor

Sn Order	Effective Multiplication Factor	Discrepancy from S16 Calculation	Comments
	k-eff	%δρ	
2	0.995114	-0.1321	FCA XXIII core 70 energy groups, mesh sizes for X,Y,Z directions=about 2.5 cm
4	0.996906	+0.0471	
6	0.996561	+0.0126	
8	0.996488	+0.0053	
12	0.996446	+0.0011	
16	0.996434	-	

Table 3-4. C/E Values for Criticality of JOYO MK-1 Core

	Effective Multiplication Factors and Errors					
	Calculated[1] (C)		Measured[2),3)] (E)		(C/E)	
Minimum Critical Core (64 core subassemblies)	0.99739	±0.00019	1.0011	±0.0018	0.9963	±0.0018
Initial Core (70 core subassemblies)	0.99473	±0.00019	0.9981	±0.0018	0.9966	±0.0018

Notes:
1) MVP continuous-energy Monte Carlo calculations with the library generated from JENDL-3.3. Total history: 100-million, Statistical error: 1σ
2) Control Rod Positions: adjusted critical positions near criticality
3) Adopted from NEA/NSC/DOC(2006)1, Table 3.15and Table 3.17. ~~Statistical error: 3σ~~

Table 3-5. Criticality C/E Values for the Enriched Uranium Cores from JENDL-3.3 Library

	Assembly	MVP2		S8	S8
		C/E	Errors	900 energy groups	70 energy groups
High Enrichment Uranium	ZPR-9/34	1.0154	0.28	1.0205	1.0400
	ZPR-3/23	0.9957	0.28	0.9973	1.0025
	ZPPR-21F	1.0047	0.25	1.0061	1.0058
	Ave/SD[3)]	1.005/0.0099	-	1.008/0.0095	1.016/0.021
Low Enrichment Uranium	ZPR-6/6A	0.9904	0.23	0.9912	0.9914
	ZPR-3/41	0.9955	0.27	0.9969	0.9977
	ZPR-6/9 U9	0.9948	0.24	0.9962	0.9947
	Ave/SD[3)]	0.9936/0.0028	-	0.9948/0.0025	0.9946/0.0031

Notes:
1) K-benchmark errors = approximately 0.25%$\delta\rho$
2) Errors by Monte Carlo calculations in %$\delta\rho$
3) Ave/SD= Averge/Standard deviation

Table 3-6. C/E Values with 900 Energy Group S8 Calculations for ZPPR-21 Benchmark Cores

Assembly	Pu/HM(%)	U5/HM(%)	S8 RZ Models with JENDL-3.3	
			70 Group	900 Group
ZPPR-21F	0.0	62.2	1.0058	1.0061
ZPPR-21E	7.8	51.3	1.0042	1.0040
ZPPR-21D	18.1	37.7	0.9992	1.0019
ZPPR-21C	27.8	28.5	0.9986	0.9945
ZPPR-21B	41.6	10.7	1.0039	1.0037
ZPPR-21A	52.3	0.1	1.0001	1.0004

Note:
1) 900 energy group S8 transport calculations in RZ benchmarked models

Table 3-7. C/E-values for Reactivity Changes for Drawer Replacements from Reflector Cell to Cavity Cell in the Reflector Worth Measurements in the FCA XXIII Cores

Case	Measurement Conditions			Measured (E)		MVP	
	ID of Measurement (1)	Cell type in "Z1"(2)	Zone ID for Void cells (3)	Value (%DK/kk')	Error (%)	C/E	Error (%)(4)
S1	Base>>21	REF	Z2	-0.282	±0.5	1.01	±3.0
S2	Base>>22	REF	Z2+Z3	-0.512	±0.6	1.03	±1.7
S3	21>>22	REF	Z3	-0.231	±0.8	1.06	±4.9
S4	41>>43	NA	Z2,Z3	-0.613	±1.7	1.02	±2.6
S5	Base>>43	NA	Z2,Z3	-0.710	±0.8	1.03	±1.4
					C/E Av STD	1.03 ±0.02	

Case	Measurement Conditions			Measured (E)		MVP	
	ID of Measurement (1)	Cell type in "Z1"(2)	Zone ID for Void cells (3)	Value (%DK/kk')	Error (%)	C/E	Error (%)(4)
L1(5)	A1>>A6	Whole 1/6 sector zone (REF to Void)		-0.744	±1.4	1.02	±1.8
L2(5)	A6>>A5			-0.727	±2.0	1.00	±2.3
L3(5)	A3a>>A3b			-0.556	±1.5	1.06	±2.1
L4(5)	A1>>A2			-0.813	±1.7	1.01	±2.0
					C/E Av STD	1.02 ±0.02	2.4 ±1.0

(1) Identifier of reactivity changes in FCA XXIII measurements for replace from 'REF' cell to 'Void' cell.
(2) Drawer cell-type in the zone1 (nearest 4 drawers in the small test zone experiments).
(3) Zone ID for Void cells in the small test zone experiments.
(4) Inclusive of measured error and statistical error due to MVP Monte Carlo calculations (100 million histories)
(5) Large Zone Experiments

Table 3-8. C/E-Values for Reactivity Changes for Drawer Replacements from Reflector Cell to Cavity Cell in the Reflector Worth Measurements in the FCA XXIII Cores

Case	Measurement Conditions			Measured (E)		S8 (70-gr)	
	ID of Measurement (1)	Cell type in "Z1"(2)	Zone ID for Void cells (3)	Value (%DK/kk')	Error (%)	C/E	Comment
S1	Base>>21	REF	Z2	-0.282	±0.5	1.07	C/E av 1.08 STD ±0.03
S2	Base>>22	REF	Z2+Z3	-0.512	±0.6	1.09	
S3	21>>22	REF	Z3	-0.231	±0.8	1.12	
S4	41>>43	NA	Z2,Z3	-0.613	±1.7	1.07	
S5	Base>>43	NA	Z2,Z3	-0.710	±0.8	1.05	
L1(5)	A1>>A6	Whole 1/6 sector zone (REF to Void)		-0.744	±1.4	1.06	C/E av 1.03 STD ±0.04
L2(5)	A6>>A5			-0.727	±2.0	1.02	
L3(5)	A3a>>A3b			-0.556	±1.5	0.98	
L4(5)	A1>>A2			-0.813	±1.7	1.05	
					C/E Av	1.06 ±0.045	Error (4)

(1) Identifier of reactivity changes in FCA XXIII measurements for replace from 'REF' cell to 'Void' cell.
(2) Drawer cell-type in the zone1 (nearest 4 drawers in the small test zone experiments).
(3) Zone ID for Void cells in the small test zone experiments.
(4) Inclusive of measured error and standard deviation of the C/E values obtained by S8 calculations
(5) Large Zone Experiments

Table 3-9. C/E-Values for Reactivity Changes for Drawer Replacements from Sodium Cell to Cavity Cell in the Reflector Worth Measurements in the FCA XXIII Cores

Case	Measurement Conditions			Measured (E)		MVP	
	ID of Measurement (1)	Cell type in "Z1" (2)	Zone ID for Void cells (3)	Value (%DK/kk')	Error (%)	C/E	Error (%)
S_cav1	Base>>21	REF	Z2	-0.167	±1.0	1.03	±7.0
S_cav2	12>>22	REF	Z2,Z3	-0.317	±1.4	0.99	±4.0
S_cav3	42>>43	NA	Z2,Z3	-0.376	±1.2	0.98	±3.5
					C/E Av STD	1.00 ±0.03	4.8 ±1.9

(1) Identifier of reactivity changes in FCA XXIII measurements for replace from 'NA' cell to 'Void' cell.
(2) Drawer cell-type in the zone1 (nearest 4 drawers in the small test zone experiments).
(3) Zone ID for Void cells in the small test zone experiments.
(4) Inclusive of measured error and statistical error due to MVP Monte Carlo calculations (100 million histories)

Table 3-10. C/E Values for Relative Reaction Rate Distributions for U-235(n,f) Reaction Rate

Foil Position		Core					Radial Blanket				Reflector	Comments
		0X	1F1	2F1	3F1	4F1	5F1	6F1	7F1	8F1	9F1	
Axial Blanket	+500	1.049 ±6.4		1.169 ±6.7	1.035 ±7.0							
	+400	1.015 ±5.6		0.979 ±5.6	1.056 ±6.0							
	+300	0.994 ±3.5		1.068 ±3.6	0.985 ±3.6							
Core	+200	1.017 ±3.4	1.011 ±3.5	1.004 ±3.4	1.001 ±3.4	1.019 ±3.5	0.967 ±5.5	1.118 ±6.5	1.093 ±7.3	1.065 ±11.1	1.051 ±10.2	Foil thickness in model: 0.5mm Upper Number: C/E-value for Lower Number: Errors(%) Average C/E-value and 1) Core Region: 1.007±3.4 2) Axial Blanket Region: 1.051±6.2 3) Radial Blanket Region 1.054±6.8 4) Reflector Region: 0.985±9.8
	+100	0.981 ±3.3	0.993 ±3.3	1.004 ±3.3	1.020 ±3.4	1.019 ±3.4	0.974 ±5.5	1.079 ±5.8	1.041 ±6.9	1.065 ±7.7	0.896 ±9.0	
	0	1.000 ±3.3	1.012 ±3.3	1.010 ±3.3	1.006 ±3.3	0.991 ±3.4	1.029 ±5.5	1.106 ±5.7	1.004 ±6.5	1.110 ±7.5	1.007 ±10.3	
	-100			1.005 ±3.3	0.993 ±3.4							
	-200											
	-300											
Axial Blanket	-400											
	-500											

Note:
Calculation: MVP with detail geometry model for pins and SS-holders, foils, JENDL-3.3 lib.

Table 3-11. C/E Values of Hf Worth at Central 3x3 Zone in FCA XXIII-1DU Core

Hf Fractions	Drawers	Measured Value (E)		MC[2]		S8[3]
		Value [%δρ]	Error [%]	C/E	Error [%]	C/E
38%	1 pack[1]	-3.80E-02	±2.8	0.80	±28	0.96
	9 packs	-3.07E-01	±0.3	0.88	±3	0.94
	15 packs	-4.84E-01	±1.0	0.87	±2	0.93
	11 packs	-2.45E-01	±1.1	0.85	±4	0.93
50%	1 pack[1]	-4.78E-01	±2.2	0.75	±23	0.97
	5 packs	-2.23E-01	±0.5	0.92	±4	0.96

Notes:
1) Central 1 pack drawer, 1pack=5.52x5.52x5.52cm^3
2) DF=diffusion calculations with XYZ geometry, 70 energy groups
3) S8=P0-S8 transport calculations with XYZ geometry, 70 energy groups

Table 3-12. C/E Values of B_4C Worth at Central 3x3 Zone in FCA XXIII-1DU Core

Core	Pos.[1]	B10/B	Measure Value (E)		MC		S8[2]
			Value [%δρ]	Error [%]	C/E	Error [%]	C/E
XXIII-1	1 pack	20%	-7.30E-02	1.6	-	-	0.99
	1 pack	60%	-1.70E-01	0.7	-	-	1.03
	1 pack	90%	-2.27E-01	0.5	-	-	1.05
XXIII-1DU	1 pack	20%	-7.73E-02	1.4	0.87	±13	1.00
	1 pack	90%	-2.27E-01	0.5	0.94	±4	1.05

Notes:
1) Pos.: Central drawer poison at core midplane
2) S8=P0-S8 transport calculations with XYZ geometry, 70 energy groups

Table 3-13. C/E-Values for Axially Integrated Sodium Void Reactivity Worth in the Core Variants of FCA XXIII

Core	Void Cell Zone		Measured Value (E)		Calculation Methods[5]		
					S8	MVP	
			Value [%δρ]	Error [%]	C/E	C/E	Error [%]
A1	T-Pu	1)	-5.86E-03	±13.9	1.27	0.39	363
	T-U	1)	-9.11E-02	±1.4	0.96	0.90	10.4
	Na	3)	-8.62E-02	±1.6	0.95	0.88	11.3
A6	T-Pu	1)	-1.18E-02	±6.9	1.17	1.88	38.8
		2)	-9.35E-02	±8.7	1.03	0.33	271
	T-U	1)	-1.07E-01	±0.8	0.95	0.95	8.4
		2)	-9.54E-02	±0.9	0.96	0.97	9.2
	Na	3)	-1.08E-01	±0.8	0.90	0.86	9.2
		4)	-9.00E-02	±1.0	0.90	0.82	11.4
A5	T-Pu	1)	-1.59E-02	±5.1	1.06	0.95	55.8
	T-U	1)	-1.11E-01	±0.7	0.95	0.87	9.5
	Na	3)	-1.02E-01	±0.9	0.94	0.89	9.4
A3a	T-Pu	1)	-1.63E-02	±5.0	1.11	1.33	39.2
	T-U	1)	-1.06E-01	±1.2	1.01	0.97	8.4
	Na	3)	-1.02E-01	±1.3	0.96	0.91	9.3
A3b	T-Pu	1)	-2.24E-02	±4.1	0.96	0.69	55.2
	T-U	1)	-1.11E-01	±1.1	1.00	0.94	8.3

Notes:
1) 1Z~11Z: summed over half core height (fixed side)
2) -1Z~-11Z: summed over half core height (movable side)
3) 1Z~13Z: half core height + two upper Na packs
4) -1Z~-13Z: half core height + two lower Na packs
5) Calculation methods: S8=P0-S8 transport with 70 energy group calculations, and MVP=continuous-energy Monte Carlo calculations

Table 3-14. Examples of C/E Values for Doppler Reactivity by the Simplified Homogeneous Models

FCA Core ID	Doppler Sample	Measured Worth (20°C – 800°C)	70 energy group S8 calculations(*)
		Unit: 1.0E-06 [%δρ]	JENDL-3.3
XVI-1	NU	-9.64±0.19	0.85
	NUO2	-4.35±0.18	0.86
XVI-2	NU	-7.47±0.21	0.89
	NUO2	-3.86±0.26	0.82

(*) with inclusion of correction factors for "heterogeneous plate cell" effect and "XYZ/RZ" effect. Those correction factors were provided in the reference "A proposal of Benchmark Calculation on Reactor Physics for Metallic Fueled and MOX Fueled LMFBR Base upon Mock-up Experiment at FCA; H. Oigawa et. al., JNST, Vol.37, No.2, p.186-201 (February 2000)"

Table 3-15. Outline of the Cores and Measured Characteristics

Assembly	FCA		
Items	XIX-1	XIX-2	XIX-3
R (cm)	33.0	35.7	35.1
H (cm)	50.8	61.0	61.0
Pu/(Pu+U)	-	23.5	100
U235/U %	93	0.7	-
Moderator	C	SS	SS
Keff Value	1.0075	1.0032	1.0031
Error %	0.06	0.03	0.03
F28/F25	0.0395	0.0408	0.035
Error %	1.3	1.4	2.0
F49/F25	-	1.056	1.083
Error %	-	1.3	1.2
Beta (pcm)	742	364	251
Error (pcm)	24	9	4

Notes:
Size: R=equivalent radius
Pu/(Pu+U): average Pu enrichment in %
Moderator: C=carbon, SS=stainless steel, O=oxygen
Reaction rate ratios: F28=U-238(n,f),F25=U-235(n,f), F49=Pu-239(n,f)

Table 3-16. C/E Values for the Benchmark Data

Assembly	FCA		
Items	XIX-1	XIX-2	XIX-3
F28/F25	1.012	0.978	0.968
F49/F25	-	1.013	0.992
$\beta_{eff.}$	0.994	0.991	0.975

Note:
70 energy group S8-FOP (First Order Perturbation), JENDL-3.3 based library JFS-3-J3.3

Table 3-17. C/E Values for Spectral Indices (70 energy group, P0-S8)

Reaction Rate Ratios	XXIII-1D (Inner Core)			XXIII-1D (Outer Core)		
	Value[1)]	Error[1)][%]	C/E(S8)	Value[1)]	Error[1)][%]	C/E(S8)
F28/F25[2)]	0.0381	1.0	1.04	0.0296	1.0	1.15
F49/F25[2)]	1.10	1.0	0.99	1.06	1.0	0.99

Notes:
1) Measured position: Reference core midplane
2) Reaction rates: F28=U-238(n,f), F49=Pu-239(n,f), F25=U-235(n,f)

Table 3-18. Burnup Reactivity Loss and Component-Wise Fractions in 4S

Items	Values	Comment
Burnup Reactivity Loss	5.06%δρ	30-year burn MVPBURN2 calculation.(2-year burn with 15 steps)
Contributors	Normalized Fraction (%)	Relative contributions due to composition shifts from BOL to EOL
Decrease of U-235	-220.8	1) Calculations by S8, 70 energy group, RZ—model . 2) Variations of number densities are taken from the MVPBURN2 calculation at the EOL stage as nodal distributions. 3)FP (fission products) is treated as a lumped cross section
Decrease of U-234	-2.9	
Decrease of U-238	+7.8	
Yield of Pu-239	+141.0	
Yield of Pu-240 (Other Pu isotopes but for Pu-239)	+0.6	
MA production	-0.2	
FP accumulation	-25.8	
Total	-100	Normalized to -100%

Table 3-19. C/E Values for Spectral Indices (70 Energy Group, P0-S8)

Reaction Rate Ratios[3)]	XXIII-1D (Inner Core)	XXIII-1D (Outer Core)
	C/E(S8)	C/E(S8)
F28/F25	1.04	1.15 (4)
F37/F25	1.04	1.10(4)
F49/F25	0.99	0.99
C28/F25	1.01	1.00

Notes:
1) Measured position: Reference core mid-plane
2) Errors for the measured values; around 1.0% for fission rate ratios, , and 1.6% for capture-to-fission ratio
3) Reaction rates: F28=U-238(n,f), F37=Np-237(n,f), F49=Pu-239(n,f), C28=U-238(n,g), F25=U-235(n,f)
4) Deviation of U-238 fission counter positioning or cell factor may affect due to steep flux gradients for higher energy neutrons.

Table 3-20. C/E Values for the Benchmark Data

Assembly	FCA			MASURCA	
	XIX-1	XIX-2	XIX-3	R2	ZONA2
F28/F25	1.012	0.978	0.968	0.901	1.039
F49/F25	-	1.013	0.992	-	1.004

Note:
1)70 energy group S8-FOP, JENDL-3.3 based library JFS-3-J3.3, Core center position
2) FCA XIX-1 and MASURCA R2; EU core
3) FCA XIX-2 and MASURCA ZONA2; EU/Pu core
4)FCA XIX-3; Pu core

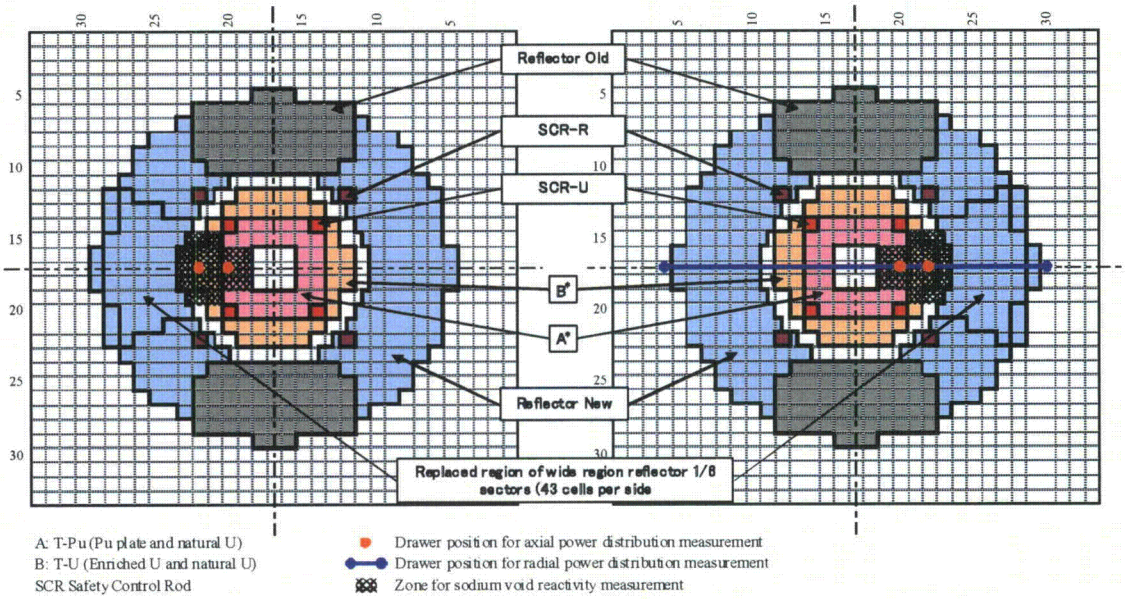

A: T-Pu (Pu plate and natural U)
B: T-U (Enriched U and natural U)
SCR Safety Control Rod

Drawer position for axial power distribution measurement
Drawer position for radial power distribution measurement
Zone for sodium void reactivity measurement

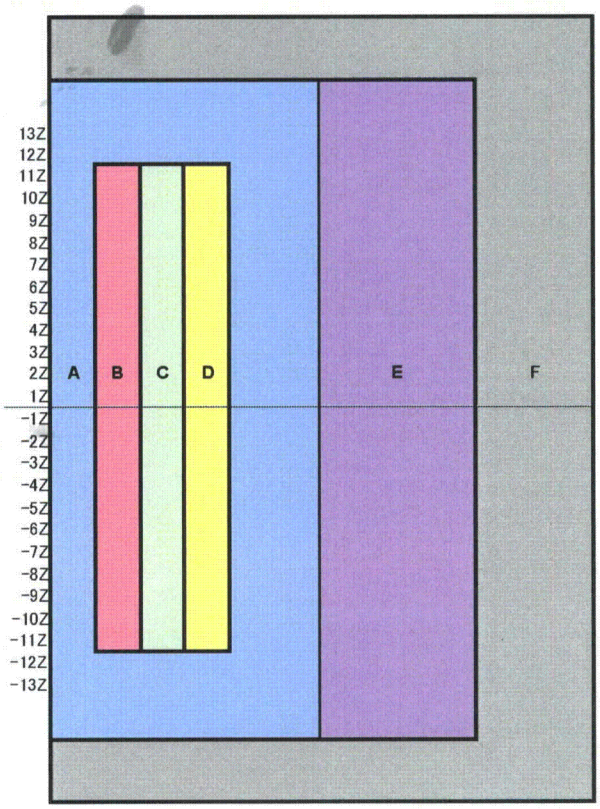

A: Na Drawer
B: T-Pu (Pu plate and natural U)
C: T-U (Enriched U and natural U)
D: Safety control rod - U
E: Reflector
F: MTX (FCA Matrix Drawer, Cavity Drawer)

Fig. 3-1. Geometry and Models for FCA XXIII-1 Core

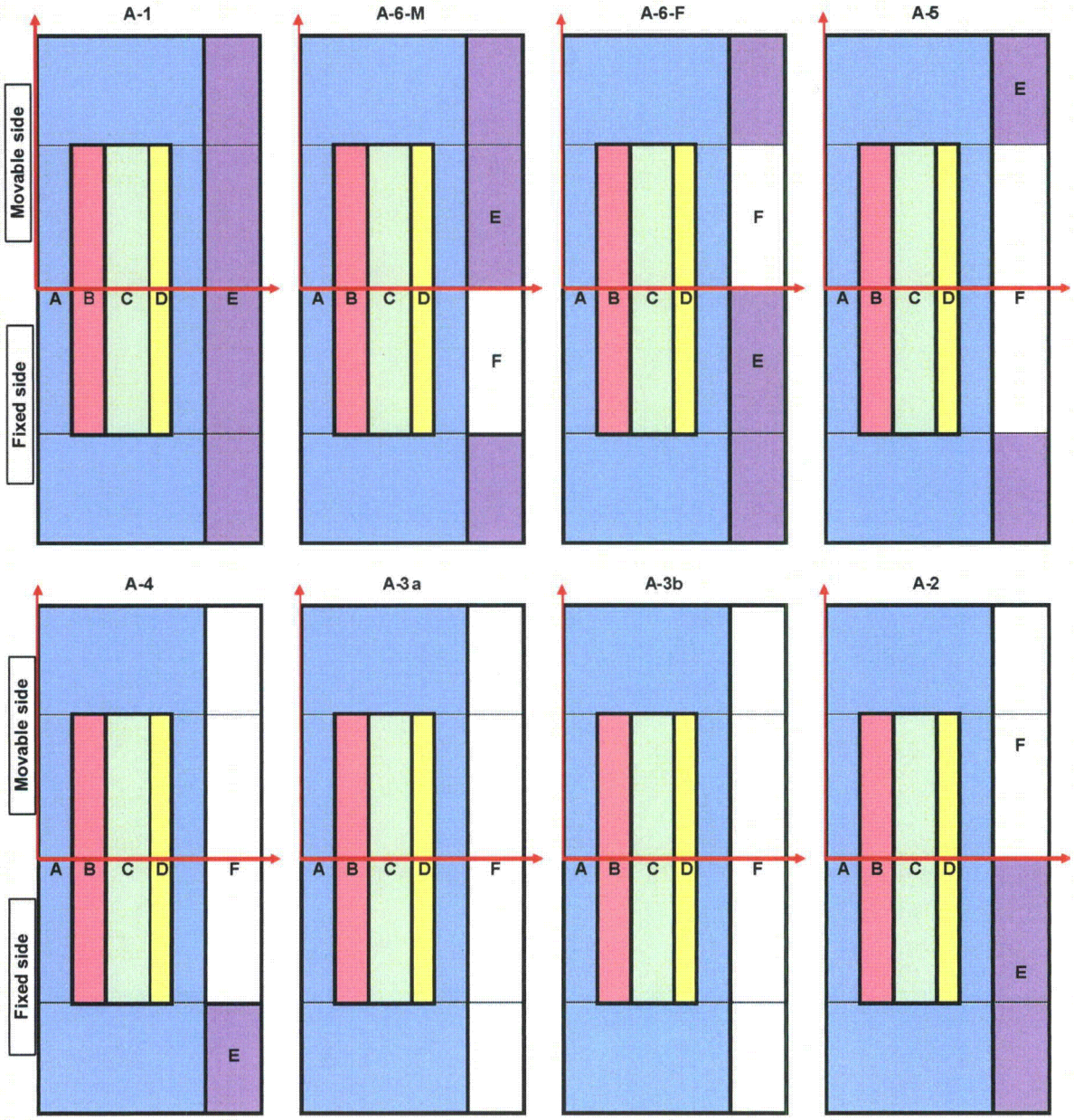

A: Na Drawer
B: T-Pu (Pu plate and natural U)
C: T-U (Enriched U and natural U)
D: SCR: Safety Control Rod
E: Reflector
F: Void

*These figures are R-Z geometry of 45°direction in X-Y cross section. SCR in T-Pu region is not drawn in these

Fig. 3-2. Core Geometries and Models for the Reflector Worth and Sodium Void Measurement and Analyses

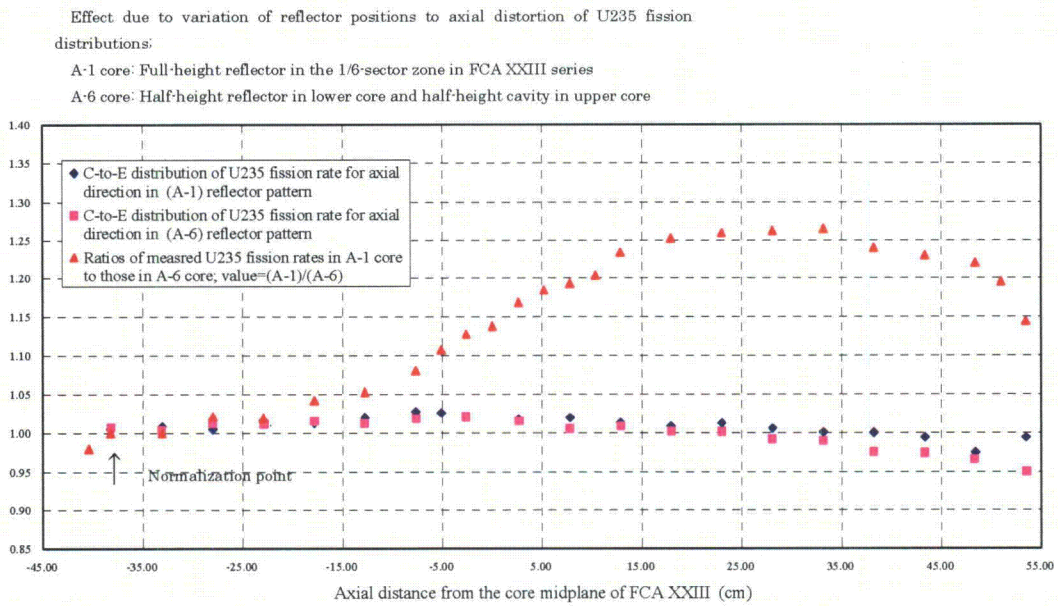

Fig.3-3. Effect due to Variation of Reflector Position to Axial Distribution of U-235 Fission of FCAXXIII Test

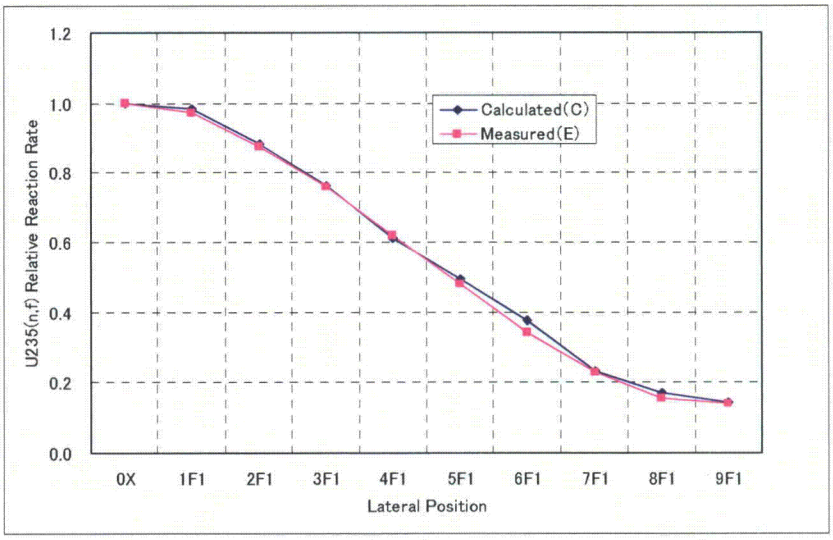

Fig.3-4. Comparison of Radial Relative Profiles for Measured and Caluclated U-235 (n,f) Reaction Rate ar Core Midplane of JOYO Experiment

4 APPLICABILITY OF THE CRITICAL ANALYSIS RESULTS TO THE 4S CORE NUCLEAR DESIGN

Although the FCA XXIII core was specifically built as a mockup of a small-sized reflector-controlled fast cores, the core size and fuel composition are not the same as those of the 4S target core. In terms of core characteristics between the FCA XXIII core and the 4S core, the similarity was evaluated by comparing reactivity components.

In sections 4.1 and 4.2, the application of sensitivity and uncertainty analysis using C/E results from FCA XXIII data to confirm the consistency of the 4S design method is discussed. This also results in an improvement of prediction accuracies by reflecting the mockup analysis results for the uncertainties of core characteristic due to the cross section errors. Those results confirmed that application of the FCA XXIII data to the 4S design methodology is appropriate.

In Chapter 4.3, the reactivity changes associated with sodium density changes such as core void coefficient (because core void coefficient of 4S is near zero) are described. Past analysis of the maximum sodium void worth had rarely considered the range near zero, because prediction accuracies for evaluation of plus or minus values around the zero-worth domain had not been needed for conventional fast reactors. It was shown that sodium void reactivity is accurately reproduced by the 4S design method in the FCA XXIII analyses. For improving accuracy of the design value of sodium void reactivity near the zero reactivity change domain, multi-component bias methods considering the physics of void reactivity are applied to determine bias factor and uncertainty for each component. The method determined the biases of the components with 95% confidence level for nonleakage and leakage components derived by perturbation calculations. This statistical method can be applicable by utilizing on the order of hundreds of measured data points obtained in the FCA XXIII experiments for demonstration of void worth distributions in the reflector-controlled fast core.

4.1 Sensitivity and Uncertainty (S&U) Analysis Using Critical Analysis Results

In this section the application of S&U analysis to some of the characteristics of the target core is outlined, taking into account the results from the analyses of the physics benchmark experiments in the FCA XXIII cores. The main emphasis is on the estimation of the uncertainties of core characteristics due to cross-section uncertainties as the first step of the S&U analyses for the 4S nuclear design.

It is important to make quantitative estimation for potential sources, especially for uncertainties due to cross-section uncertainties of the major nuclides and reactions, for demonstration of the approaches associated with the Bayesian approach using the measured data from the physics mockups.

First, S&U analyses were done to assess the consistencies of the C/E values obtained from the analyses of the FCA XXIII experiments. The S&U analysis requires uncertainty data for cross-section E values and C values, in addition to C/E values and cross-section sensitivity coefficients.

Cross-section sensitivity coefficients were calculated by S8-transport calculations using generalized perturbation theory (GPT, equivalent GPT: SAGEP-SNT [4-1], [4-2], [4-3], [4-4]) for the effective multiplication factor, the reflector reactivity worth, sodium void worth, and Hf reactivity worth for the FCA XXIII cores.

(1) C/E Values Selected for Evaluation of Applicability of the Approach

From the various integral data and the analysis results from the FCA XXIII cores, 20 C/E values were chosen as examples in this demonstration, as shown in Table 4.1-1. Table 4.1-2 lists the selected measured characteristics and their estimated errors. Table 4.1-3 shows the C/E values and their estimated errors associated with method errors. Those C/E values were obtained from the S8-transport analyses. C/E values of sodium void worth were categorized into two parts. For larger void worth, C/E values are scattered around a value of 1.0.

(2) Analysis of an Error of Measurement

Reactivity measurements were made for over 150 items in the course of FCA XXIII experiments. It was assumed that only strong correlations for the same characteristics were included between criticality and the worth measurements, but .measurement errors in reflector worth and those in sodium void worth are treated as independent in the cross-section adjustment approach trial analysis.

(3) Cross-Section Sensitivity Coefficients

Target nuclides and reactions for cross-section adjustments are shown in Table 4.1-4.

(4) Analysis Method Error Uncertainty

The analysis results from the 70 energy group S8 transport calculations were taken. Methodology errors were estimated from the differences of C/E values from those obtained by the MVP detailed calculations in this demonstration. Correlations between analysis errors were also inferred; strong positive correlations were given among the same characteristics and no correlations were assumed for inter-different characteristics. Contributions from the sodium void worth measurements and analyses are reduced by giving larger relative errors associated with method errors to small void worth in the absolute basis.

(5) Cross-Section Covariance Data

Cross-section covariance data processed from JENDL-3.3 were used in an 18 energy group structure [4-5].

4.2 Prediction Accuracies of the Selected Characteristics of the Target Cores

4.2.1 Cross-Section Sensitivity Coefficients

In planning the FCA XXIII critical experiments, basic geometry and fuel compositions were determined to simulate those of the 4S core to have as much similarity as possible in terms of neutron spectra and flux distributions. However, average fuel composition, core size, and reflector-cavity volume impose restrictions in the available fuel, sodium, and structure materials. As a good measure for evaluating the similarity of the benchmark core to the 4S core, comparisons of cross-section sensitivity coefficients are widely accepted for the core-wide integral characteristics.

The sensitivity coefficient is defined as follows:

$$S_{ij} = \left(\frac{dR/R}{d\sigma_{ij}/\sigma_{ij}} \right) \quad \text{(Uncorrelated sensitivity coefficient)}$$

where R corresponds to integral characteristics such as k-effective, reflector worth, sodium void worth, etc.,

i: nuclide reaction index
j: energy group.

For the FCA XXIII cores, cross-section sensitivity coefficients were calculated with criticality, reflector reactivity worth, sodium void reactivity, and Hf reactivity worth for the selected patterns.

4.2.2 Prediction Accuracies by Application of the Bias Factors

The first step in this process uses the C/E value of the various integral data from the FCA XXIII core to apply the "cross-section adjustment" technique [4-6] with the Bayesian approach, which adjusts C/E values toward 1.00 within the predetermined uncertainty ranges (using utility program ABLE code [4-7]). At this stage, the cross-section covariance data (uncertainties) are updated by reflecting information from the experiment analyses. The second step then estimates the prediction accuracy of the specified characteristics in the target core through the related cross-section sensitivity coefficients, calculation errors, and updated cross-section covariance data. This step obtains the expected basis factor and its uncertainty due to the updated cross-section uncertainties by use of the utility program ACCEPT code [4-7].

(1) Evaluation of Applicability of the Adjustment Approach

Table 4.2-1 provides the results of the adjustment approach in the FCA XXIII analysis. The results suggest that C/E values for the effective multiplication factors and for reflector worth can

be consistently improved toward 1.00 within cross-section uncertainties. It is not expected that the C/E values for the sodium void worth can be improved significantly. But the uncertainty originating from cross-section uncertainties can be reduced by about 25%-50% for other cases.

This demonstration indicates good consistencies among the C/E values obtained from the S8-transport base results in the FCA XXIII analyses. It also indicates that S&U analysis provides a reasonable basis or guideline for determining uncertainties due to cross-section errors and calculation method errors. More specifically, looking at the C/E values for sodium void worth, C/E values were shifted about 5–10% from the S8-transport calculation results as a whole and uncertainties due to cross-section errors can be reduced to the 3% level with one-sigma. But in the case of large deviation of C/E values from 1.0, improvement of the C/E values was not obtained in this trial. One reason can be attributed to the large relative errors given as an initial value for adjustment. This example suggests that the C/E adjustment approach has some limitations to near-zero reactivity worth at the plus/minus boundary domain. For sodium void worth including near-zero values, an alternative approach is required to reflect information and experiences through measured data.

(2) Uncertainty Estimation of the 4S Core Characteristics due to Cross-Section Errors

For the 4S core (EOL core), the uncertainty reduction potential was estimated using the cross-section adjustment approach, combining the 14 integral data sets selected from the FCA XXIII measurements and analyses, updated cross-section covariance data with the FCA XXIII data, and various sensitivity coefficients of FCA XXIII cores and the 4S core for selected characteristics.

For the 4S core, criticality, reflector worth, and sodium void worth were selected to assess applicability of the adjustment approach. The results in Table 4.2-2 also indicate that the FCA XXIII results can have good similarity to the 4S core, because the trend of uncertainty reduction has similar to those obtain in the adjustment approach for the integral characteristics of the FCA XXIII core. Further extension of the database from experience obtained from FCA XXIII and other cores can assist the applicability of the cross-section adjustment approach.

4.3 Direct Application of the Measured Sodium Void Worth Results to the Target Cores

4.3.1 Multi-Component Approach for Predicting Core Sodium Void Worth

The statistical regression approach was applied to the sodium void worth prediction for the 4S cores using the measured sodium void worth in the physics benchmark FCA XXIII cores.

The S8-transport calculations with 70 energy group JFS-3-J3.3 data generally reproduced measured sodium void worth for various situations in the vicinity of zero reactivity. However, the simple bias approach is to be reevaluated for prediction of the uncertainties for sodium void worth near zero in the absolute value basis.

Complementary efforts for determining uncertainties of core void reactivity near zero values are being made from application of the demonstrated database directly measured in the benchmark experiments. As noted, at the FCA XXIII cores, more than 100 measured data points were acquired in the measurements of the sodium void worth distributions by changing neutron leakage situations under various patterns of the reflectors in the sector region around the core region. These data can be applied to estimates of the uncertainties of the design parameters relating to reactivity effects, such as sodium density coefficients, assumed sodium void effects, and so on.

Past experience shows typically two methods have been used to generate bias factors from the critical experiments database.

The first method is to use the reciprocal of the mean of the C/E values obtained from the analysis of the experimental data set and to determine an uncertainty based on the standard deviation of the mean. Selection of data is influential to determine this simple bias factor near zero-reactivity domains, because the balance of the total nonleakage components and total leakage components heavily depends on the locations in the core and vicinity regions.

The second method is to determine separate bias factors for the nonleakage and leakage components, and leakage components of the calculated reactivity. The rationale for this approach is that those components are driven by rather distinct mechanisms. The nonleakage components are mainly attributed to cross-sections that determine the flux and, more importantly, the adjoining flux spectra. Reactor configuration and flux gradients determine leakage components. This approach is called the "Two component fitting method," which uses statistical regression techniques.

Using these data, fitting is done to minimize the residual errors.

$$\text{Residual}=\text{Sum}(i)[\ E(i)-(\alpha*NL(i)+\beta*L(i))]^2$$

where,

E(i)=measured sodium void worth

C(i)=NL(i)+L(i): calculated sodium void worth

NL(i): nonleakage component, L(i): leakage component

Fitted coefficients α and β correspond to energy-integrated bias factors to the calculated worth.

In this context, the results from the S8-transport calculations were taken to show applicability of the method. Figure 4.3-1 shows the energy dependence of calculated components of sodium void worth in the FCA XXIII core. As shown, the general trends confirmed that cancellation between nonleakage and leakage components occurred near zero and slight positive domains of the reactivity.

The fitted coefficient sets were determined using 105 measured data points for sodium void worth distributions in the FCA XXIII core, and calculated nonleakage and leakage components with 70 energy group S8-transport exact perturbation calculations. It was found that the sodium void worth by the first-order perturbation (FOP) method agreed well with that obtained by the exact perturbation calculation and slight underestimations were seen for the leakage terms between 0.1 MeV and several MeV in neutron energy.

Table 4.3-1 includes bias factors for sodium void worth. The table includes the upper and lower limits of 95% confidence level. By the one-component bias approach, the nominal bias factor was determined to be 1.033 with small spreads for the upper and lower limits of 95% confidence levels. By the two-component bias approach, the regression approach showed that the fitted coefficients were statistically appropriate. The bias factor for the leakage components was determined to be 1.040. On the other hand, the bias factor for the nonleakage term reached to deviations of 14% from the calculated components on average.

Those bias factors were applied to the FCA XXIII data for checking predicted versus measured values. The ratio P/E values were stable for large negative sodium void patterns, but the values had large volatilities around the near-zero-worth domain. In addition, the one-component approach could not predict for plus or minus values around the zero-worth domain. The two-component approach provides a proper trend around the zero-worth domain in this application.

Table 4.3-2 summarizes a comparison of the average P/E value and its standard deviation for 105 cases between the one- and two-component approaches. The two-component approach is superior to the one-component approach with higher accuracies in the wider combination of the nonleakage and leakage components.

However, as the FCA XXIII core configuration and fuel average compositions are different from the target cores, another complementary method was used to evaluate the uncertainties associated with the one energy group two-component approach mentioned above. The complimentary approach employed a four-component approach with two energy groups in a regression analysis, because two-energy groups can better reflect higher and lower neutron energy behaviors for nonleakage and leakage terms in the FCA XXIII and the 4S cores, respectively.

Based on Fig. 4.3-1, the two-group approach at least seems to be suitable for taking into account position dependence with energy of above and below 1 MeV. It is expected that the two-group approach, which requires four parameters, can be appropriate using 105 data points due to about 25 data points for one-parameter as a simple average. Table 4.3-3 shows the bias set for the two energy groups approach. The results indicate that more than 30% corrections are required both for nonleakage and leakage terms in the higher-energy region over 1 MeV (group 1). The bias factor with small deviation from the value of 1.00 is determined to the nonleakage component of group 2, and small deviations from the calculated value are anticipated for the bias to the leakage component in group 2. It was found that the bias factor for the nonleakage component is less sensitive to the total worth with a small absolute value from 1.00. This indicates that the measured data provided small contributions to the nonleakage components due to the size and configuration of the FCA XXIII core.

This evaluation suggests that differences of the predicted values indicate the estimated uncertainty due to extrapolation from the FCA data to the target parameters.

4.3.2 Estimated Uncertainty of Core Sodium Void Worth

From these results obtained from the FCA XXIII analyses on the bias factors due to two-component or four-component approaches, the uncertainty of the sodium void worth of the end-of-life (EOL) core was estimated to evaluate the reactivity uncertainty relating to the direct use of the measured reactivity data to the target core parameters.

The core-wide sodium void worth was calculated by the two-dimensional RZ S8 70-group transport method with perturbation calculations for the EOL core. Table 4.3-4 summarizes the nonleakage and leakage terms. Appling the bias factors, two types of predicted core-wide sodium void worth are shown in Table 4.3-5. It shows that the deviation from the nominal value to the 95% confidence levels is approximately ±0.04%$\Delta\rho$ (6 cents) both for two- and four-component approaches. Other uncertainties associated with differences of core compositions and other factors are to be determined in the design.

References

[4-1] M. Kawashima, Y. Tsuboi, M. Yamaoka, "Comparisons of cross section sensitivity coefficients in a small fast reactor", FR09 P1345 CN-176

[4-2] M. Kawashima et al., " Sensitivity Analyses for Small Fast Reactor Nuclear Characteristics with a Discrete Ordinate Transport Calculation Method", Proceedings of PHYSOR2010, PHYSOR 2010 – Advances in Reactor Physics to Power the Nuclear Renaissance, Pittsburgh, Pennsylvania, USA, May 9-14, 2010, on CD-ROM, American Nuclear Society, LaGrange Park, IL (2010)

[4-3] G. Aliberti et al. "Nuclear data sensitivity, uncertainty and target accuracy assessment for future nuclear systems", Annals of Nuclear Energy 33 (2006) 700-733

[4-4] A. Gandini et al., "Equivalent generalized perturbation theory (EGPT)", Annals of Nuclear Energy 13(1986) pp109

[4-5] G. Chiba, et al., "Benchmark Test of Evaluated Nuclear Data Files for Fast Reactor Neutronics Application," JAEA-Research 2007-051 [in Japanese].

[4-6] T. Takeda, et al., "Prediction Uncertainty Evaluation Method of Core Performance Parameters in Large Liquid-Metal Fast Breeder Reactors," Nuclear Science and Engineering, 103, p. 157 (1989).

[4-7] M. Ishikawa et al., PNC PN9440 94-004, "Maintenance of a nuclear design basic database of a maintenance (IV)-nuclear-characteristics analysis code system," Power Reactor and Nuclear Fuel Development Corporation O-arai Engineering Center, Section 4.8 (ABLE), Section 4.9 (ACCEPT), March 1994,

Table 4.1-1. Measured Integral Parameters and their Identification Numbers

Parameter*	Selected items for Integral Parameters
1	Criticality of the reference core of the FCA XXIII-1
2	Reflector worth relative to sodium cell for zone-1 in the small zone
3	Reflector worth relative to cavity cell for zone-2 and -3 in the small zone
4	Sodium cell worth to cavity cell for zone-2 and -3 in the small zone
5	Reflector worth to cavity cell in the 1/6-sector zones (A1>A2; half length)
6	Smaller cavity to large cavity cell in the 1/6-sector zones (A3a>A3b)
7	Sodium void worth(**) in inner zone (TPU) for A1-variant(***)
8	Sodium void worth in inner zone (TPU) for A1-variant
9	Sodium void worth in inner core zone (TPU) for A6-variant
10	Sodium void worth in outer core zone (TU) for A6-variant
11	Sodium void worth in inner core zone (TPU) for A3b-variant
12	Sodium void worth in outer zone (TU) for A3b-variant
13	B4C worth to sodium in the central sodium zone (1-pack height)
14	Hafnium worth to sodium in the central sodium zone (8-pack height)

Notes:
(*) Identification number used in Table 4.1.1-2, 4.1.1-3 and 4.1.2-1)
(**) see Table 3.2 for core variations (A1, A3a, A3b and A6) in the FCA23 assembly)
(**) axially integrated for selected one-drawer area using measured axial distributions

Table 4.1-2 Measured Integral Parameters and their Errors

Parameter*	Integral Parameters; δρ(%)	Relative Error (%)
1	1.00209 (Keff)	0.023
2	0.238	1.8
3	0.613	1.7
4	0.376	1.2
5	-0.813	1.7
6	-0.556	1.5
7	-0.586	13.7
8	-9.1	1.4
9	-1.18	6.8
10	-10.7	0.8
11	-2.24	5.6
12	-1.11	1.1
13	-0.227	0.5
14	-0.277	0.4

*) Explanation of parameters is shown in Table 4.1.1-1

Table 4.1-3 Analysis Results (C/E Values) and the Examples of Method Uncertainties

Parameter	C/E(S8)	Relative Error (%)
1	0.993	0.2
2	1.03	3
3	1.07	4
4	1.10	5
5	1.06	3
6	0.99	3
7	1.22	15
8	1.01	3
9	1.18	10
10	1.00	3
11	1.00	3
12	1.06	3
13	1.05	2.5
14	0.94	4

*) Explanation of parameters is shown in Table 4.1.1-1

Table 4.1-4. Nuclides and Reactions for Cross-Section Sensitivity Analysis

Nuclide	Reactions
Na-23	Capture, elastic scattering, inelastic scattering, scattering directional cosine; mu
Cr	Scattering directional cosine; mu dispersion direction cosine mu
Fe	Capture, elastic scattering, inelastic scattering, scattering directional cosine; mu
Ni	Scattering directional cosine; mu
U-235	Capture , fission, nu-value, elastic scattering, inelastic scattering, scattering directional cosine; mu
U-238	Capture, fission, nu-value, elastic scattering, inelastic scattering, scattering directional cosine; mu
Pu-239	Capture , fission, nu-value, elastic scattering, inelastic scattering, scattering directional cosine; mu
Pu-240	Capture, fission, nu-value
Pu-241	Capture, fission, nu-value

Table 4.2-1 Examples of Evaluated Uncertainties for Core Characteristics of FCA XXIII Core

Parameter	C/E 1)	P/E 2)	VE(%)3)	VM (%) 4)	GMG (%) 5)	GM'G (%)6)
1	0.993	0.999	0.023	0.2	0.6	0.3
2	1.03	1.02	1.8	3	5.2	3.8
3	1.07	1.05	1.7	4	5.1	4.3
4	1.10	1.07	1.2	5	6.1	5.3
5	1.06	1.04	1.7	3	4.4	3.4
6	0.99	0.97	1.5	3	4.3	3.3
7	1.22	1.04	13.7	15	100.	23.5.
8	1.01	0.98	1.4	3	5.3	3.5
9	1.18	1.12	6.8	10	27.	11.1
10	1.00	0.98	0.8	3	5	3.4
11	1.00	0.96	5.6	3	13.5	4.2
12	1.06	1.03	1.1	3	4.8	3.4
13	1.05	1.03	0.5	2.5	4.	2.9
14	0.94	0.92	0.4	4	5.1	4.3

Notes:
1) C/E (input) before adjustment, 2) P/E (result) after adjustments,
3) VE (%) input: measurement uncertainty,, 4) VM (%) input: analysis uncertainty,
5) GMG: uncertainty due to cross-section uncertainty before adjustment
6) GM'G: uncertainty due to cross-section uncertainty after adjustment

Table 4.2-2 Examples of Evaluated Uncertainties for Core Characteristics of the Target Core

Core Characteristics	Before Adjustment: Uncertainty due to Cross-Section Uncertainty; GMG'	After Adjustment: Uncertainty due to Cross-Section Uncertainty; GM'G'
Criticality	0.6%	0.4%
Reflector worth	5.8%	4.9%
Core void worth	10.5%	9.8%

Table 4.3-1. Fitted Bias Factors by One Energy Group from the FCA XXIII Results

Bias Approach (1 energy-group model)	Bias	Fitting Coefficients		
		95% Lower	Nominal	95% Upper
One-Component Bias Approach $Y=\alpha(NL+L)$	α	1.022	1.033	1.044
Two-Component Bias Approach $Y=\alpha NL+\beta L$	α	1.085	1.139	1.193
	β	1.029	1.040	1.051

Notes:
Y: Predicted value for the bias approach
NL: Total nonleakage term of reactivity worth (sodium void worth)
L: Total leakage term of reactivity worth (sodium void worth)

Table 4.3-2. Predicted Average Bias for the FCA XXIII Results

Using Information From S8-Transport Calculations	P/E Value for FCA XXIII Measurements	
	Average	Standard Deviation
One-Component Bias Approach	0.931	0.234
Two-Component Bias Approach	0.946	0.161

Table 4.3-3. Fitted Bias Factors by Two-Energy Group from the FCA XXIII Results

Bias Approach (2 energy group model)	Bias	Fitting Coefficients		
		95% Lower	Nominal	95% Upper
Two-Component Bias Approach $Y=\alpha_{1g} NL_{1g} +\beta_{1g} L_{1g} +\alpha_{2g} NL_{2g} +\beta_{2g} L_{2g}$	α_{1g}	1.196	1.328	1.461
	β_{1g}	1.006	1.393	1.780
	α_{2g}	-0.728	0.029	0.786
	β_{2g}	0.874	0.984	1.093

Notes:
Y: Predicted value for the bias approach
Energy group 1: 10.0–1.05 MeV, Energy group 2: less than 1.05 MeV
NL_{1g}: Energy group 1 nonleakage term of reactivity worth (sodium void worth)
L_{1g} : Energy group 1 leakage term of reactivity worth (sodium void worth)
NL_{2g}: Energy group 2 nonleakage term of reactivity worth (sodium void worth)
L_{2g} : Energy group 2 leakage term of reactivity worth (sodium void worth)
*1) The coefficient α_{2g} is statistically of less importance in the regression analysis due to the large p value in this case.

Table 4.3-4. Core-Wide Sodium Void Worth at the EOL Core in the Target Core

	Energy group	Worth %Δρ		
		Nonleakage Term	Leakage Term	Sum
Two-Component Approach	1-70g total	0.85	-0.90	-0.05
Four-Component Approach	1-9g	0.43	-0.18	0.25
	10-70g	0.41	-0.72	-0.30

Table 4.3-5. Predicted Sodium Void Worth Using Fitted Bias Factors

	Energy group	Worth %Δρ		
		95% Lower	Nominal	95% Upper
Two-Component Approach	1-70g total	-0.001	0.04	0.07
Four-Component Approach	1-9g	0.34	0.33	0.32
	10-70g	-0.93	-0.70	-0.46
	1-70g total	-0.59	-0.37	-0.14

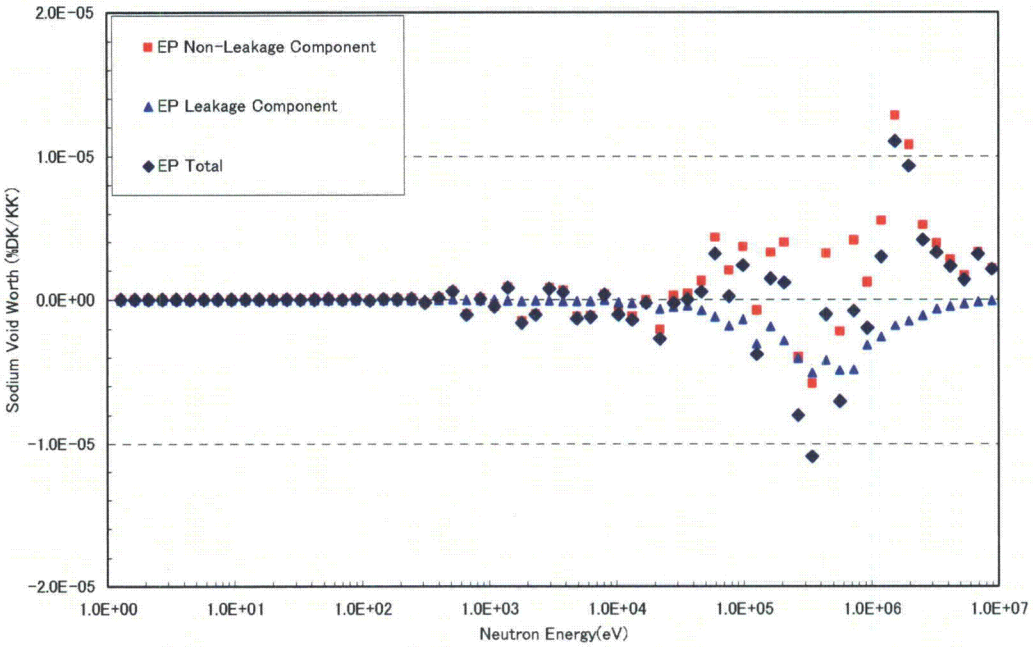

Position; axial 2 packs of FCA fuel cell near core –mid-plane of the inner core

Fig.4.3-1. Energy Dependence of Calculated Components of Sodium Void Worth for the FCA XXIII

5 CONCLUSIONS

The nuclear design code and methods for the 4S are as follows:

a) The continuous-energy Monte Carlo code MVP

b) The Discrete-ordinate transport codes, THREEDANT and TWODANT, for deterministic calculations

c) The evaluated cross-section file JENDL-3.3 based library for the MVP code and 70 energy group constant set for fast reactor JFS-3-J3.3 generated by the cell homogenization code SLAROM from the evaluated cross-section file JENDL-3.3.

The two types of transport methods a) and b) are used for the design in complementary ways. Other related calculation codes include perturbation code groups were used in connection with Sn-transport calculations.

The 4S nuclear design methods were applied to the analysis of the measured characteristics of the FCA XXIII series cores. Selected critical benchmark data analyses were made for criticality, sample Doppler reactivity, and effective delayed neutron fraction. For consideration of the fast experimental reactor JOYO MK-1, criticality and reaction rate were analyzed.

Good agreement was confirmed for the principal neutronic characteristics as summarized in Table 5-1. Those biases and uncertainties make up a portion of the prediction uncertainties in the 4S nuclear design.

Table 5-1. Summary Analysis Accuracies Obtained from the FCA XXIII Experiments and Analyses

Nuclear Characteristics Item	Design Method	C/E Bias	Method Uncertainty	Remarks
Criticality	MC Method[1)]	0.997	0.3%	–
Reflector Reactivity Worth	MC Method	1.03	6%	Total reflector worth
	Sn Transport[2)]	1.06	10%	Stroke-worth curve
Power Distribution	MC Method	1.007	6%	(S/A power)
	Sn Transport	1.01	2%	Power distribution in S/A
Absorber reactivity worth(B_4C)	MC Method	0.94	6%	Total worth
	Sn Transport	1.02	6%	Stroke –worth curve
Absorber reactivity worth (Hf)	MC Method	0.88	6%	Total worth
	Sn Transport	0.94	6%	Stroke –worth curve
Sodium Void reactivity (Core region)	Sn Transport	NL=1.139	5%	Two component Bias Approach NL: Nonleakage term L: Leakage term
		L=1.040	5%	
Doppler Reactivity	Sn transport	0.85	10%	-
Effective delayed Neutron Fraction	Sn transport	1.00	6%	-
Burnup reactivity loss	MC Method[3)]	1.00	10%	-

Notes:
1) Continuous-energy Monte Carlo (MC) MVP-library processed from JENDL-3.3
2) 70 energy group JFS-3-J3.3 processed from JENDL-3.3
3) Continuous-energy Monte Carlo (MC) MVPBURN-library processed from JENDL-3.3

APPENDIX. EXPERIMENTAL ANALYSES BY THE 4S NUCLEAR DESIGN METHODS

A.1 Critical Experiment Analysis in the FCA XXIII Core

The experimental core (FCA XXIII core) was constructed as a physics mockup assembly of the 4S core to focus on measurements of major core characteristics in leakage-dominant situations. In this physics mockup experiment, the focus was on understanding the relationships between reflector positions controlling core-wide neutron leakages and major characteristics, such as criticality, reflector worth, power distribution and sodium void reactivity worth. Therefore, measurements of important nuclear characteristics, such as sodium void reactivity, reflector worth value, neutron absorber reactivity worth of B_4C and Hf-plates, and reaction rate ratios were performed to confirm the applicability of the nuclear design methods for the 4S core design.

A.1.1 Outline of the Experiments and Analysis Method

The FCA is a table-split type critical facility with fixed (stationary) and movable halves of the assembly, and hence inherently has a small gap between the two sides at the core midplane. The measurements were done around an average temperature of 20°C.

The core went critical on July 23, 2005, with 45 drawers in the fixed half and 44 in the movable side. The core consists of the Pu-plate cell region (T-Pu region), Pu-plate, and enriched U-plate region (T-U region). The as-built core layout of the phase I and the basic fuel cell patterns are shown in [A.1-1].

The FCA XXIII-1 core included a central 3-by-3 zone composed of sodium plate drawers and surrounded by simulated reflector drawers consisting of stainless steel and sodium plates. The core consisted of enriched uranium (EU) and plutonium (Pu) plates with averages of 15% Pu-enrichment and 11% U-235 in total heavy metals with 82 fuel drawers. These major geometries and compositions were selected to provide appropriate similarity of the principal neutron spectra under leakage-dominant circumstances achievable in the mockup core.

The FCA XXIII-1DU core was also built with a slight adjustment associated with depleted uranium blocks placed outside the reflector regions based on operational requests for lowering neutron dose around the facility.

Table A.1.1-1 compares the outline of fissile fractions and core geometries. The measured core characteristics in the FCA XXIII core series included the following:

1) Criticality

2) Reflector reactivity worth:

   — Substitution worth with reflector cells to sodium plate or cavity cells in the small zone

— Substitution worth with reflector cells to cavity cells in the 1/6 sector zone of the core periphery.

3) Sodium void reactivity worth distributions:

— With variations of reflector position variants in the 1/6 sector zone at the core periphery.

4) Power distribution (reaction rate distributions and reaction rate ratios)

— With variations of reflector position variants in the 1/6 sector zone at the core periphery.

5) Absorber reactivity worth for B_4C and Hf

The nuclear data set JENDL-3.3 [A.1-2] has been used in the design analyses. The Monte Carlo code with continuous-energy MVP [A.1-3] and the group constant set with a 70 energy group structure generated from JENDL-3.3 and JFS-3-J3.3 [A.1-4], has been used for the analyses.

Applicability of the MVP with JENDL-3.3 library was considered as a part of validation efforts through the FCA XXIII analyses. Exact plate geometry models were used in the MVP calculations for fuel plates, cans, and matrices of the drawers. This model can provide heterogeneous corrections, which are important in application of the FCA results for the target cores.

As the principal deterministic methods with 70 energy group, discrete-ordinate P0-S8 transport calculations are applied to the 4S-design and benchmark analyses using the DANTSYS code system [A.1-5] (THREEDANT with XYZ geometry and TWODANT with RZ geometry model). A conventional diffusion approximation, DIF3D [A.1-6] code, was also applied to compute the plate anisotropy corrections associated with the FCA plate-type fuel drawer configuration through the directional effective diffusion coefficients for the fuel drawer characteristics.

The effective cross-sections for various drawers used in the FCA XXIII cores were calculated by the cell homogenization code SLAROM [A.1-7], which has been used in FCA analyses as the standard method in combination with 70 energy-group reactor constant library JFS-3-J3.3 for fast reactors. The collision probability method was used to homogenize the heterogeneous plate structures for the T-Pu and the T-U drawers. Anisotropic diffusion coefficients were calculated for fuel drawer cells with the Benoist's model. For the P0-S8 transport calculations, homogenized average transport cross-sections are defined as the $1/(3*D_{AVE})$, where D_{AVE} corresponds to the cell averaged diffusion coefficients over fuel drawer plate arrangements. The D_{AVE} values are calculated by the directional diffusion coefficients derived from the cell calculation. The directional anisotropic diffusion coefficients correspond to those parallel to the plates and perpendicular to the plates, respectively. Anisotropy effects due to the FCA plate fuel cell alignments were estimated from the diffusion calculations with the directional anisotropic diffusion coefficients and with isotropic average diffusion coefficients.

For the FCA analytical calculations, the standard node size was 2.76 cm in X- and Y-directions, and 2.54 cm in the Z-direction.

As for the rationale for determining the order of the discrete-ordinate transport (Sn-transport) calculations, surveys were performed to identify the relevant influences to an effective multiplication factor and a sodium void reactivity distribution in the context of the subsequent analyses for the FCA XXIII experiments.

Table A.1.1-2 shows examples of Sn-order effects (n from 4 to 16) on the effective multiplication factor. The survey showed that the "S8 calculation" is accurate enough with appropriate computational efficiency for design calculations.

Regarding examples of the rationale for the reactivity worth calculations by the Sn-transport models, cases of the effects of sodium void reactivity were investigated on the variants of the Sn-order. While sodium void worth in the FCA measurements was determined by the balance of the positive nonleakage term and the negative leakage term, surveys can indicate adequate Sn-order selection to the nonleakage term (spectral term) and leakage term, individually, as well as total reactivity. Table A.1.1-3 exemplifies the calculated sodium void worth distributions with various Sn-orders. Details of the analyses are given in the subsequent sections. Characteristic features of those cases covered three types of sodium void worth profiles. First, positive nonleakage terms dominate rather than negative terms in the regions '1Z-2Z', and '3Z-4Z'. Second, small reactivity changes are given at the region '5Z-6Z' in the vicinity of near-zero reactivity balances. Third, leakage terms dominate at the regions '7Z-8Z' and '9Z-11Z' in the core, and at the region '12Z-13Z' above the core. The Sn-order effects on the sodium void reactivity were investigated by comparing the ratios of the worth of Sn to that by S16 calculations at each region. For most regions, S8 calculations provide good agreement with the S16 calculations. In the vicinity of the near-zero-worth region, approximately 30% differences were observed at the region '5Z-6Z'. However, in this reactivity domain, as the absolute values are small, it is judged that the S8 calculations are acceptable even for the sodium void worth analyses.

TableA.1.1-4 compares reactivity components of sodium void worth in FCA XXIII between the exact and the first-order perturbation methods by the S8-transport calculations. The results indicate that several percent differences are observed in the leakage-dominant regions and some more complicated trends are shown in the vicinity of the near-zero void domains. The analyses are done by the exact perturbation method as the reference method, but the first-order perturbation method is used for the simplified method as well in some cases.

A.1.2 Criticality

The measured criticalities were corrected to the reference effective multiplication factors through the standardized processes at FCA, taking into account the reference geometry models in temperature, the split-gaps, and so on for the analyses.

Monte Carlo calculations were selected as the reference analysis method for criticality analyses with rigorous geometry models. The number of histories of the MVP calculation was set at 10 million, and as a result, the statistical errors are 0.02%.

The calculated multiplication factor (k_{eff} value) was compared with the measured one in the form of calculation-to-experiment ratio (C/E value). The reference model provided C/E values of 0.9965 for the FCA XXIII-1 core and of 0.9976 for the FCA XXIII-1DU core. The biases are consistent between the two, and the calculated values of MVP resulted in underestimating experimental values by 0.2% to 0.3% with the JENDL-3.3 library. As complementary results, Table A.1.2-1 shows criticality based on the measured data and C/E values of the deterministic methods. From the table, the C/E values of the P0-S8 transport methods are confirmed to be adequate with the deterministic 70 energy group approach. A conventional diffusion calculation (DF) significantly underestimated by more than 2% for the effective multiplication factors.

A.1.3 Reflector Reactivity Worth

The reflector reactivity worth measurements were made by replacing various combinations of sodium plates and steel plates in the reflector zone.

For the small reactivity changes due to replacement of the reflector drawers (REF: about 85% stainless steel plates and 15% sodium plates) with sodium plate drawers (NA) or the stainless steel void canned plates drawers (VOID) in the small zones briefly described in Appendix A, C/E values by the deterministic calculations using P0-S8 transport and diffusion (DF) methods are summarized in Table A.1.3-1.

P0-S8 transport calculations reproduced the substitution worth from the REF-drawers to the NA-drawers quite well within 5% except for case 41 (C/E=0.92). The C/E values for the worth from the REF-drawers to void-drawers tend to increase by several percent (C/E=1.06, 1.08) with the homogenized drawer models. The C/E values for the P0-S8 transport calculations are in the range of 0.92 to 1.08 for REF-NA and REF-VOID replacements with stable behavior.

Otherwise, the conventional diffusion calculations provide large deviations around 30% in C/E values for the substitution worth.

For the larger reactivity changes measured in the 1/6 sector reflector zone, continuous-energy Monte Carlo methods were applied for the analysis. In the analysis of reflector reactivity worth, the MVP calculations with exact geometry models were carried out with an effective 10 million histories. The statistical error in the calculation of each effective multiplication factor is 0.02%

The C/E results are shown in Table A.1.3-2, where the P0-S8 transport calculations with the 70 energy groups are also summarized. For the case of larger reactivity changes (along with configuration changes: A1>>A6, A6>>A5, A3a>>A3b and A1>>A2 in the Table A.1.3-2), the C/E values by the Monte Carlo calculations are placed in the range of 1.00 to 1.06, and are in good agreement within about ±5%. On the other hand, in the case of smaller reactivity changes (along with configuration changes: A5>>A4 and A4>>A3a in Table A.1.3-2), C/E values are

scattered in the range of 0.9 to 1.3 and the degree of agreement is reduced. In addition, this tendency is also observed in the P0-S8 transport calculations.

These results support the conclusion that the P0-S8 transport calculation model is suitable and applicable to the worth analyses at the reflecting and cavity regions of the 4S core.

A.1.4 Reaction Rates (Power Distributions and Reaction Rate Ratios)

Axial distortion of power distributions was experimentally investigated in relation to the reflector worth measurements in the 1/6-sector region. Comparisons of the normalized measured and calculated U-235 fission reaction rate distributions for the A1 core and A6-F core were made as shown in Fig3-3. As the A1 core was fully covered by reflector drawers, the U-235 fission rate was distributed symmetrically in the axial direction near the core center (marked with a black circle and x). On the other hand, as the A6-F core has a cavity region, which was created by replacing steel drawers with void drawers, the U-235 fission rate is distributed asymmetrically in the axial direction (marked with black triangles and +). Comparisons using the P0-S8 transport calculations showed that reflector movement can be adequately predicted for neutron flux distortions.

Reaction rate ratios were also measured in the FCA XXIII-1 and XXIII-1DU reference cores at the T-Pu and T-U zones near the midplane. The small fission chambers were used for this investigation. A foil activation technique was applied to obtain the ratios of fission rates of U-238 and Np-237, and the capture rate of U-238 vs. the fission rate of U-235. The 93% enriched U and depleted U foils were placed on the fuel plate in the selected cell of the core irradiated under the appropriate power level. Fission rates of U-235 and capture rates of U-238 were measured through the standard procedures used at FCA.

Table A.1.4-2 provides the C/E values for reaction rate ratios measured in the FCA XXIII-1DU core. Fission rates were measured by micro-fission chambers and capture rates of U-238 were measured with foil activation methods. For the comparisons with the calculated values, cell average factors were provided using Monte Carlo calculations for reaction rates in the fuel drawer cell including the micro-fission chamber positions.

The C/E values showed generally satisfactory agreement with unity by deterministic analyses. However, C/E values of the reaction rate ratios on F28/F25 and F37/F25 are overestimated by over 10% at the outer core region. This indicated that further corrections may be needed for steep flux gradient effects to fission chambers for threshold fission reactions in the calculations.

A.1.5 Sodium Void Worth

The sodium coolant void reactivity distributions were measured in the core as well as around the core region by replacing sodium with void. More than 100 patterns of sodium void reactivity changes were compared to P0-S8 transport calculations with 70 energy groups.

As for the general trends, the best agreement is found with slight biases between measured values by the P0-S8 transport calculations with 70 energy group JFS-3-J3.3 library in absolute value near zero sodium reactivity changes.

The results confirmed that P0-S8 transport calculations provided stable agreement in the upper and lower halves of the core, where asymmetric replacement of reflector and void regions in the 1/6-sector portion were used for reflector reactivity worth measurements. As anticipated, diffusion calculations provided more negative-worth distribution due to overestimation of the leakage effects.

Table A.1.5-1 summarizes the C/E values for the axially integrated sodium void reactivity in the variations of core configuration with various combinations of reflectors and void regions as denoted by A1, A3a, A3b, A5, and A6 configurations.

The P0-S8 transport calculations provide good agreement with unity for wide ranges of the near-zero sodium reactivity changes. It is confirmed that continuous-energy Monte Carlo calculations can be applicable within the range of "less than 10% statistical error" with the MVP code as well.

A.1.6 Absorber Worth

Boron carbide (B_4C) and hafnium (Hf) are candidate materials for reactor shutdown and compensation of burnup reactivity losses. B_4C and Hf reactivity worth measurements were made by replacing sodium plates with absorber material plates in the central region.

Analyses were made by deterministic methods (P0-S8 transport and diffusion calculations) using homogeneous models for sodium, B_4C, and Hf drawers at the central 3-by-3 region. Plate heterogeneity correction factors for B_4C-drawers and Hf-drawers were calculated for typical situations with the detailed plate layouts with continuous-energy Monte Carlo calculations. Analyses showed small plate heterogeneity effects with the selected plate patterns for the reactivity worth measurements in FCA XXIII cores. The correction factors for Hf and B_4C (natural boron) estimated were 0.99-1.00, and correction to the calculated values with the homogeneous model was 0.98 for the B_4C with at most 90% enriched B-10 in a 38% volume ratio in the drawer.

TableA.1.6-1 and Table A.1.6-2 summarize measured values and C/E results for Hf-plates and B_4C plates, respectively, with the homogeneous model basis. Additional analysis also confirmed that transport corrections, of a magnitude of up to 4% in those cases, are necessary for the worth predictions when the diffusion base calculations are used as the simplified design calculations.

The deterministic analyses provided stable C/E values in the ranges from 0.93 to 0.97 for Hf reactivity worth, and from 0.99 to 1.05 for B_4C reactivity worth.

A.1.7 Summary

A series of critical experiments was carried out in the JAEA fast critical facility (FCA) FCA XXIII cores with emphasis on reflector reactivity worth and sodium void reactivity, which are especially important from the viewpoint of the safety features of the 4S. The analyses of those physics mockup experiments have been carried out by the neutron transport calculation methods with the continuous-energy Monte Carlo code MVP and 70 energy group discrete-ordinate P0-S8 transport code DANTSYS using libraries processed from the JENDL-3.3 data file. The results showed that a combination of the stochastic and deterministic transport calculation methods (Monte Carlo and Sn) provided good prediction bases for criticality, reflector worth, sodium void reactivity, reaction rate ratios, and absorber reactivity worth for the 4S nuclear design.

References

[A.1-1] S. Okajima, M. Fukushima, T. Takeda "Development of Neutronics Analysis Technique for Non-refueling Core (Part1 Critical experiments)", *Trans. Am. Nucl. Soc.*, Vol. 93, p. 54 (2005)

[A.1-2] K. Shibata, et al., "Japanese Evaluated Nuclear Data library Version 3 Revision-3: JENDL-3.3' J. Nucl. Sci. Technol. Vol.39. [11], 1125 (2002).

[A.1-3] T. Mori, M. Nakagawa, M. Sasaki, "Vectorization of Continuous Energy Monte Carlo Method for Neutron Transport Calculation", J. Nucl. Sci. Technol., Vol. 29, [4], 325 (1992).

[A.1-4] http://rpg.jaea.go.jp/code/JFS-3-J33/index.html (In Japanese) .

[A.1-5] R. E. Alcouffe, et al., "DANTSYS: A Diffusion Accelerated Neutral Particle Transport Code System," LA-12969-M (1995).

[A.1-6] R. D. Lawrence, "The DIF3D Nodal Neutronics Option for Two- and Three-Dimensional Diffusion Theory Calculations in Hexagonal Geometry, Argonne-83-1, Argonne National Laboratory (1983).

[A.1-7] M. Nakagawa, et al., "A Code for Cell Homogenization of Fast Reactor," JAERI 1294 (1984)

[A.1-8] N. Ueda, et al., "Development of the 4S and Related Technologies (7) : Summary of the FCA XXIII Experiment Analyses towards Evaluation of Prediction Accuracies for the 4S Core Characteristics"、 Proceedings of ICAPP '09, Tokyo, Japan, May 10-14, 2009, Paper 9493

[A.1-9] Y. Tsuboi , S. Matsuyama and M. Kawashima, "Development of The 4S and Related Technologies (8) An Analysis of Delayed Neutron Fraction Benchmark Results Using Nuclear Design Methodology", Proceedings of ICAPP '09, Tokyo, Japan, May 10-14, 2009, Paper 9184

Table A.1.1-1. Comparison of the Outline of Fissile Fractions and Core Geometries

Assembly	Pu[1)]	U5[2)]	R (cm)	H (cm)	Core
4S(BOL)	---	17.6	10/47[3)]	250	LEU-Zr 29a%
FCA XXIII	15	11	9/32[3)]	112	Pu/LEU-Zr 23a%

Notes:
1) Pu=Pu fraction in total heavy metal (Pu+U)
2) U5=U235 fraction in total heavy metal
3) Equivalent inner radius/outer radius of core

Table A.1.1-2. Examples of Sn-Order Effects on the Effective Multiplication Factor

Sn Order	Effective Multiplication Factor	Discrepancy from S16 Calculation	Comments
	k-eff	%δρ	
2	0.995114	-0.1321	FCA XXIII core 70 energy groups, mesh sizes for X,Y,Z directions=about 2.5 cm
4	0.996906	+0.0471	
6	0.996561	+0.0126	
8	0.996488	+0.0053	
12	0.996446	+0.0011	
16	0.996434	-	

Table A.1.1-3. Examples of Sn-order Effects on the Sodium Void Reactivity

(1) Examples of Sodium Void Worth Map in FCA XXIII

FCA XXIII-1 A-1 Core	Status of Reflector 1/6-sector Zone	Void Cell Region	Sodium Void Worth in T-Pu Zone (unit: %δρ) Sn-order[1] S4	S6	S8	S12	S16
Above-Core	R [2]	12Z—13Z	-8.21E-03	-8.24E-03	-8.24E-03	-8.25E-03	-8.25E-03
(Core Top) Core (Midplane)	R	9Z—11Z	-7.97E-03	-7.99E-03	-7.99E-03	-7.99E-03	-7.98E-03
		7Z—8Z	-2.73E-03	-2.76E-03	-2.76E-03	-2.76E-03	-2.76E-03
		5Z—6Z	6.26E-04	5.64E-04	5.50E-04	5.44E-04	4.02E-04
		3Z—4Z	3.16E-03	3.08E-03	3.06E-03	3.05E-03	3.05E-03
		1Z—2Z	4.52E-03	4.43E-03	4.41E-03	4.40E-03	4.39E-03

Notes:
1) 70 energy group, S8, XYZ transport calculations
2) Reflector cells

(2) Examples of Sn-order effects on the sodium void reactivity

FCA XXIII-1 A-1 Core	Status of Reflector 1/6-sector Zone	Void Cell Region	Deviation of Sodium Void Worth in T-Pu Zone 2-(Sn/S16) Sn-order[1] S4	S6	S8	S12	S16
Above-Core	R [2]	12Z—13Z	1.01E+00	1.01E+00	1.00E+00	1.00E+00	1.00E+00
(Core Top) Core (Midplane)	R	9Z—11Z	1.00E+00	1.00E+00	1.00E+00	1.00E+00	1.00E+00
		7Z—8Z	1.01E+00	1.00E+00	1.00E+00	1.00E+00	1.00E+00
		5Z—6Z	4.43E-01	5.97E-01	6.32E-01	6.47E-01	1.00E+00
		3Z—4Z	9.63E-01	9.88E-01	9.94E-01	9.98E-01	1.00E+00
		1Z—2Z	9.71E-01	9.91E-01	9.96E-01	9.98E-01	1.00E+00

Notes:
1) 70 energy group, S8, XYZ transport calculations
2) Reflector cells

Table A.1.1-4. Comparisons of Reactivity Components of Sodium Void Worth Map in FCA XXIII between Exact and First-Order Perturbation Methods[1)]

FCA XXIII-1	Status of Reflector 1/6-sector Zone	Void Cell Region	Worth Ratio [FOP/EP][5)] S8,70g,XYZ								
			T-Pu Zone			T-U Zone			Na Zone		
A-1 Core			NL[2)]	L[3)]	Total	NL	L	Total	NL	L	Total
Above-Core	R[4)]	12Z—13Z	0.95	0.94	0.94	0.96	0.94	0.94	1.01	0.94	0.94
(Core Top) Core (Midplane)	R	9Z—11Z	0.96	0.93	0.92	0.95	0.94	0.94	0.94	0.95	0.95
		7Z—8Z	0.97	0.94	0.90	0.95	0.95	0.94	0.70	0.95	0.96
		5Z—6Z	0.97	0.94	1.23	0.95	0.95	0.94	2.78	0.96	0.96
		3Z—4Z	0.97	0.93	1.01	0.95	0.95	0.95	1.45	0.96	0.96
		1Z—2Z	0.97	0.93	0.99	0.94	0.95	0.95	1.46	0.96	0.97

Notes:
1) 70 energy group, S8, XYZ transport calculations
2) NL: Nonleakage component
3) L: Leakage component
4) Reflector cells
5)FOP(First order perturbation)/EP(Exact Prediction)

Table A.1.2-1. C/E Values for Effective Multiplication Factors

FCA Cores	Measured Values		C/E Values		
	Value	Uncertainty	MVP (Continuous-Energy Monte Carlo)*	P0-S8 Transport (70 energy groups)*	Diffusion (70 energy groups)*
XXIII-1	1.00209	±0.00023	0.9965±0.0002	0.9926	0.9694

Note:
(*) Calculated by using the JENDL-3.3-based-libraries

Table A.1.3-1. C/Es of the Reflector Worth in the Small Zones

Case	Zone Conditions			Measured (E)		C/E Values	
	1	2	3	Value [%δρ]	Error [%]	DF	S8
Base	REF	REF	REF	-	-	-	-
11	REF	NA	VOID	-0.115	0.9	1.25	1.00
12	REF	NA	NA	-0.196	1.3	1.33	1.04
12Y	REF	NA	NA	-0.223	0.4	1.32	1.03
21	REF	VOID	REF	-0.282	0.5	1.42	1.06
22	REF	VOID	VOID	-0.512	0.6	1.56	1.08
41	NA	REF	REF	-0.096	1.5	1.23	0.92
42	NA	NA	NA	-0.334	0.9	1.29	0.99
43	NA	VOID	VOID	-0.710	0.8	1.48	1.04

Table A.1.3-2. C/E for Reflector Worth in the 1/6 Sector Zone

Configuration Changes*	Measured (E)		S8	MVP	
	Value [%δρ]	Error [%]	C/E	C/E	Error [%]
A1>>A6	-0.744	±1.4	1.06	1.02	±1.8
A6>>A5	-0.739	±2.0	1.02	1.00	±2.3
A5>>A4	-0.059	±1.1	1.1	0.9	±16.
A4>>A3a	-0.059	±1.4	1.1	1.3	±12.
A3a>>A3b	-0.556	±1.5	0.98	1.06	±2.1
A1>>A2	-0.813	±1.7	1.05	1.01	±2.0

*) See figure 3.2 in chapter 3

Table A.1.4-1. Comparison of Measured Value of Reaction Rate Ratio, and Calculated Value

FCA	Measurement			Measured Data		Calculated Data[1)]		C/E Value	
ID	R-pos.	Z-pos.	Ratio[2)]	Meas.	Error [%]	DF	S8	DF	S8
XXIII-1	T-Pu	Midplane	F28/F25	0.0388	±3.0	0.0398	0.0398	1.02	1.03
			F37/F25	0.304	±3.0	0.307	0.307	1.00	1.00
			F49/F25	1.14	±3.1	1.10	1.10	0.96	0.96
			C28/F25	----	----	0.116	0.116	----	----
XXIII-1D	T-Pu		F28/F25	0.0381	±1.0	0.0396	0.0397	1.04	1.04
			F37/F25	0.295	±1.0	0.305	0.305	1.04	1.04
			F49/F25	1.10	±1.0	1.09	1.09	0.99	0.99
			C28/F25	0.115	±1.6	0.116	0.116	1.01	1.01
	T-U		F28/F25	0.0296	±1.0	0.0325	0.0340	1.10	1.15
			F37/F25	0.235	±1.0	0.253	0.260	1.08	1.10
			F49/F25	1.06	±1.0	1.05	1.06	0.99	0.99
			C28/F25	0.119	±1.6	0.120	0.119	1.01	1.00

Notes:
1) 70 energy group, P0-S8)
2) Reaction rates: F28=U238(n,f), F37=Np237(n,f), F49=Pu239(n,f), C28=U238(n,g), F25=U235(n,f)

Table A.1.4-2. C/E Values for Spectral Indices (70 energy group, P0-S8)

Reaction Rate Ratios	XXIII-1D (Inner Core)			XXIII-1D (Outer Core)		
	Value[1)]	Error[1)] [%]	C/E(S8)	Value[1)]	Error[1)] [%]	C/E(S8)
F28/F25[2)]	0.0381	1.0	1.04	0.0296	1.0	1.15
F37/F25[2)]	0.295	1.0	1.04	0.235	1.0	1.10
F49/F25[2)]	1.10	1.0	0.99	1.06	1.0	0.99
C28/F25[2)]	0.115	1.6	1.01	0.119	1.6	1.00

Notes:
1) Measured position: Reference core midplane
2) Reaction rates: F28=U-238(n,f), F37=Np-237(n,f), F49=Pu-239(n,f), C28=U-238(n,g), F25=U-235(n,f)

Table A.1.5-1. C/E-Values for Axially Integrated Sodium Void Reactivity Worth in the Core Variants of FCA XXIII

Core	Void Cell Zone		Measured (E)		Calculation Methods [5]			
					DF	S8	MVP	
			Value [%δρ]	Error [%]	C/E	C/E	C/E	Error
A1	T-Pu	1)	-5.86E-03	±13.9	3.17	1.27	0.39	363
	T-U	1)	-9.11E-02	±1.4	1.13	0.96	0.90	10.4
	Na	3)	-8.62E-02	±1.6	1.26	0.95	0.88	11.3
A6	T-Pu	1)	-1.18E-02	±6.9	2.33	1.17	1.88	38.8
		2)	-9.35E-02	±8.7	2.34	1.03	0.33	271
	T-U	1)	-1.07E-01	±0.8	1.17	0.95	0.95	8.4
		2)	-9.54E-02	±0.9	1.15	0.96	0.97	9.2
	Na	3)	-1.08E-01	±0.8	1.19	0.90	0.86	9.2
		4)	-9.00E-02	±1.0	1.21	0.90	0.82	11.4
A5	T-Pu	1)	-1.59E-02	±5.1	1.99	1.06	0.95	55.8
	T-U	1)	-1.11E-01	±0.7	1.16	0.95	0.87	9.5
	Na	3)	-1.02E-01	±0.9	1.22	0.94	0.89	9.4
A3a	T-Pu	1)	-1.63E-02	±5.0	2.02	1.11	1.33	39.2
	T-U	1)	-1.06E-01	±1.2	1.23	1.01	0.97	8.4
	Na	3)	-1.02E-01	±1.3	1.23	0.96	0.91	9.3
A3b	T-Pu	1)	-2.24E-02	±4.1	1.78	0.96	0.69	55.2
	T-U	1)	-1.11E-01	±1.1	1.25	1.00	0.94	8.3

Notes:
1) 1Z~11Z: summed over half core height (fixed side)
2) -1Z~-11Z: summed over half core height (movable side)
3) 1Z~13Z: half core height + two upper Na packs
4) -1Z~-13Z: half core height + two lower Na packs
5) Calculation methods: DF=diffusion, S8=P0-S8 transport with 70 energy group calculations, and MVP=continuous-energy Monte Carlo calculations

Table A.1.6-1. C/E Values of Hf Worth at Central 3x3 Zone in FCA XXIII-1DU Core

Hf Fractions	Drawers	Measured Value (E)		DF[2)]	S8[3)]
		Value [%δρ]	Error [%]	C/E	C/E
38%	1 pack[1)]	-3.80E-02	2.8	0.99	0.96
	9 packs	-3.07E-01	0.3	0.98	0.94
	15 packs	-4.84E-01	1.0	0.96	0.93
	11 packs	-2.45E-01	1.1	0.96	0.93
50%	1 pack[1)]	-4.78E-01	2.2	1.00	0.97
	5 packs	-2.23E-01	0.5	0.99	0.96

Notes:
1) Central 1 pack drawer, 1pack=5.52x5.52x5.52cm**3
2) DF=diffusion calculations with XYZ geometry, 70 energy group
3) S8=P0-S8 transport calculations with XYZ geometry, 70 energy group

Table A.1.6-2. C/E Values of B_4C Worth at Central 3x3 Zone in FCA XXIII-1DU Core

Core	Pos.[1)]	B10/B	Measure (E)		DF [2)]	S8 [3)]
			Value [%δρ]	Error[%]	C/E	C/E
XXIII-1	1 pack	20%	-7.30E-02	1.6	1.02	0.99
	1 pack	60%	-1.70E-01	0.7	1.06	1.03
	1 pack	90%	-2.27E-01	0.5	1.09	1.05
XXIII-1DU	1 pack	20%	-7.73E-02	1.4	1.02	1.00
	1 pack	90%	-2.27E-01	0.5	1.09	1.05

Notes:
1) Pos.: central drawer poison at core midplane
2) DF=diffusion calculations with XYZ geometry, 70 energy groups
3) S8=P0-S8 transport calculations with XYZ geometry, 70 energy groups

A.2 Critical Experiment Analysis for Benchmark Data

A.2.1 Outline of Benchmark Experiments and Analyses

(1) Criticality Benchmark Data for Enriched Uranium Small-Sized Fast Spectra

Criticality benchmark experiments were selected from the Handbook [A.2-1] to validate the nuclear cross-section libraries employed in the 4S nuclear design method. First, three LEU cores were analyzed (ZPR-U9, ZPR-3/41 and ZPR-6/6A) under the fast reactor spectra. Second, ZPPR-21F was selected as a MEU core. Finally, two HUE cores were analyzed (ZPR-3/23 and U/Iron cores). Through these benchmark data analyses, the applicability of the cross-section libraries processed from JENDL-3.3 was confirmed for the 4S core for the beginning of life (enriched uranium fast-spectrum core). [A.2-2]

Additionally, the benchmarked ZPPR-21 cores were analyzed to confirm the consistencies in prediction accuracies of fission contributions between enriched uranium and plutonium cores, to understand the relationship between the analyzed results for the FCA XXIII cores and other fast spectrum benchmark results from the past ZPPR and ZPR cores.

Table A.2.1-1 presents the outline of the uranium benchmark cores with inclusion of the target 4S and the FCA XXIII cores. Table A.2.1-2 shows the outline of the ZPPR-21 cores.

(2) Sample Doppler Benchmark Data (FCA XVI)

Sample Doppler reactivity measurements have been performed in the past with physics benchmark assembly, FCA XVI-1 and -II cores, which simulated metallic-fueled LMFBR core characteristics [A.2-3.]. As sample Doppler measurements were not done in the FCA XXIII cores, applicability of the neutron cross-section libraries generated from the JENDL-3.3 data set was evaluated for Doppler effects with the benchmark data obtained in the metal-fueled fast reactor spectra. [A.2-4]

(3) Benchmark Data for Effective Delayed Neutron Fraction

To improve the accuracy of predictions of the effective delayed neutron fraction, a program of benchmark experiments was carried out as an international collaboration [A.2-5]. Three different core configurations were selected including the enriched uranium core (FCA XIX-1), the plutonium/natural-uranium core (FCA XIX-2), and the plutonium core without uranium (FCA XIX-3). In parallel, two additional core configurations provided independent benchmark data, namely the R2 (U-core) and Zona2 (MOX-core) of MUSARCA of CEA/Cadarache. In those cores, criticality and central spectrum indices were measured as well. The independent benchmark data were provided as simplified models with correction factors. [A.2-2]

Basic delayed neutron fraction data were taken from the JENDL-3.3 file for the 4S design methods. Through analyses of the above benchmark data, validation was conducted for the effective delayed neutron fractions.

A.2.1.2 Criticality

(1) Analysis Methods for the Benchmark Data

The calculations for the benchmark data utilized homogeneous two-dimensional RZ models that were provided in the open literature [A.2-1], applying the 4S nuclear design methodology (combination of basic calculation methods and cross-section libraries). Necessary correction factors associated with homogenization of the plate cells used in the FCA cores were applied to the calculated characteristics to compare them with the measured data.

In addition to the standardized 4S nuclear design methods, several comparisons were performed in terms of the calculated results from the continuous-energy Monte Carlo codes, MVP vs. MCNP, with nuclear data libraries, MVP-library vs. MCNP-library, which were generated from the JENDL-3.3 nuclear files. For the deterministic discrete-ordinate transport calculations, two types of energy groups were compared. Although the standard method uses the 70 energy group structure with SLAROM code for preparation of the effective cross-sections, for this comparison, a more detailed 900 energy group structure with the SLAROM-UF code was used.

All analyses were done with the RZ geometries and homogenized compositions specified for the benchmark calculations. Two continuous-energy Monte Carlo codes were used with the libraries processed from JENDL-3.3 [A.2-6] in combinations of MVP [A.2-7], and MCNP5 [A.2-8]/FXLIB-J33 [A.2-9]. Deterministic discrete-ordinate transport calculations were also performed with the 900-group S8-approximation by TWODANT [A.2-10] as well as the conventional 70-group S8-calculations using the JFS-3-J3.3 library [A.2-11]. The 900 energy group calculation with SLAROM-UF code [A.2-12] incorporated the ultra-fine group treatments for resonances for the low-energy region and improved slowing down treatments from the original SLAROM [A.2-13] code.

(2) Comparison of Results

The calculated multiplication factors were compared with the benchmarked effective multiplication factors evaluated in the handbook, as tabulated in Table A.2.2-1.

Using the 4S nuclear design methods, for the three LEU cores, MVP2 calculations showed an average C/E of 0.9936 with a standard deviation of 0.0028, and 70 energy group S8-transport calculated an average C/E as 0.9946 with a standard deviation of 0.0031. The S8-transport calculations with conventional 70 energy group calculations also reproduced very close C/E values with MVP results within 0.15%$\delta\rho$ for a wide range of fast spectra. For HEU cores, C/E values higher by +1.2%$\delta\rho$ than those for the LEU cores were shown. The results indicate that the 900-group calculations predicted multiplication factors close enough relative to those obtained by the MVP rather than those from the 70 energy group calculations.

Additional useful information (refer to Table A.2.1-1 (core identification and U enrichment) and Table A.2.2-1 (C/E-values for the top three HUE core and lower three LEU cores)) was obtained through inter-comparison of results by using different codes and libraries.

- Good agreement was confirmed between the results from the MVP and MCNP5 codes within statistical uncertainties. The averaged C/E values and standard deviations through the MVP calculations are 0.9936 +/- 0.0028 for the LEU cores, and 0.9924 +/- 0.0023 with MCNP.

- The relative relationship was seen in the HEU cores, that is, the averaged C/E values and standard deviations through the MVP calculations are 1.0053 +/- 0.0099, and 1.0049 +/- 0.0099 with MCNP.

- The advanced 900 energy group calculations produced similar trends to the continuous-energy results with +0.12% bias in the LEU cores and +0.27% bias in the HEU cores, respectively. C/E values obtained with JENDL-3.3 libraries showed dependence on the enrichment level.

- For the ZPR-9/34, EU/Fe core, the 900 energy group calculation significantly improved the C/E value from 1.040 calculated by the standard 70 energy group structure of the JFS-3 type constant set, to 1.021 obtained from the 900 energy group structure with the SLAROM-UF code, compared to the results from the MVP calculation. This core consists of 93% enriched uranium metal and large fractions of iron plates. It has been recognized that the standard 70-group JFS3-type energy structure was not suitable for pure iron-rich mixed compositions. For mixtures such as stainless steel, this problem does not appear because the scattering resonance is appropriately self-shielded. It is recognized that the C/E values for the ZPR-9/34 core derived by the continuous-energy Monte Carlo calculations are within the ordinary deviations of the k-effective values in benchmark analyses.

- The average C/E values of three LEU cores are 0.9936, with standard deviations (std) of 0.0028 for Monte Carlo, and 0.9946 with std of 0.0032 for the 70 energy group S8 calculations with the JENDL-3.3 basis, respectively. The present homogenized benchmark problems provided good consistency between the two calculation methods selected as the basis for the nuclear design methods.

Additional ZPPR-21 core series were analyzed with the 900 energy group S8 calculations in RZ models including comparisons of benchmarked criticalities between JENDL-3.3 and ENDF/B-VII.0 bases [A.2-14]. The results are tabulated in Table A.2.2-2.

The C/E trends are similar between the two libraries and provided stable biases among the ZPPR-21 cores, despite the wide ranges for combinations of U-235, U-238, and Pu-239. The C/E values obtained using the S8 calculation for the ZPPR-21F core are 1.0058 for the JENDL-3.3 based 900 energy group library, and 1.0102 for the ENDF/B VII.0 based library. Those numbers are as much as 1.1%$\delta\rho$ higher than those for the LEU cores mentioned above,

because the U-235 enrichment was about 36%. For Pu cores in ZPPR-21 series, similar discrepancies of about 0.6%$\delta\rho$ were observed between the JENDL-3.3 and ENDF/B VII.0 data.

The overall trend demonstrated that the C/E values obtained with the JENDL-3.3 libraries showed dependence on the U-235 enrichment. However in the LEU range, the C/E values remained stable.

Those results support the adequacy of the 4S nuclear design method especially from the BOL to EOL ranges.

A.2.3 Sample Doppler Reactivity

Validation efforts were made by the benchmark analyses provided from the FCA XVI-1 and -2 cores using S8 transport calculations in combination with the JFS-3-J3.3 70 energy group library. A two-dimensional RZ model for the reactor and sample region with an isolated Doppler sample cell model was used to get the effective sample cross-sections with the SLAROM code as shown in the reference. Simplified homogeneous models for the FCA fuel cells ignore the heterogeneous effects due to thin and dense plate fuels used in the FCA XVI cores.

Detailed correction factors associated with the FCA fuel heterogeneity effects were taken from [A.2-3]. The 70 energy group [A.2-11]-S8 and 900 energy group [A.2-14]-S8 calculations were made using constant sets generated from JENDL-3.3. The results are shown in Table A.2.3-1. As discussed in chapter A.2.2-2, the 900 energy group calculations predicted multiplication factors close enough relative to those obtained by the MVP rather than those from the 70 energy group calculations. As treatment for the self-shielding factors in the Doppler regions has been improved in the 900 energy group library, it is anticipated that the continuous-energy Monte Carlo calculation can provide good C/E values near 1.00 with the detailed models in the MVP calculations for adequate amounts of the Doppler reactivity.

The results for the reported correction factors are tabulated in Table A.2.3-1. The JENDL 70 energy group set can predict the U-238 Doppler reactivity changes with C/E values in the range of 0.91-1.00. The C/E value had some variation between the Doppler samples (NU-metal or NU-oxide) and the benchmark cores.

A.2.4. Effective Delayed Neutron Fractions

Delayed neutron fraction analyses were made to estimate the uncertainty of the delayed neutron fractions (β_{eff}) in the 4S core, applying the 4S nuclear design methods using the JENDL-3.3 file. The analyses selected the international benchmark experiments for effective delayed neutron fraction from the FCA XIX core series [A.2-3]. Three cores, FCA XIX-1, -2 and -3, cover a wide variety of contributions from U-235, U-238 and Pu-239 fission within the fast spectrum ranges. The report also included the simplified core data for the benchmark core R2 and ZONA cores in the MASURCA facility. The outline of the cores is provided in Table A.2.4-1.

Two of the cores (FCA XIX-1 and MASURCA R2) corresponded to enriched uranium fuel compositions in which approximately 80% of the beta-effective values consist of contributions from U-235 fission. Beta-effective values of two of the plutonium cores (FCA XIX-2 and MASURCA ZONA2) consist of contributions of U-238 and Pu-239 fissions with more than 40% of the total combined, respectively. About 80% of the total β-effective value in the FCA XIX-3 core was attributed to Pu-239 fission.

Analyses were made by S8-transport (TWODANT) calculations using the 70 energy group JFS-3-J3.3 set with RZ models. Nuclide-wise delayed neutron data were also taken from the JENDL-3.3 library file.

For the measured values, correction factors due to plate-heterogeneity provided in the FCA fuel drawers in [A.2-3] were directly applied in this analysis. Geometry model correction factors were quoted from [A.2-3] as well. On the other hand, no specifications for heterogeneous and model correction factors were given for the above reported data for MASURCA experiments. No larger corrections are expected than corrections in the FCA case, because rodlet-type fuel drawers were used in the MASURCA experiments.

Table A.2.4-2 summarizes the comparison with the calculated values for the corresponding characteristics. The C/E results for the beta-effective showed the JENDL-3.3 base data can predict within 3% uncertainties for the very wide combinations of the fission contributions of U-235, U-238, and Pu-239, which cover range of nuclides fractions that changes during the 4S lifetime.

A.2.5 Remarks

Combining the C/E value trends for the LEU cores and the ZPPR-21 cores, the results imply that large bias factor shifts of the multiplication factors during the reactivity life time for the 4S core are not anticipated.

The analysis results provided stable C/E values near 1.00 plus or minus several percent for the beta-effective, fission spectrum indexes, and criticality in large composition variants. Concerning criticality, almost all of the C/E values from the JENDL-3.3 libraries are kept consistent for the FCA XXIII and FCA XIX experiments with those uranium benchmarked model analyses.

Therefore it is concluded that the evaluation provides appropriate uncertainty evaluation bases for the nuclear characteristics for safety analyses in the 4S design

Reference

[A.2-1] Nuclear Energy Agency, "International Handbook of Evaluated Criticality Safety Benchmark Experiments," September, 2005 Edition. NEA/NSC/DOC(95)/03/III. IEU-MET-FAST-010 (U9), IEU-COMP-FAST-001 (ZPR-6/6A), IEU-MET-FAST-012 (ZPR-3/41), HEU-MET-FAST-061(ZPPR-21F), HEU-MET-FAST-061(ZPPR-21F), HEU-MET-FAST-061(ZPPR-21F), HEU-MET-FAST-055(ZPR-3/23), HEU-MET-FAST-060(ZPR-9/3),

HEU-MET-INTER-001(U/Iron), PU-MET-FAST-033(ZPPR-21A), MIX-MET-FAST-011 (ZPPR-21B,21C,21D,21E).

[A.2-2] Y. Tsuboi , S. Matsuyama and M. Kawashima, "Development of The 4S and Related Technologies (8) An Analysis of Delayed Neutron Fraction Benchmark Results Using Nuclear Design Methodology", Proceedings of ICAPP '09, Tokyo, Japan, May 10-14, 2009, Paper 9184

[A.2-3] H. Oigawa, et al., "A proposal of Benchmark Calculation on Reactor Physics for Metallic Fueled and MOX Fueled LMFBR Based upon Mock-up Experiment at FCA," Journal of Nucl. Sci. and Technol., Vol. 37, No. 2, pp. 186-201 (February 2000).

[A2-4] Y. Tsuboi, Y. Moriki, M. Kawashima, "Criticality and Doppler Benchmark Calculations for Small Fast Core", Trans. Am. Nucl. Soc., November,11, 2008, Reno, Nevada

[A.2-5] S. Okajima, et al., "Summary on International Benchmark Experiments for Effective Delayed Neutron Fraction (β_{eff})," Progress in Nuclear Energy, Vol. 41, No. 1-4, pp. 285-301, 2002.

[A.2-6] K. Shibata, et.al "Japanese Evaluated Nuclear Data library Version 3 Revision-3: JENDL-3.3' J. Nuclear Sci. Technol. Vol.39. [11], 1125 (2002).

[A.2-7] T. Mori., M. Nakagawa, M. Sasaki, "Vectorization of Continuous Energy Monte Carlo Method for Neutron Transport Calculation", J. Nucl. Sci. Technol., Vol. 29, [4], 325 (1992).

[A.2-8] X-5 Monte Carlo Team, "MCNP – A General Monte Carlo N-Particle Transport Code, Version-5," LA-UR-03-1987, LANL (April 2006).

[A.2-9] K. Kosako et al., "The Libraries FSXLIB and MATXSLIB Based on JENDL-3.3," JAERI, JAERI-Data/Code 2003-011 (July 2003).

[A.2-10] R. E. Alcouffe, et al., "DANTSYS: A Diffusion Accelerated Neutral Particle Transport Code System," LA-12969-M (1995).

[A.2-11]http://rpg.jaea.go.jp/code/JFS-3-J33/index.html (In Japanese) .

[A.2-12] T. Hazama et al., "Development of a Fine and Ultra-Fine Group Cell Calculation Code SLAROM-UF for Fast Reactor Analyses" J. Nucl. Sci. and Technol., 43, 908 (2006).

[A.2-13] M. Nakagawa, et al., "A Code for Cell Homogenization of Fast Reactor," JAERI 1294 (1984).

[A.2-14] G. Chiba, et al., "Benchmark Test of Evaluated Nuclear Data Files for Fast Reactor Neutronics Application," JAEA-Research 2007-051 [in Japanese].

Table A.2.1-1. Outline of the Selected Enriched Uranium Fast-Spectrum Cores

Assembly	Pu [1]	U5 [2]	R(cm)	H(cm)	Core
4S(BOL)	---	17.6	10/47 [3]	250	Zr 29a%
FCA XXIII	15	11	9/32 [3]	112	Zr 23a%
ZPR-9/34		93	62.2	183.2	EU/Fe
ZPR-3/23		93	30.8	50.9	HEU
ZPPR-21F		62	19.0	41.4	EU
ZPR-6/6A		16.5	91.2	91.2	EU/oxide
ZPR-3/41		17.0	41.6	81.5	EU/Al
ZPR-U9		9.0	41.0	76.4	EU

Notes:
1) Pu=Pu fraction in total heavy metal (Pu+U)
2) U5=U-235 fraction in total heavy metal
3) Equivalent inner radius/outer radius of core

Table A.2.1-2. Outline of the ZPPR-21 Cores

Assembly	Pu [1]	U5 [2]	R(cm) [3]	H(cm)	Core
ZPPR-21E	7.8	51.3	19	41	Zr 31a%
ZPPR-21D	18.1	37.7	19	41	Zr 31a%
ZPPR-21C	27.8	28.5	19	41	Zr 31a%
ZPPR-21B	41.6	10.7	19	41	Zr 31a%
ZPPR-21A	52.3	0.1	19	41	Zr 31a%

Notes:
1) Pu=Pu fraction in total heavy metal (Pu+U)
2) U5=U-235 fraction in total heavy metal
3) Equivalent inner radius/outer radius of core

Table A.2.2-1. Criticality C/E Values for the Enriched Uranium Cores from JENDL-3.3 Library

Assembly	MVP2		MCNP		S8	S8
	C/E	Errors	C/E	Errors	900Gr	70Gr
ZPR-9/34	1.0154	0.28	1.0150	0.29	1.0205	1.0400
ZPR-3/23	0.9957	0.28	0.9953	0.28	0.9973	1.0025
ZPPR-21F	1.0047	0.25	1.0043	0.25	1.0061	1.0058
Ave/SD [3]	1.005/0.0099		1.0049/0.0099			1.016/0.021
ZPR-6/6A	0.9904	0.23	0.9897	0.24	0.9912	0.9914
ZPR-3/41	0.9955	0.27	0.9941	0.27	0.9969	0.9977
ZPR-6/9 U9	0.9948	0.24	0.9933	0.24	0.9962	0.9947
Ave/SD [3]	0.9936/0.0028		0.9924/0.0023			0.9946/0.0031

Notes:
1) K-benchmark errors = approximately 0.25%$\delta\rho$
2) Errors by Monte Carlo calculations in %$\delta\rho$
3) Ave/SD= Averge/Standard deviation

Table A.2.2-2. C/E Values with 900 Energy Group S8 Calculations for ZPPR-21 Benchmark Cores

Assembly	Pu/HM	U5/HM	900 Energy Group S8 RZ Models [1]	
			JENDL-3.3	ENDF/B-VII.0
ZPPR-21F	0.0	62.2	1.0061	1.0097
ZPPR-21E	7.8	51.3	1.0040	1.0083
ZPPR-21D	18.1	37.7	1.0019	1.0065
ZPPR-21C	27.8	28.5	0.9945	0.9990
ZPPR-21B	41.6	10.7	1.0037	1.0086
ZPPR-21A	52.3	0.1	1.0004	1.0056

Note:
1) 900 energy group S8 transport calculations in RZ benchmarked models

Table A.2.3-1. Examples of C/E Values for Doppler Reactivity by the Simplified Homogeneous Models

FCA Core ID	Doppler Sample	Measured Worth (20°C – 800°C) [1.0E-06 δρ]	C/E value	
			70 energy group S8 with JENDL-3.3	900 energy group S8 with JENDL-3.3
XVI-1	NU	-9.64±0.19	0.85	0.94
	NUO_2	-4.35±0.18	0.86	0.97
XVI-2	NU	-7.47±0.21	0.89	0.98
	NUO_2	-3.86±0.26	0.82	0.92
Average			0.85	095
Standard Deviation			0.03	0.03

Table A.2.4-1. Outline of the Cores and Measured Characteristics

Assembly	FCA			MASURCA	
Test No.	XIX-1	XIX-2	XIX-3	R2	ZONA2
R (cm) [1]	33.0	35.7	35.1	48.4	49.8
H (cm)	50.8	61.0	61.0	61.0	61.0
Pu/(Pu+U) [2]	---	23.5	100	---	27
U235/U %	93	0.7	---	30	0.3
Moderator [3]	C	SS	SS	O	O
Value	1.0075	1.0032	1.0031	0.9988	0.9995
Error %	0.06	0.03	0.03	0.012	0.006
F28/F25 [4]	0.0395	0.0408	0.035	0.0413	
Error %	1.3	1.4	2.0	1.5	
F49/F25 [4]	-----	1.056	1.083	-----	
Error %	-----	1.3	1.2	-----	
Beta (pcm)	742	364	251	721	349
Error (pcm)	24	9	4	11	6

Notes:
1) Size: R=equivalent radius
2) Pu/(Pu+U): average Pu enrichment in %
3) Moderator: C=carbon, SS=stainless steel, O=oxygen
4) Reaction rate ratios: F28=U-238(n,f),F25=U-235(n,f), F49=Pu-239(n,f)

Table A.2.4-2. C/E Values for the Benchmark Data

Assembly	FCA			MASURCA	
Items	XIX-1	XIX-2	XIX-3	R2	ZONA2
Criticality	0.990	0.996	1.017	0.990	0.992
F28/F25	1.012	0.978	0.968	0.901	1.039
F49/F25	-----	1.013	0.992	-----	1.004
$\beta_{eff.}$	0.994	0.991	0.975	1.017	0.991

Note:
70 energy group S8-FOP, JENDL-3.3 based library JFS-3-J3.3

A.3 Selected Topics from Small Fast Reactor JOYO MK-1 Benchmark Data Analyses

A.3.1 Benchmark Data and Analyses

In addition to the analyses of the critical experimental data, the previous fast reactor data have been analyzed with the 4S nuclear design methods (combination of the transport calculations and the cross-section libraries generated from the JENDL3.3 data file).

The measurement data and models were taken from the JOYO nuclear characteristics evaluation data [A.3-1] for the International Reactor Physics Experiment Evaluation (IRPhE) project that has been promoted by OECD/NEA.

In this context, Criticality Two benchmark critical experimental configurations are described and evaluated. The first core has 64 core fuel subassemblies, and the second core, 70.

The power distribution measurements in the initial low-power physics testing and burnup reactivity losses were also traced with the 4S nuclear design method.

In 1977 and 1978, prior to the first power ascension to 50 MW in the MK-I core, various nuclear characteristics including the criticality, control rod worth, sodium void reactivity worth, fuel reactivity worth at the core periphery relative to a blanket subassembly, and isothermal temperature coefficient, were measured under very low-power conditions. It is expected that those data are more appropriate for benchmark modeling compared with those measured under higher burnup conditions, because neither fuel burnup nor component deformation by irradiation had yet occurred to a significant degree.

Power operation testing in JOYO provided measured results for reactivity losses, which had not been obtained from the critical experiments.

The 4S nuclear design methods were applied to analyses for those nuclear characteristics demonstrated in the small leakage-dominant JOYO MK-1 core.

A.3.2 Criticality

In the JOYO reactor, criticality is achieved by control rod operation. Under stable temperature conditions and a constant sodium flow rate, the control rod positions are carefully adjusted to realize a stable criticality condition according to the neutron flux monitors. When the operators or experimenters judge the criticality condition has been achieved, all the control rod positions are recorded, as well as the coolant temperature (virtually equivalent to the core temperature in low-power conditions), and the core layout. The coolant temperature is measured as an average value of the reactor vessel outlet and inlet temperature signals. The combined uncertainty of the experimental values was consolidated with the possible factors relating to measurements including control rod worth, excess reactivity, isothermal temperature effects, and so on.

For the analysis of criticality, a pin-by-pin detailed MVP model was used for the isothermal temperature 250°C conditions (geometries and compositions in [A.3-2]) including control rod absorber modeling. Figure A.3.2-1 shows the cross-section view of the calculation model. Figure A.3.2-2 shows the MVP models (whole core and pin-wise configurations) used in these calculations.

Table A.3.2-1 shows a comparison of measured and calculated criticality data. The C/E values for the two cores are 0.9963±0.0018 and 0.9966±0.0018, respectively. Those numbers are close to those C/E values obtained from the MVP analysis for the critical experiments in the FCA XXIII cores (C/E values: 0.997 for the FCA-XXIII-1 core, 0.998 for the FCA-XXIII-1DU core).

A.3.3 Reaction Rates

During the low-power test period, reaction rate distributions were measured using special subassemblies in the core and blanket regions. Five special subassemblies were prepared to place various kinds of foils in the core and blanket, respectively. In the special core-type fuel subassembly, seven central fuel pins were replaced with a tube containing stainless steel pellets (foil-holder SS) to place various thin foils in the axial direction for the core fuel. In the special blanket-type fuel assembly, the one central pin was replaced with a tube.

By replacing the reference core and blanket fuel subassemblies with the special assemblies, 12 irradiation tests were carried out to measure power distributions in the core and blanket region.

The irradiated foils were recovered after the testing and reaction rates were obtained by measurements of radioactivity of each foil. The reaction rates obtained were U-235(n,f), U-238(n,f), (n,g), Pu-239(n,f), Th-232(n,f), Au-197(n,g),Na-23(n,g), Ni-58(n,p), and Cu-63(n,g),(n,a).

Three different types of loading patterns of the test subassemblies were chosen for the runs. The test subassemblies were loaded in a row from the core center to the radial reflector position for the first case. For the second case, some were placed in fuel storage rack position surrounding blanket region. Also, they were loaded into the core-blanket boundary and positions adjacent to the control rods, which were half inserted.

Relative reaction rate distributions were analyzed with the pin-by-pin model, which covers the irradiated foil and foil-holders' geometry, as well, using continuous-energy Monte Carlo MVP calculations for U-235(n,f), Pu-239(n,f), U-238(n,f), and U-238(n,g) reaction rates.

The results are shown in the form of C/E values from Table A.3.3-1 to Table A.3.3-4. Also, comparisons are depicted in Fig. A.3.3-1 to Fig.A.3.3-8 between the measured and calculated distributions. It is confirmed that the C/E values in the core region are very close to 1.00. In Tables A.3.3-4 to A.3.3-8, correction factors due to foil-holder and foil effects are shown. The results reveal that reaction rates measured by the foils are closely correlated to the actual reaction rates in the fuel pins, at least in the core region.

Those analysis results support that the 4S design methodology is adequate for the past actual fast cores.

References

[A.3-1] NEA/NSC/DOC (2006)1, "Japan's Experimental Fast Reactor JOYO MK-I core: Sodium-Cooled Uranium-Plutonium Fueled Fast Core Surrounded by UO_2 Blanket"

[A.3-2] K. Yokoyama et al., "Reevaluation on Experimental Data and Analysis with the Latest Reactor Physics Calculation Method on Fast Experimental Reactor", JNC-TN9400 2005-024

Table A.3.2-1. C/E Values for Criticality of JOYO MK-1 Core

	Effective Multiplication Factors and Errors					
	Calculated[1] (C)		Measured[2),3)] (E)		(C/E)	
Minimum Critical Core (64 core subassemblies)	0.99739	±0.00019	1.0011	±0.0018	0.9963	±0.0018
Initial Core (70 core subassemblies)	0.99473	±0.00019	0.9981	±0.0018	0.9966	±0.0018

Notes:

1) MVP continuous-energy Monte Carlo calculations with the library generated from JENDL-3.3. Total history: 100-million, Statistical error: 1σ
2) Control Rod Positions: adjusted critical positions near criticality
3) Adopted from NEA/NSC/DOC(2006)1, Table 3.15and Table 3.17. Statistical error: 3σ

Table A.3.3-1. C/E Values for Relative Reaction Rate Distributions for U-235(n,f) Reaction Rate

Foil Position		Core					Radial Blanket				Reflector	Comments
		0X	1F1	2F1	3F1	4F1	5F1	6F1	7F1	8F1	9F1	
Axial Blanket	+500	1.049 ±6.4		1.169 ±6.7	1.035 ±7.0							
	+400	1.015 ±5.6		0.979 ±5.6	1.056 ±6.0							
	+300	0.994 ±3.5		1.068 ±3.6	0.985 ±3.6							
Core	+200	1.017 ±3.4	1.011 ±3.5	1.004 ±3.4	1.001 ±3.4	1.019 ±3.5	0.967 ±5.5	1.118 ±6.5	1.093 ±7.3	1.065 ±11.1	1.051 ±10.2	Foil thickness in model: 0.5mm
	+100	0.981 ±3.3	0.993 ±3.3	1.004 ±3.3	1.020 ±3.4	1.019 ±3.4	0.974 ±5.5	1.079 ±5.8	1.041 ±6.9	1.065 ±7.7	0.896 ±9.0	Upper Number: C/E-value for Lower Number: Errors(%)
	0	1.000 ±3.3	1.012 ±3.3	1.010 ±3.3	1.006 ±3.3	0.991 ±3.4	1.029 ±5.5	1.106 ±5.7	1.004 ±6.5	1.110 ±7.5	1.007 ±10.3	Average C/E-value and 1) Core Region: 1.007±3.4 2) Axial Blanket Region: 1.051±6.2 3) Radial Blanket Region 1.054±6.8 4) Reflector Region: 0.985±9.8
	-100			1.005 ±3.3	0.993 ±3.4							
	-200											
	-300											
Axial Blanket	-400											
	-500											

Note:
Calculation: MVP with detail geometry model for pins and SS-holders, foils, JENDL-3.3 lib.

Table A.3.3-2. C/E Values for Relative Reaction Rate Distributions for Pu-239 (n,f) Reaction Rate

Foil Position		Core					Radial Blanket				Reflector	Comments
		0X	1F1	2F1	3F1	4F1	5F1	6F1	7F1	8F1	9F1	
Axial Blanket	+500	1.153 ±6.3										
	+400	1.109 ±7.7										
	+300	1.019 ±3.5										
Core	+200	1.053 ±3.3	1.040 ±3.3	1.036 ±3.3	1.065 ±3.4	1.070 ±3.6	1.125 ±5.7	1.122 ±6.4	1.133 ±8.2	1.022 ±10.1	1.455 ±20.1	Foil thickness in model: 0.5mm
	+100	0.997 ±3.3	1.015 ±3.3	1.027 ±3.3	1.000 ±3.3	1.034 ±3.4	1.067 ±5.5	1.077 ±6.1	1.116 ±8	1.045 ±11.7	0.785 ±10	Upper Number: C/E-value for Lower Number: Errors(%)
	0	1.000 ±3.3	1.017 ±3.3	1.012 ±3.3	1.052 ±3.3	1.030 ±3.4	1.071 ±5.5	1.172 ±6.2	1.056 ±8.9	1.326 ±14.9	0.974 ±12.3	Average C/E-value and 1) Core Region: 1.028±3.3 2) Axial Blanket Region: 1.131±7.0 3) Radial Blanket Region 1.111±8.1 4) Reflector Region: 1.072±14.1
	-100	1.009 ±3.3										
	-200											
	-300											
Axial Blanket	-400											
	-500											

Note:
Calculation: MVP with detail geometry model for pins and SS-holders, foils, JENDL-3.3 lib.

Table A.3.3-3. C/E Values for Relative Reaction Rate Distributions for U-238(n,f) Reaction Rate

Foil Position		Core					Radial Blanket				Reflector	Comments
		0X	1F1	2F1	3F1	4F1	5F1	6F1	7F1	8F1	9F1	
Axial Blanket	+500	1.039 ±12		0.896 ±13.9	1.339 ±16.6							Foil thickness in model: 0.5mm Upper Number: C/E-value for Lower Number: Errors(%) Average C/E-value and 1) Core Region: 1.074±5.2 2) Axial Blanket Region: 1.171±12.0 3) Radial Blanket Region 1.214±16.2 4) Reflector Region: 0.717±37.1
	+400	1.239 ±9.5		1.091 ±8.9	1.423 ±11.0							
	+300	1.111 ±5.5		1.179 ±5.9	1.243 ±6.4							
Core	+200	1.045 ±5.0	1.059 ±5.1	1.047 ±5.2	1.099 ±5.4	1.175 ±5.8	1.308 ±9.3	1.466 ±12.7	0.986 ±21.9	1.085 ±23.5	0.638 ±41.4	
	+100	1.026 ±4.8	1.000 ±4.8	1.025 ±4.9	1.053 ±5.1	1.157 ±5.5	1.222 ±8.4	1.245 ±11.3	1.165 ±16	1.581 ±23.3	1.010 ±35.8	
	0	1.000 ±4.7	1.059 ±4.7	1.058 ±4.8	1.104 ±5.0	1.130 ±5.4	1.344 ±8.2	0.995 ±10.1	1.008 ±16.2	1.160 ±33.2	0.504 ±34.1	
	-100	1.036 ±4.8		0.974 ±4.9	0.964 ±5							
	-200											
	-300											
Axial Blanket	-400											
	-500											

Note:
Calculation: MVP with detail geometry model for pins and SS-holders, foils, JENDL-3.3 lib.

Table A.3.3-4. C/E Values for Relative Reaction Rate Distributions for U-238(n,γ) Reaction Rate

Foil Position		Core					Radial Blanket				Reflector	Comments
		0X	1F1	2F1	3F1	4F1	5F1	6F1	7F1	8F1	9F1	
Axial Blanket	+500	0.811 ±10.1										Foil thickness in model: 0.5mm Upper Number: C/E-value for Lower Number: Errors(%) Average C/E-value and 1) Core Region: 0.994±6.9 2) Axial Blanket Region: 0.824±9.5 3) Radial Blanket Region 1.092±16.2 4) Reflector Region: 0.415±21.7
	+400	0.837 ±9.0										
	+300	0.931 ±7.7										
Core	+200	1.003 ±6.5										
	+100	1.002 ±6.3										
	0	1.000 ±6.8	1.022 ±6.5	0.995 ±6.7	1.007 ±6.6	1.019 ±8.3	1.008 ±8.1	1.087 ±13.0	1.090 ±25.3	1.182 ±18.5	0.415 ±21.7	
	-100	0.965 ±7.3										
	-200											
	-300											
Axial Blanket	-400											
	-500											

Note:
Calculation: MVP with detail geometry model for pins and SS-holders, foils, JENDL-3.3 lib.

Table A.3.3-5. Correction Factors Due to Foil and SS-holder Effects for U-235(n,f) Reaction Rates

Foil Position		Core					Radial Blanket				Reflector	Comments
		0X	1F1	2F1	3F1	4F1	5F1	6F1	7F1	8F1	9F1	
Axial Blanket	+500	0.952 ±4.7		0.850 ±5.0	0.953 ±5.6							Foil thickness in model: 0.5mm Upper Number: C/E-value for Lower Number: Errors(%) Average C/E-value and 1) Core Region: 0.980±1.9 2) Axial Blanket Region: 0.951±4.2 3) Radial Blanket Region 0.889±5.3
	+400	0.992 ±3.0		1.032 ±3.1	0.929 ±3.8							
	+300	1.000 ±2.1		0.947 ±2.5	0.969 ±2.4							
Core	+200	0.969 ±1.8	0.973 ±2.0	0.991 ±1.9	0.967 ±2.0	0.959 ±2.2	0.938 ±2.9	0.830 ±4.8	0.866 ±6.2	0.864 ±11.0		
	+100	0.982 ±1.6	0.979 ±1.6	0.996 ±1.8	0.997 ±1.9	0.989 ±2.0	0.882 ±2.8	0.850 ±3.6	0.940 ±5.7	0.925 ±7.4		
	0	1.000 ±1.6	0.982 ±1.6	0.977 ±1.7	0.981 ±1.7	0.961 ±1.9	0.857 ±2.7	0.845 ±3.6	0.934 ±5.1	0.936 ±7.9		
	-100			0.983 ±1.7	0.993 ±1.8							
	-200											
	-300											
Axial Blanket	-400											
	-500											

Table A.3.3-6. Correction Factors Due to Foil and SS-holder Effects for Pu-239(n,f) Reaction Rates

Foil Position		Core					Radial Blanket				Reflector	Comments
		0X	1F1	2F1	3F1	4F1	5F1	6F1	7F1	8F1	9F1	
Axial Blanket	+500	0.959 ±5.1										Foil thickness in model: 0.5mm Upper Number: C/E-value for Lower Number: Errors(%) Average C/E-value and 1) Core Region: 0.996±1.7 2) Axial Blanket Region: 0.937±5.7 3) Radial Blanket Region 0.892±7.9
	+400	0.916 ±6.3										
	+300	0.986 ±2.1										
Core	+200	0.989 ±1.7	0.989 ±1.7	1.016 ±1.7	1.004 ±1.9	0.974 ±2.3	0.934 ±3.6	0.861 ±5.4	0.798 ±7.8	0.940 ±11.7		
	+100	0.995 ±1.5	0.984 ±1.6	1.014 ±1.7	1.027 ±1.7	0.990 ±1.9	0.931 ±3.9	0.836 ±4.2	0.857 ±7.3	1.027 ±14.6		
	0	1.000 ±1.5	0.990 ±1.5	0.992 ±1.6	0.989 ±1.7	1.001 ±1.9	0.844 ±2.9	0.825 ±4.4	1.049 ±12.1	0.804 ±17.5		
	-100	0.985 ±1.6										
	-200											
	-300											
Axial Blanket	-400											
	-500											

Table A.3.3-7. Correction Factors Due to Foil and SS-holder Effects for U-238(n,f) Reactions Rates

Foil Position		Core					Radial Blanket				Reflector	Comments
		0X	1F1	2F1	3F1	4F1	5F1	6F1	7F1	8F1	9F1	
Axial Blanket	+500	0.882 ±13.5		0.957 ±15.2	0.780 ±17.9							Foil thickness in model: 0.5mm Upper Number: C/E-value for Lower Number: Errors(%) Average C/E-value and 1) Core Region: 0.976±4.9 2) Axial Blanket Region: 0.848±12.6 3) Radial Blanket Region 0.838±19.9
	+400	0.787 ±9.2		0.888 ±8.9	0.796 ±10.9							
	+300	0.956 ±5.5		0.902 ±5.9	0.939 ±6.5							
Core	+200	0.982 ±4.6	0.962 ±4.8	0.987 ±4.9	0.965 ±5.2	1.016 ±5.8	0.799 ±9.6	0.732 ±15.2	1.282 ±25.7	0.881 ±32.6		
	+100	0.954 ±4.3	1.003 ±4.3	1.004 ±4.6	1.019 ±4.8	0.993 ±5.4	0.846 ±8.3	0.734 ±12.9	0.723 ±20.1	0.639 ±35.3		
	0	1.000 ±4.3	0.925 ±4.3	0.942 ±4.4	0.945 ±4.7	1.006 ±5.3	0.731 ±7.9	0.824 ±11.8	1.022 ±19.4	0.839 ±39.4		
	-100	0.932 ±4.4		1.015 ±4.5	1.048 ±4.7							
	-200											
	-300											
Axial Blanket	-400											
	-500											

Table A.3.3-8. Correction Factors Due to Foil and SS-holder Effects for U-238(n,γ) Reaction Rates

Foil Position		Core					Radial Blanket				Reflector	Comments
		0X	1F1	2F1	3F1	4F1	5F1	6F1	7F1	8F1	9F1	
Axial Blanket	+500	0.802 ±9.3										Foil thickness in model: 0.5mm Upper Number: C/E-value for Lower Number: Errors(%) Average C/E-value and 1) Core Region: 0.973±5.2 2) Axial Blanket Region: 0.896±9.5 3) Radial Blanket Region 0.633±16.2
	+400	0.989 ±9.8										
	+300	0.968 ±6.4										
Core	+200	0.966 ±4.4										
	+100	0.988 ±4.0										
	0	1.000 ±4.8	0.977 ±4.7	0.987 ±4.8	0.961 ±4.6	0.885 ±7.2	0.792 ±7.2	0.650 ±13.2	0.610 ±25.5	0.481 ±18.9		
	-100	1.029 ±5.6										
	-200											
	-300											
Axial Blanket	-400											
	-500											

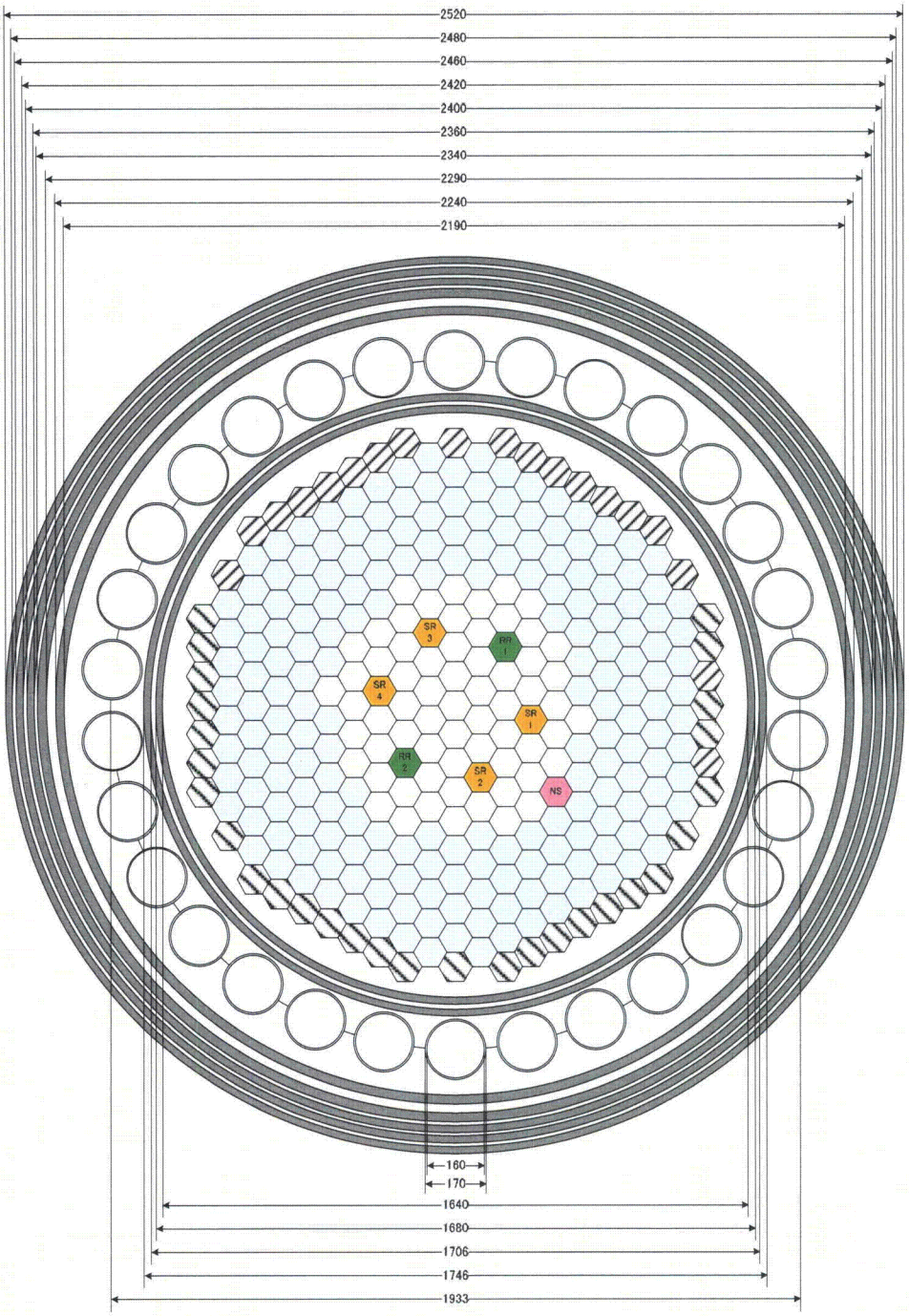

Fig. A.3.2-1. Cross-Sectional View of JOYO MK-1 Core

: Special subassembly (Core –type x = 1 to 4)

: Special subassembly (Blanket-type x=1)

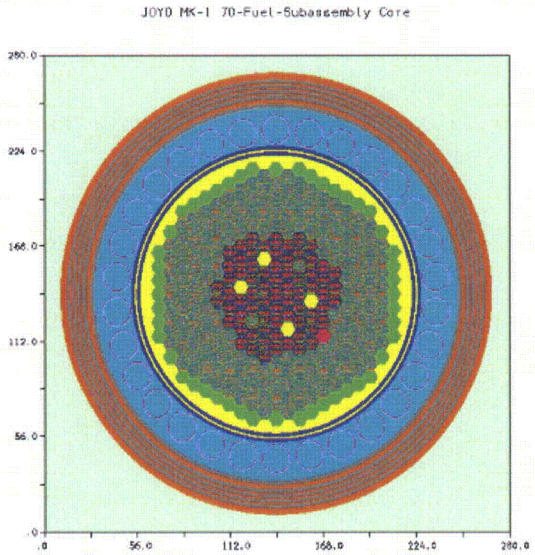

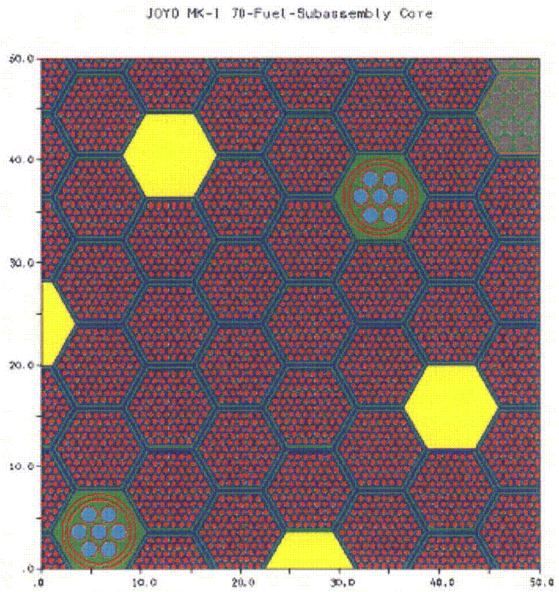

Fig. A.3.2-2. MVP Model for Criticality Analysis

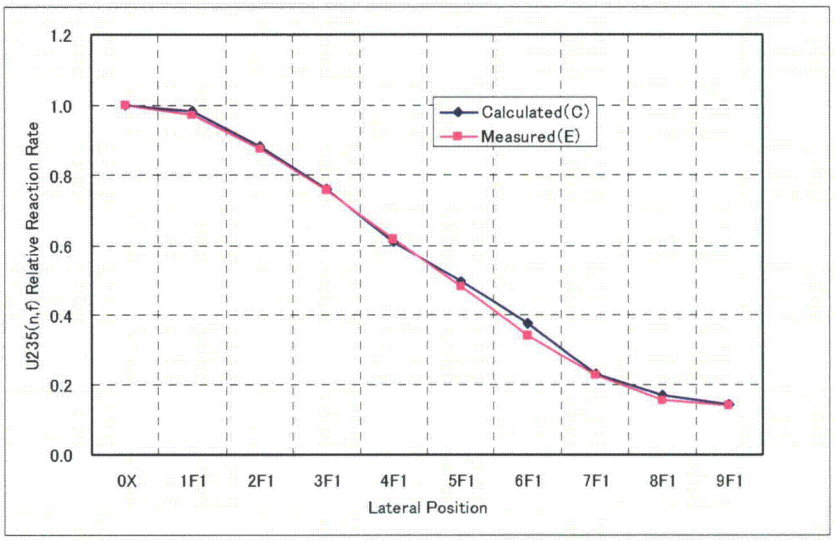

Fig. A.3.3-1. Comparison of Radial Relative Profiles for Measured and Calculated U-235(n,f) Reaction Rates at Core Midplane

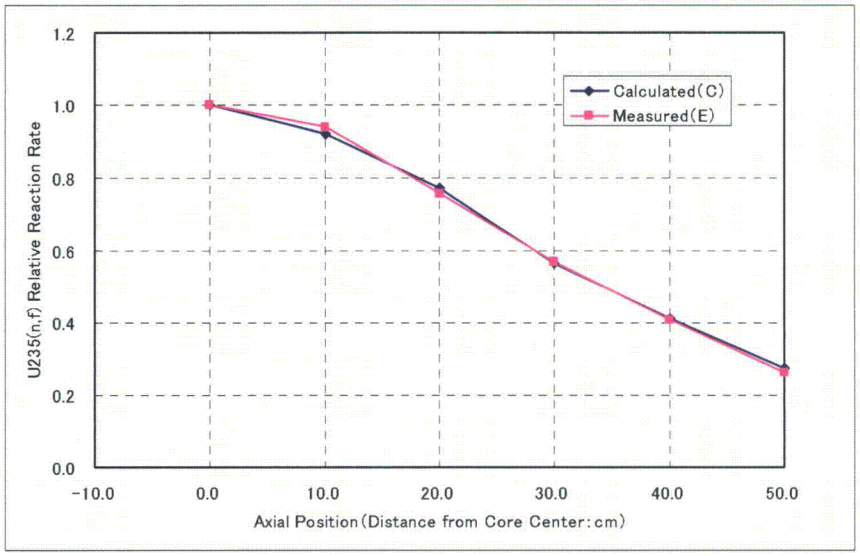

Fig. A.3.3-2. Comparison of Axial Relative Profiles for Measured and Calculated U-235(n,f) Reaction Rates at Core Center Assembly

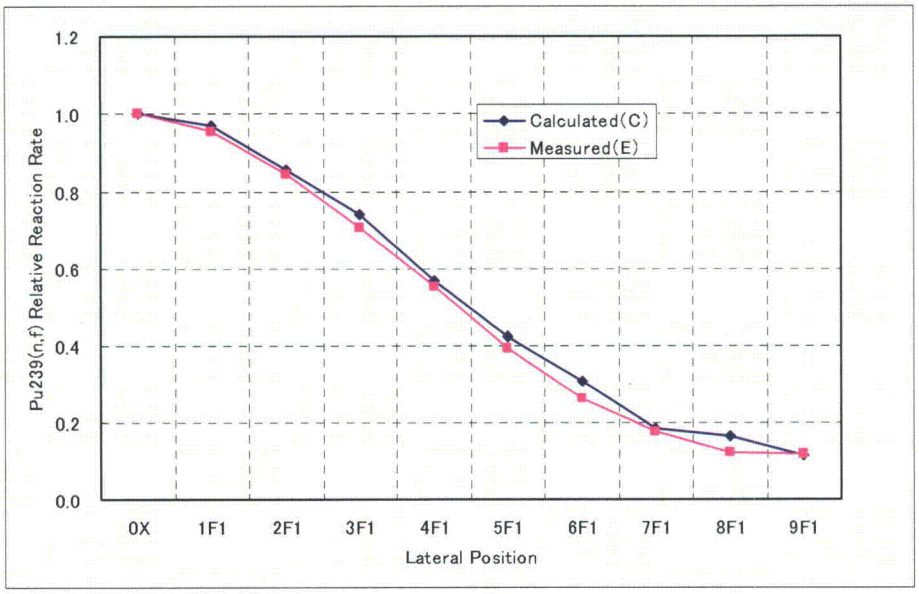

Fig. A.3.3-3. Comparison of Radial Relative Profiles for Measured and Calculated Pu-239(n,f) Reaction Rates at Core Midplane

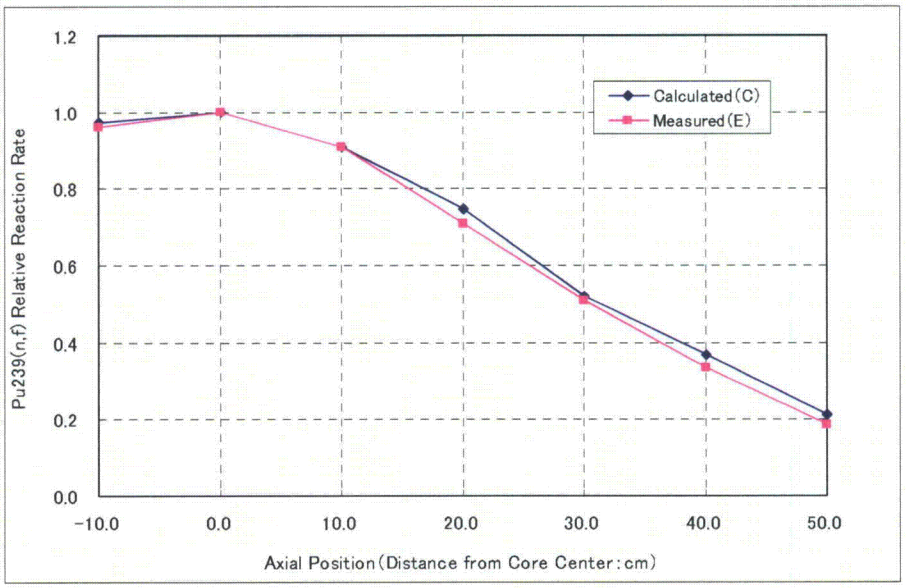

Fig. A.3.3-4. Comparison of Axial Relative Profiles for Measured and Calculated Pu-239(n,f) Reaction Rates at Core Center Assembly

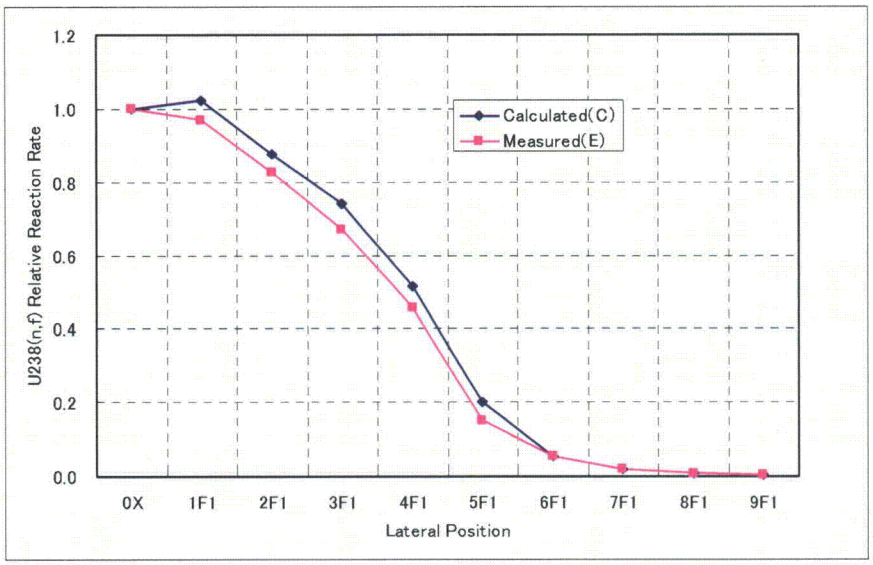

Fig. A.3.3-5. Comparison of Radial Relative Profiles for Measured and Calculated U-238(n,f) Reaction Rates at Core Midplane

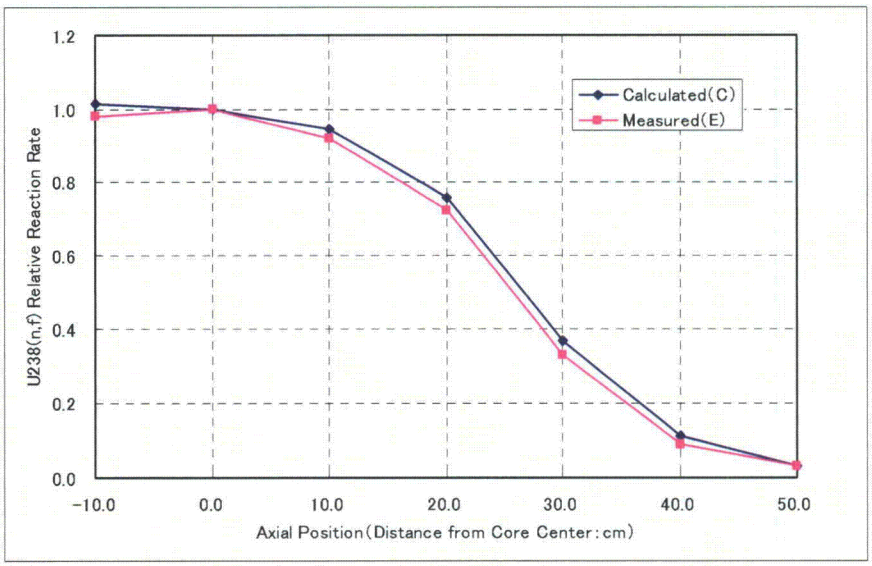

Fig. A.3.3-6. Comparison of Axial Relative Profiles for Measured and Calculated U-238(n,f) Reaction Rates at Core Center Assembly

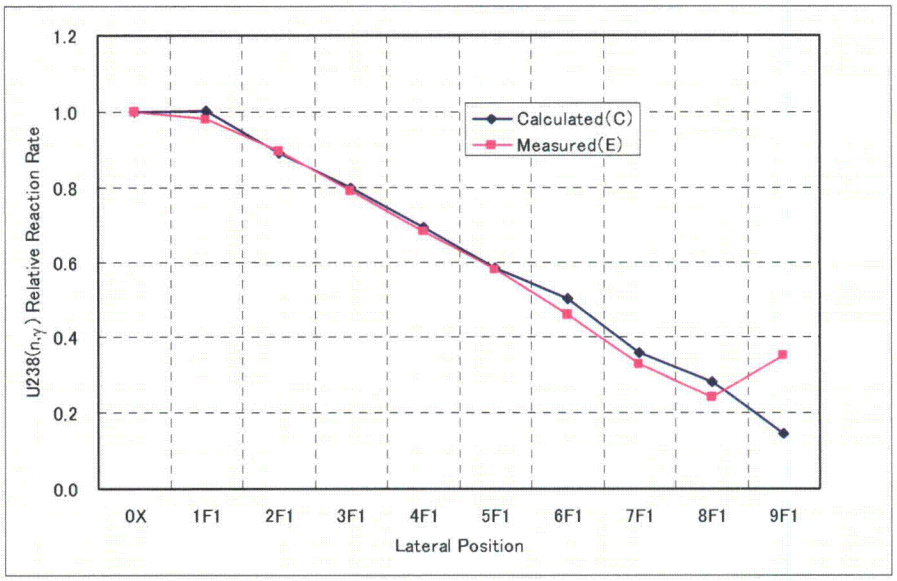

Fig. A.3.3-7. Comparison of Radial Relative Profiles for Measured and Calculated U-238(n,g) Reaction Rates at Core Midplane

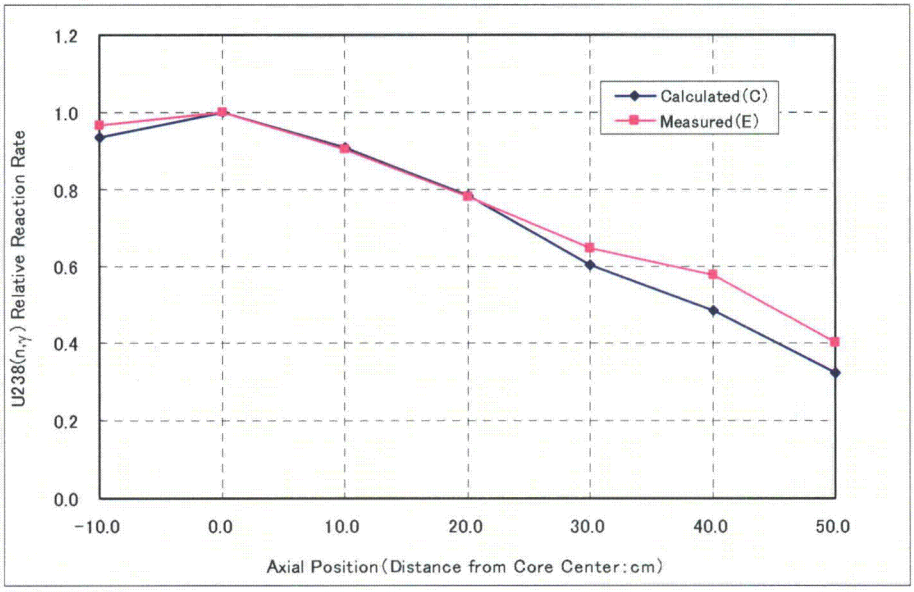

Fig. A.3.3-8. Comparison of Axial Relative Profiles for Measured and Calculated U-238(n,g) Reaction Rates at Core Center Assembly